

Mechanisms of High Frequency Activity in Epileptic Foci

Gareth Liam Morris

A thesis submitted to
the University of Birmingham
for the degree of
DOCTOR OF PHILOSOPHY

Neuronal Networks
School of Clinical and Experimental Medicine
College of Medical and Dental Sciences
The University of Birmingham
October 2014

UNIVERSITY OF
BIRMINGHAM

University of Birmingham Research Archive

e-theses repository

This unpublished thesis/dissertation is copyright of the author and/or third parties. The intellectual property rights of the author or third parties in respect of this work are as defined by The Copyright Designs and Patents Act 1988 or as modified by any successor legislation.

Any use made of information contained in this thesis/dissertation must be in accordance with that legislation and must be properly acknowledged. Further distribution or reproduction in any format is prohibited without the permission of the copyright holder.

ABSTRACT

High frequency activity (HFA) is oscillatory brain activity faster than ~ 100 Hz. It is subdivided into physiological ripples (~ 100 -250 Hz) and pathological fast ripples (~ 250 -500 Hz). Ripples in the hippocampus are paced by recurrent inhibition from interneurons. The mechanism for pathological HFA is unknown, but may be the same as for ripples and could provide new insight into the pathological nature of epileptic tissue.

HFA was induced using the high potassium (*in vitro*) and tetanus neurotoxin (*ex vivo*) models of epilepsy. Field HFA was recorded simultaneously with action potentials from visually targeted interneurons, made possible using VGAT-Venus A rats and a membrane chamber. The phase relationship between HFA and interneuron firing was examined.

In both models, HFA frequency was normally distributed between 100-300 Hz. Interneurons increased their firing rate during epileptiform bursts and were subdivided into four groups based on their firing patterns. The most pertinent group fired at >100 Hz throughout epileptiform bursts and were candidates to pace HFA. Of this group, significant phase relationships were seen in four interneurons using high potassium and one interneuron with tetanus neurotoxin.

These interneurons were compatible with the hypothesis that they pace HFA, but blockade of GABAergic signalling using bicuculline did not abolish HFA, suggesting a modulatory rather than causative role for interneurons.

This work is dedicated to

Caroline Buck

ACKNOWLEDGEMENTS

Throughout my three years studying for this PhD, many people have taught, guided, assisted or contributed in some other way to my progress and it is impossible to thank each and every one of them. For this reason, the list of thanks is by no means exhaustive.

I begin by thanking John Jefferys and Andy Powell, who have supervised me throughout the PhD, for their patience, guidance and never-ending support. I could not have wished for better supervisors and reiterate my sincere thanks to both of them. I also thank Premek Jiruska, who obtained the funding for the work along with John and Andy, but unfortunately left the University only a few months into the project.

Thank you to Karri Lamsa and Mike Lacey for all of their helpful comments, suggestions and insights as examiners.

Next I thank the many colleagues with whom I have been lucky enough to share the 'write-up room' (i.e. the office where all PhD students, post-docs, technicians and other undesirables were hidden away). Early on, Wei-Chih Chang was always happy to share his experience and ideas with me and was almost like a supervisor himself. Atif Saghir was a self-styled 'well wicked' technician and was incredibly patient when teaching and continually helping me to do PCR. Kali Gill and Lucy Foss only get a passing mention as I was not acknowledged in their theses! Towards the end of the PhD, Sahar Avazzadeh took over as go-to

technician as well as Persian teacher (merci, Sahar). Alex Lumsden provided much welcome distraction from work and also contributed a figure to this thesis. Thanks also to Ashleigh Wilcox for all the cups of tea.

I am extremely grateful to the neuronal networks group as a whole (in no particular order): Martin Vreugdenhil, Attila Sik, Emil Toescu and Andor Magony. Thanks for all of your comments, questions and discussions about this work both during lab meetings and otherwise. Thanks also to Barbara Harrison, who was always kind and supportive to the whole group.

Finally, thank you to Epilepsy Research UK, who funded the work. Thanks also to Guarantors of Brain and the Physiological Society, who awarded me travel grants to attend the American Epilepsy Society conference in Washington, D.C..

TABLE OF CONTENTS

1.	Introduction	1
1.1	Temporal lobe epilepsy	1
1.1.1	Epilepsy	1
1.1.2	The hippocampus	1
1.1.3	Morphological changes in the hippocampus during epileptogenesis.....	2
1.2	High frequency activity	4
1.2.1	Definition.....	4
1.2.2	Physiological HFA	4
1.2.3	HFA in epilepsy.....	5
1.2.4	Hypothesised mechanisms of pathological HFA	7
1.3	Models of temporal lobe epilepsy.....	18
1.3.1	General.....	18
1.3.2	The high potassium model	18
1.3.3	The tetanus neurotoxin model of epilepsy	19
1.4	The membrane chamber	22
1.5	VGAT-Venus rats.....	24
1.6	Aims and hypotheses.....	26
2.	Methods.....	27
2.1	Breeding and maintenance of rat colony	27
2.2	Polymerase chain reaction (PCR).....	27
2.3	Slice preparation.....	30
2.4	Data acquisition and experimental protocols.....	31
2.4.1	Refining a model of high frequency activity.....	31
2.4.2	The role of interneurons in the high potassium (9mM) model of epilepsy	32
2.4.3	The role of interneurons in the tetanus neurotoxin model	35
2.5	Data analysis	37
2.5.1	Interictal periods	37
2.5.2	Power spectra.....	39
2.5.3	Event detection	40
2.5.4	Average waveforms.....	43

2.5.5	Autocorrelation	44
2.5.6	Phase relationships using MatLab.....	45
2.5.7	Cell visualisation.....	46
3.	Results – Designing a Protocol.....	48
3.1	Slice parameters	48
3.1.1	Slice orientation – Horizontal vs Sagittal.....	48
3.1.2	Region of interest – CA3 vs CA1	49
3.1.3	Slice thickness – 300 μm vs 400 μm	52
3.2	The membrane chamber	54
3.2.1	Imaging.....	54
3.2.2	Single-cell recording	56
3.2.3	High potassium recordings.....	59
4.	Results – The high potassium model of epilepsy.....	61
4.1	Characterising HFA induced by high potassium in the membrane chamber	61
4.1.1	Epileptic-like activity is induced by high potassium.....	61
4.1.2	High potassium induces HFA superimposed on pathological sharp waves	64
4.1.3	The induced HFA spans both the ripple and fast ripple frequency bands	65
4.2	Investigating the behaviour of interneurons during epileptiform bursts.....	69
4.2.1	Interneuron firing frequency is increased during pathological sharp waves.....	70
4.2.2	Interneuron action potential amplitude is decreased during HFA	72
4.2.3	Interneurons show a variety of firing patterns during HFA	74
4.3	Examining the relationship between interneuronal firing and HFA cycles	76
4.3.1	HFA cycles and action potentials both occur primarily during epileptiform bursts	76
4.3.2	Phase-domain correlations using HFA cycles as the trigger.....	77
4.3.3	Phase-domain correlations using interneuron firing as the trigger	77
4.3.4	Laminar distribution of correlated interneurons	81
5.	Results – The tetanus toxin model of epilepsy.....	83
5.1	Response to tetanus toxin injection <i>in vivo</i>	83
5.1.1	Time course of seizures.....	83
5.2	Characterising the HFA seen <i>ex vivo</i> after TeNT injection.....	86
5.2.1	Potassium thresholds for the induction of HFA	86
5.2.2	Time course of seizure activity.....	86

5.2.3	Ripples (100-300 Hz)	88
5.2.4	Fast ripples (300-500 Hz).....	90
5.3	The behaviour of interneurons in the tetanus toxin model	93
5.3.1	Firing frequencies.....	93
5.3.2	Action potential amplitude	95
5.3.3	Firing patterns	97
5.4	Phase relationships between interneuron firing and HFA cycles in the tetanus toxin model	98
5.4.1	Phase relationships between ripple cycles and interneuron firing.....	98
5.4.2	Phase relationships between fast ripple events and interneuron firing.....	101
6.	Discussion	105
6.1	Protocol development	105
6.1.1	Slice parameters.....	105
6.1.2	The membrane chamber.....	107
6.2	HFA in the high potassium and tetanus toxin models.....	111
6.2.1	HFA in high potassium.....	111
6.2.2	Dominant HFA in TeNT	113
6.2.3	Fast ripple HFA in TeNT	114
6.3	Interneuron involvement in epileptic-like HFA.....	115
6.3.1	Interneuron participation in pathological 100-300 Hz HFA	115
6.3.2	Interneurons as a rate-limiting step in pathological 100-300 Hz HFA	122
6.4	Further experimental work.....	126
6.4.1	Anatomical identification of interneuron subtypes	126
6.4.2	Establishing causality.....	128
6.4.3	Use of a different chronic model	130
6.4.4	Studying non-synaptic mechanisms.....	131
6.5	Concluding remarks	132
	Reference List.....	134
	Appendix – Pharmacological Manipulation of HFA.....	150
	Appendix – Published Abstracts.....	152
	Appendix – Matlab Scripts	158

LIST OF FIGURES

Figure 1.1 – Schematic diagram of the membrane chamber.	24
Figure 2.1 – Sample PCR results.	29
Figure 2.2 – Defining the interictal/ictal periods.....	38
Figure 2.3 – Sample power spectrum.....	39
Figure 2.4 – HFA event detection.....	42
Figure 2.5 – Action potential detection.....	42
Figure 2.6 – Average waveforms for high frequency activity.....	43
Figure 2.7 – Autocorrelation.	44
Figure 3.1 – Horizontal slices are more prone than sagittal slices to seizure-like events.	49
Figure 3.2 – Epileptiform bursts in CA3 precede those in CA1.....	51
Figure 3.3 – HFA in CA3 has greater power than that in CA1.....	52
Figure 3.4 – Interneurons expressing VGAT-Venus can be visualised in the membrane chamber.	56
Figure 3.5 – Photograph illustrating the use of the membrane chamber.....	56
Figure 3.7 – Extracellular HFA can be recorded simultaneously with single-cell traces in 9mM K ⁺ in the membrane chamber.	60
Figure 4.1 - High potassium induces epileptic-like activity, including HFA, in brain slices.	63
Figure 4.2 - High frequency activity occurs primarily on the rising phase of pathological sharp waves.....	65
Figure 4.3 –‘Ripple band’ high frequency activity induced by high potassium.	67
Figure 4.4 – ‘Fast ripple band’ activity induced by high potassium.....	68
Figure 4.5 – The peak frequencies of induced HFA are normally distributed and span both the ripple and fast ripple bands.....	69
Figure 4.6 – Action potential firing frequency increases during epileptiform bursts.....	72

Figure 4.7 – The amplitude of action potentials recorded from interneurons decreases during epileptiform bursts.	73
Figure 4.8 – Different firing patterns of interneurons during epileptiform bursts.	75
Figure 4.9 – A significantly correlated interneuron.	78
Figure 4.10 – Oscillations which correlated to interneuron firing were slower.	80
Figure 4.11 – Laminar distribution of correlated and uncorrelated interneurons.	82
Figure 5.1 – Time course of epileptic response to TeNT injection.	85
Figure 5.2 – Continuous and discrete morphologies of epileptic-like activity in ex vivo TeNT treated slices.	88
Figure 5.3 – Ripple band (100-300 Hz) HFA is dominant in the TeNT model.	89
Figure 5.4 – Peak HFA frequencies from all slices were normally distributed	90
Figure 5.5 – The TeNT model featured both ripples and fast ripples.	92
Figure 5.6 – Ripples and fast ripples occurred primarily during pathological sharp waves.	92
Figure 5.7 – The timing of ripples and fast ripples was not correlated.	93
Figure 5.8 – Interneurons fire action potentials at higher frequency during epileptiform bursts in the TeNT model.	95
Figure 5.9 – Interneuron action potential amplitude decreases during epileptiform bursts.	97
Figure 5.10 – Significant phase relationships between ripple-band HFA and interneuron firing.	101
Figure 5.11 – Correlations between fast ripples and interneuron firing.	104
Figure 6.1 – Phase relationships in an anatomically reconstructed putative O-LM cell.	120
Figure 6.2 - Hypothesised mechanisms for the transition from physiological to pathological HFA.	124

LIST OF TABLES

Table 4.1 – Summary characteristics of continuous epileptic-like fields induced by 9mM potassium	64
Table 4.2 – Properties of significant phase relationships.....	82
Table 5.1 – Laminar distribution of interneurons with respect to firing patterns.	98

LIST OF ABBREVIATIONS

ABC	-	avidin/biotinylated enzyme complex
AC	-	alternating current
aCSF	-	artificial cerebrospinal fluid
AMPA	-	α -amino-3-hydroxy-5-methyl-4-isoxazolepropionic acid
BSA	-	bovine serum albumin
CA	-	cornu ammonis
CCK	-	cholecystokinin
DAB-Ni	-	3'-3'-diaminobenzidine nickel
DC	-	direct current
DNA	-	deoxyribonucleic acid
EDTA	-	ethylenediaminetetraacetic acid
EEG	-	electroencephalogram
eGFP	-	enhanced green fluorescent protein
EPSC	-	excitatory post-synaptic current
EPSP	-	excitatory post-synaptic potential
FFT	-	fast Fourier transform
FIR	-	finite impulse response
GABA	-	γ -aminobutyric acid

GAD	-	glutamate decarboxylase
GIN	-	GFP-expressing inhibitory neuron
HEPES	-	4-(2-hydroxyethyl)-1-piperazineethanesulfonic acid
HFA	-	high frequency activity
IPSC	-	inhibitory post-synaptic current
IPSP	-	inhibitory post-synaptic potential
KA	-	kainic acid
O-LM	-	oriens-lacunosum moleculare
PB	-	phosphate buffer
PBS	-	phosphate buffered saline
PCR	-	polymerase chain reaction
PV	-	parvalbumin
SD	-	standard deviation
SDS	-	sodium dodecyl sulphate
SEM	-	standard error of the mean
SL		stratum lucidum
SLE	-	seizure-like event
SNARE	-	soluble NSF attachment protein receptor
SO	-	stratum oriens
SP	-	stratum pyramidale
SPW	-	sharp wave
SPW-R	-	sharp wave-ripple complex
SR	-	stratum radiatum
TBE	-	tris/borate/EDTA
TeNT	-	tetanus neurotoxin
TLE	-	temporal lobe epilepsy
VAMP	-	vesicle associated membrane protein
VGAT	-	vesicular GABA transporter
YFP	-	yellow fluorescent protein

1. INTRODUCTION

1.1 Temporal lobe epilepsy

1.1.1 *Epilepsy*

Epilepsy is the third most common neurological disease (Kohrman 07), with around 50 million cases worldwide (Banerjee et al 09). Epilepsy is characterised by pathological hyperexcitability of neuronal networks and abnormal synchrony of pyramidal cell firing. This manifests clinically as seizures, which have different clinical presentations depending on the specific brain regions affected. Seizures can be more systematically described using the classification system set out by the International League Against Epilepsy in 2001 (Engel, Jr. 01).

1.1.2 *The hippocampus*

Temporal lobe epilepsy (TLE), where pathological discharges arise from an epileptic focus in the hippocampus, or anatomically related structures such as the amygdala (Wiebe et al 01), is the most common form of focal epilepsy (Tellez-Zenteno and Hernandez-Ronquillo 12). In physiological brain tissue, the activity flow through the hippocampus can be simplified to a tri-synaptic circuit (Amaral 93). Briefly, the structure receives input from the entorhinal cortex, which then passes through three hippocampal sub-regions – the dentate gyrus, CA3 and CA1 – before outputting to the subiculum. Each region is connected to the next by excitatory projections which relay signals between them. Locally, each of these

sub-regions contains recurrent excitatory connections, which allow normal tissue to generate epileptiform activity, as in acute models of epilepsy such as the high potassium model (Traynelis and Dingledine 88). The amount and nature of recurrent excitation varies between sub-regions. CA3 features strong monosynaptic excitation of other pyramidal cells. More sparse monosynaptic recurrent excitation is seen in CA1 (Deuchars and Thomson 96) and the dentate gyrus features disynaptic feedback, via mossy fibres. Local hippocampal circuits are also interspersed with inhibitory interneurons which modulate the temporal firing patterns of excitatory pyramidal cells (Klausberger and Somogyi 08) and can entrain them into network oscillations, with the frequency of the interneuron's firing determining the frequency of the field activity (Whittington et al 95). Interconnections between the regions of the hippocampus show activity-dependent plasticity, supporting its role in learning and memory (Bliss and Lomo 73).

1.1.3 Morphological changes in the hippocampus during epileptogenesis

The plastic nature of the hippocampus confers a susceptibility to the formation of aberrant excitatory loops, which can facilitate spontaneous seizure generation (Coulter et al 11). Indeed, it has been shown that alterations in network connectivity can give rise to epilepsy (Cavazos et al 04). In the kindling model of TLE in rats, new axons and synapses form in the mossy fibre pathway, which is the excitatory pathway between the dentate gyrus and CA3 (Cavazos and Sutula 90). These changes are long-lasting, and correspond with the time course of the

resulting epileptic-like behaviour. This finding is consolidated by findings from the kainate (KA) model, where seizures follow the time course of axonal sprouting, rather than the precipitating cell loss (Allen et al 92). However, blockade of axonal sprouting has no clear effect on seizure patterns and it has been suggested that other related phenomena, such as the formation of ectopic granule cells, may be involved (Buckmaster and Lew 11).

Pathological connectivity has also been shown between the CA3 and CA1 regions of the hippocampus. Rats with KA-induced epilepsy show an increased density of projections in the Schaffer collateral pathway from CA3 to CA1, as well as novel outputs directly to the entorhinal cortex from CA3 (Siddiqui and Joseph 05).

Because the entorhinal cortex is the main input into the dentate gyrus, this sets up a recurrent excitatory loop which could pathologically alter hippocampal activity.

Changes in CA1 axonal projections have been shown using both acute (KA and pilocarpine (Cavazos et al 04)) and chronic (tetanus neurotoxin (Vreugdenhil et al 02), kindling and pentylentetrazol (Cavazos et al 04)) rat models. In these cases, pyramidal cell projections extend beyond their normal reach both dorsally and ventrally, creating excessive output into the subiculum and novel pathways into stratum lacunosum-moleculare. All of these changes would serve to excessively amplify the normal routing of signals in the hippocampus and to create modified pathways.

1.2 High frequency activity

The hippocampus shows oscillatory brain waves with frequencies ranging from <1 Hz (delta) up to >100 Hz (high frequency activity or HFA). HFA is of particular interest as it is more prevalent in epileptic tissue, and specific patterns of this phenomenon are closely linked to epileptic foci (Bragin et al 99b).

1.2.1 Definition

High frequency activity (also termed high frequency oscillations or HFOs) consists of brain oscillations with a frequency of greater than ~100 Hz (Jefferys et al 12). HFA can be subdivided into the ripple band, ~100-~250 Hz, and the fast ripple band, ~250-~500 Hz. The exact cut-offs for these bands are ill-defined in the literature, with ripple activity ranging from 100-300 Hz and fast ripples from 200-600 Hz (Foffani et al 07). Clearly, there is some overlap between these two bands and frequency is not a reliable classifier. To this end, it has been suggested that HFA could be further classified by three properties: transient vs continuous, narrow frequency band vs broad frequency band and whether or not it is linked to a causative event (Jefferys et al 12).

1.2.2 Physiological HFA

Physiological HFA occurs in the ripple band and has been reported at frequencies ranging from 80 Hz (Jiruska et al 10b) to 300 Hz (Foffani et al 07). HFA in this band has been reported *in vivo* in the hippocampal CA1 region of behaving rats (Buzsaki et al 92; Csicsvari et al 99; Li et al 92; Ylinen et al 95) during behavioural

immobility (Foffani et al 07), slow-wave sleep (Buzsaki et al 92; Foffani et al 07; Li et al 92) and consummatory behaviour (Ylinen et al 95). HFA, with lower power and frequency than that in CA1, can also be observed in CA3 *in vivo* (Buzsaki et al 92). Functionally, hippocampal HFA has been linked to memory consolidation (Axmacher et al 06; Karlocai et al 14); indeed, the abolition of ripples using electrical stimulation of the ventral hippocampus impaired spatial learning in rats (Girardeau et al 09). Mechanistically, physiological HFA is thought to be generated by the synchronisation of a local population of pyramidal cells due to the temporal constraints imposed by recurrent IPSPs from fast-spiking GABAergic interneurons (see section 1.2.4.1).

1.2.3 HFA in epilepsy

Abnormal high frequency field oscillations, initially termed 'high-frequency gamma' (Fisher et al 92), are present in human epileptic brain tissue and have been observed in various structures (Fisher et al 92), including the hippocampus (Bragin et al 99a) and frontal lobe (Allen et al 92). Pathological HFA is replicated in chronic animal models, including the tetanus neurotoxin (Jefferys 89), KA (Bragin et al 99b) and pilocarpine (Levesque et al 11) models, where it occurs primarily during behavioural immobility and sleep (Bragin et al 99b). Pathological-like HFA is also seen in acute *in vitro* models such as high potassium (Karlocai et al 14) and low calcium (Jiruska et al 10a). Fast ripple activity, in excess of 200 Hz, was first systematically described in 1999 (Bragin et al 99c) and is unique to epileptic foci. Specifically, increased power in the fast ripple band is associated with the onset of

hypersynchronous seizures (Bragin et al 05). The spatial limitation of fast ripples to the epileptic focus is stable over the timescale of days to months (Bragin et al 03). As a result of this, the presence of pathological HFA provides a reliable biomarker for seizure-generating tissue and indeed resection of this tissue correlates with a positive surgical outcome (Kerber et al 13).

Fast ripple activity is distinct from ripple activity (Bragin et al 99a) and there is no precise temporal relationship between the pathological and physiological oscillations, though the two can often coincide where they are superimposed on the same epileptiform discharge (Bragin et al 99a). Indeed, power spectral analysis of HFA during seizure onset can reveal bimodal profiles, which can be interpreted as two separate oscillations occurring at the same time (Bragin et al 04). This suggests that the two phenomena may not be directly mechanistically linked, but can both be triggered locally by the strong excitatory input of an interictal discharge. On a cellular level, extracellular recordings from chronic rat models have shown that pyramidal cells exhibiting a complex spiking pattern correlate with fast ripple activity, which suggests that the pathological oscillation may reflect the synchronisation of these cells into population spikes (Bragin et al 99b). Recordings from putative interneurons in the same study did not reveal any correlation with fast ripples, though this was not studied systematically. Thus, it is desirable to investigate the mechanism leading to the synchronisation of complex-spiking pyramidal cells into a fast ripple oscillation, and to compare and contrast this with the proposed mechanism of ripple generation, by recurrent IPSPs.

1.2.4 Hypothesised mechanisms of pathological HFA

In order to create fast ripple band HFA, groups of pyramidal cells must be synchronised on a sub- 5 millisecond timescale. There are several hypothesised mechanisms for this – some involve synaptic transmission and some are non-synaptic (Jiruska et al 10b).

1.2.4.1 Pacing by interneurons

As was mentioned in section 1.2.2, physiological HFA is thought to arise from the synchronisation of pyramidal cells by inhibitory interneurons (Csicsvari et al 99; Ylinen et al 95) and so this is a logical starting point for investigation into mechanisms of epileptic HFA. Physiological HFA is often superimposed on a sharp wave (SPW) which is a relatively slow event, lasting from 40-120 ms (Ylinen et al 95), that arises from hypersynchronous dendritic input. For *in vivo* physiological ripples in CA1, it has been shown that sharp waves are triggered by the synchronous discharge of pyramidal cells in CA3 (Li et al 92). This creates a powerful wave of excitation through the Schaffer collateral pathway, resulting in the formation of a sharp wave in CA1. The arrival of this sharp wave causes simultaneous excitatory input into all of the local circuitry and, in this hypothesis, the interplay between excitatory pyramidal cells and inhibitory interneurons within the cell line is thought to underlie ripple activity. The activation of local interneurons causes them to release GABA onto all of their synaptically connected target cells. This means that a large population of pyramidal cells receive a synchronous inhibitory input and, for a short time (~5 ms), are all silenced.

Because the excitatory drive of the sharp wave is still present, those pyramidal cells which are able to fire will do so in synchrony, as soon as they are released from their inhibitory constraints. This can be recorded extracellularly as a single HFA cycle. Once the interneuron recovers from hyperpolarisation, the continuing sharp wave drive causes it to fire again, repeating the cycle. This can happen multiple times during one sharp wave, creating an oscillation where the frequency is determined by the firing rate of the interneuron and the rate at which it thus imposes IPSPs on its targets.

There are several pieces of evidence to support this hypothesis. Firstly, for physiological HFA, interneurons in stratum pyramidale and stratum oriens (Csicsvari et al 99), including basket cells (Ylinen et al 95) exhibit firing which is strongly correlated to the field oscillation. This means that the dynamics of local interneuronal firing are compatible with the hypothesis and theoretically the frequency of the oscillation could reach the fast ripple band, if the interneuron were to fire at this frequency. Computational simulations of local hippocampal networks provide further support for this hypothesis. In CA1, each basket cell innervates around 1440 pyramidal cells, averaging 25 inputs onto each cell (Traub et al 99). Thus the firing of one basket cell is sufficient to entrain a small aggregate of pyramidal neurons to fire synchronously. In turn, the pyramidal cells could provide excitatory feedback to other interneurons and entrain their target cells. This would cause a gradual build up in the power and synchrony of the oscillation, consistent with the 'locking in phase' described by Bikson et al. (03). Another piece of supporting evidence is that spike transduction between interneurons and

pyramidal cells is very reliable; in CA3, a single IPSP is sufficient to prevent action potential firing in target cells (Traub et al 99). Taken together, these ideas show that the high frequency interneuronal firing described by Ylinen et al. would be capable of having a strong influence over its targets. Finally, it has been suggested that fast-spiking interneurons are capable of maintaining firing frequencies up to 1 kHz (Rudy and McBain 01). This is sufficient to pace oscillations throughout both the ripple and fast ripple ranges.

However, some experimental observations cast doubt on this hypothesis. Whilst fast-spiking cells are capable of firing action potentials at sufficiently high frequency to pace HFA, it has been shown that the second in a pair of IPSCs elicited in a pyramidal cell is suppressed at frequencies as low as 0.5 Hz (Khazipov et al 95). Similarly, in the high K^+ model of TLE, it has been shown that there is a depression in synaptic transmission from parvalbumin positive basket cells to pyramidal cells as pathological HFA develops (Karlocai et al 14). Indeed, basket cells and some axo-axonic cells do not fire at all during epileptiform bursts¹, which has been attributed to depolarisation block (Karlocai et al 14), though this mechanism may be unrealistic on a 200 ms timescale HFA can also be observed in other models where inhibitory transmission is impaired including the tetanus neurotoxin (Jiruska et al 10b) and low calcium (Jiruska et al 10a) models. It must also be noted that the temporal relationship between interneuron firing and HFA described by Ylinen et al. does not establish a causative relationship between the

¹ In this work, the term 'epileptiform burst' refers to a sharp wave-ripple complex which occurs in a pathological situation. Thus pathological and physiological events can be differentiated. When referring only to the slower component of epileptiform bursts, they will be termed 'pathological sharp waves'.

two. A correlation between the two signals does not prove causality and, due to the cyclical nature of both signals, it is hard to determine which is the cause and which the consequence. Further, both signals could, in theory, be mediated by a third event and not directly mechanistically related (van Drongelen 10).

1.2.4.2 Synaptic coupling of pyramidal cells

The second theoretical mechanism for the generation of pathological HFA is that the required synchrony is caused by direct excitatory synaptic coupling between pyramidal cells (Dzhala and Staley 04; Jiruska et al 10b). Around 20% of pyramidal neurons in CA3 are capable of generating spontaneous bursts of action potentials (Dzhala and Staley 04). Indeed, in the intact physiological hippocampus, most action potentials recorded from CA3 pyramidal cells do not show any detectable underlying post-synaptic potentials. This is in contrast with interneurons, which appear to mostly rely on glutamatergic input to trigger action potentials (Cohen and Miles 00). Therefore, single pyramidal cells are capable of acting as isolated cellular oscillators (Jefferys et al 12). In the normal hippocampus, individual cellular oscillators display a range of inter-spike intervals and burst lengths (Dzhala and Staley 04). This asynchronous and comparatively disorganised firing would be insufficient to generate an EEG oscillation (Jefferys et al 12). Therefore, although synaptic coupling is not necessary for a single cell to oscillate, the network interconnections between them must be considered in the formation of an HFA-band field oscillation.

Fast ripples could be generated if a homogeneous population of cellular oscillators were to fire at the same time. The intrinsic cellular bursts are generated and modulated by ion channels in the apical dendrites of the neurons (Dzhala and Staley 04). Logically, blockade of excitatory signalling decreases spontaneous firing and suppression of inhibition increases the levels of firing (Cohen and Miles 00). It follows that, with the collapse of inhibitory signalling which is seen in models of TLE (Ferecsko et al 14; Karlocai et al 14), excitatory signalling between pyramidal cells should have a greater contribution to network activity (Cohen and Miles 00). As discussed in section 1.1.3, aberrant excitatory interconnections and even autapses form during epileptogenesis. Therefore, the epileptic brain features a greater number of excitatory synaptic connections, which are poorly organised and have abnormally high efficacy due to the collapse of inhibitory restraint. It is thus hypothesised that these pathological interconnections give rise to fast ripples.

1.2.4.3 Non-synaptic coupling of pyramidal cells

One non-synaptic mechanism for the synchronisation of pyramidal cells is electrotonic coupling via gap junctions (Draguhn et al 98; Jiruska et al 10c). A gap junction is a continuous pore between adjacent cells which allows any sufficiently small water soluble molecule to pass through it. Thus, the two cells are electrically (through the passage of current carrying ions) and metabolically coupled (Alberts et al 08). It follows that an action potential in one pyramidal cell should propagate almost instantaneously into an electrotonically coupled cell, resulting in

synchronisation between the two. This is supported by electrophysiological studies in which the activation of one cell has been shown to induce small, transient depolarisations, referred to as either fast pre-potentials (MacVicar and Dudek 81) or spikelets (Vivar et al 12). Moreover, this type of electrical transmission is faster than chemical synapses (Vivar et al 12), and so would seem like a leading candidate as a mechanism of HFA, as it could provide faster temporal synchronisation. The main argument supporting this hypothesis is that gap junction blockers such as carbenoxolone (Draguhn et al 98; Vivar et al 12), halothane (Draguhn et al 98) and octanol (Draguhn et al 98) reversibly block HFA. However, gap junction blockers are not specific; it has been shown, for example, that carbenoxolone irreversibly blocks AMPA-mediated EPSCs and reversibly reduces GABA_A-mediated IPSCs (Tovar et al 09). Whilst Vivar et al (12) controlled for this by studying spikelets in the absence of synaptic transmission (and so blocking these currents anyway), the effects of carbenoxolone on the membrane properties of both pyramidal cells and interneurons - attenuated repolarisation, spike rate and input resistance (Tovar et al 09) – could also underlie the abolition of HFA in the presence of gap junction blockers.

Further doubt about this mechanism arises when considering the extent and nature of electrotonic coupling in the hippocampus. For quite some time it was widely considered that the presence of gap junctions in the mature mammalian CNS was limited, with such structures only seen in significant numbers during development and following injury (Jefferys 95). Though several studies have reported the presence of gap junctions in the main hippocampal regions: CA1

(Perez-Velazquez et al 94), CA3 (MacVicar and Dudek 81; Schmitz et al 01) and the mossy fibre pathway (Hamzei-Sichani et al 12; Vivar et al 12), several confounding factors cast doubt upon some of these studies. For example, Perez-Velazquez et al (Perez-Velazquez et al 94) reported the presence of gap junctions in CA1 and presented evidence of both dye-coupling and the propagation of electrophysiological events between pyramidal cells. However, the study was carried out in juvenile rats and it has been shown that both the presence of gap junctions and levels of connexins are highly related to brain development (Schmitz et al 01) and that, at least in the cortex, there is negligible coupling in adult animals (Peinado et al 93). Whilst the evidence for gap junctional coupling between pyramidal cells in CA3, using paired intracellular recordings in slices prepared from adult rats (MacVicar and Dudek 81), seems to be more convincing, there is still doubt as to whether this would be sufficient to produce HFA. Firstly, computational models of CA3 pyramidal cells have shown that for a gap junction to reliably elicit a spikelet in the target cell, the coupling must take place at the axo-axonal level, as this is the only part of the cell membrane with sufficiently low capacitance and so fast time constants (Draguhn et al 98). However, several studies have reported that gap junctions are located between dendrites. Thus it is not surprising that the propagation of spikelets into target cells is very infrequent (MacVicar and Dudek 81; Vivar et al 12). Further, even when a spikelet is elicited, it is by definition a very small depolarisation and may not cause the membrane potential of the target cell to cross the threshold for action potential firing. This makes it seemingly unlikely that gap junctions would be reliable enough to

synchronise a large ensemble of cells to fire at very high frequency as is required to pace HFA. Perhaps though, spikelets might act to enhance synchronisation in cells which are already hyperexcitable, as in epileptic tissue, because in this case the small depolarisation of a spikelet might be sufficient to trigger an action potential (Perez-Velazquez et al 94).

It must also be considered that gap junctions could act in conjunction with other mechanisms. Electron microscopy studies have provided strong evidence of dendro-dendritic coupling between fast-spiking, parvalbumin-containing interneurons (Fukuda and Kosaka 00; Hamzei-Sichani et al 12). Perhaps, when these interneurons become hyperexcitable due to the continuous excitatory drive in the epileptic hippocampus, these gap junctions could act to synchronise fast-spiking interneurons, thus exerting the same rhythmic inhibition on all of the pyramidal cell targets of all of the interneurons. This hypothetical compound mechanism would therefore cause a very large network of cells to fire rhythmically at very high frequency, as is seen in ripple and fast ripple activity. It has also been suggested that, where epileptic discharges occur in the absence of synaptic transmission, gap junctions could play a complementary role in fine tuning HFA (Dudek et al 98), which is brought about by electric field interactions (Jefferys and Haas 82).

1.2.4.4 Field effects and ephaptic interactions

The final hypothesised mechanism for the synchronisation of pyramidal neurons into high frequency oscillations is by electrical field effects, including ephaptic

interactions (Jefferys 95). These two phenomena are very similar and will thus be discussed together, but it is important to note that ephaptic interactions specifically denote the impact of the electrical fields generated by a single neuron on another in very close proximity (Arvanitaki 42; Jefferys 95). In contrast, field effects are generated by a population of neurons and can modulate other excitable cells over a longer distance (Jefferys 95).

Several studies have demonstrated experimentally that electrical fields can modulate neuronal excitability. Uniform DC electrical fields applied across acute hippocampal brain slices can induce or suppress activity in CA1 pyramidal cells (Bikson et al 04; Francis et al 03) and in granule cells in the dentate gyrus (Jefferys 81), depending on the polarity of the applied field. These effects can be achieved with fields as small as $140 \mu\text{Vmm}^{-1}$ (Francis et al 03) and the magnitude of polarisation is directly proportional to the strength of the applied field (Bikson et al 04). Electrical fields can also modulate cells in CA3, though this region is less sensitive than CA1. This is due to a lower density of cell packing in CA3, which increases the ratio of extracellular: intracellular space (Francis et al 03). Indeed, the extracellular volume fraction in CA1 is 0.12, compared with 0.18 in CA3 (McBain et al 90). This lowers extracellular resistivity, which has a linear relationship with field strength (Jefferys 95). The response of neurons to DC fields also depends on the orientation of the field with respect to the cells. Fields applied parallel to the somato-dendritic axis are capable of polarising cells, whilst perpendicular fields can alter the excitability of afferent inputs to the cells (Bikson et al 04). Similarly, the application of local DC currents via a monopolar

stimulating electrode is capable of modulating neuronal activity and indeed suppressing epileptiform bursts (Lian et al 03). In this case, the strength of the applied field is not uniform throughout the slice and attenuates as distance from the stimulating electrode increases. Cellular excitability can also be modulated using AC stimulation (Deans et al 07; Lian et al 03). In this case, the membrane potential fluctuates in phase with the stimulation. This effect has a linear relationship with the strength of the applied field and does not outlast the duration of stimulation (Deans et al 07). At 10 Hz, the efficacy of AC stimulation is comparable to that of DC stimulation, though this decreases at higher frequency (Deans et al 07), perhaps arguing against a role in high frequency synchronisation of pyramidal cells. Unlike DC stimulation, there is no orientation-dependent effect for AC stimulation (Lian et al 03).

All of the studies described above used *in vitro* recordings and relied on the application of electrical fields through stimulating electrodes. Whilst this is clearly not the case in the intact brain, the same mechanisms could play a role.

Physiological hippocampal sharp waves in the awake rat generate a local electrical field of up to 14 mVmm^{-1} (Buzsaki 86). This is substantially greater than $140 \text{ }\mu\text{Vmm}^{-1}$, the threshold for recruiting CA1 neurons into synchronous firing (Francis et al 03). Further, as mentioned above, the hippocampus is particularly susceptible to field effects due to the close packing and regular orientation of pyramidal neurons. Therefore, within the hippocampus, there is a naturally occurring phenomenon which generates sufficient electrical fields to recruit its

susceptible neighbouring neurons to fire. It thus follows that field effects are likely to play a role in normal hippocampal function.

In the epileptic brain, large pathological epileptiform bursts arise in the epileptic focus and can cause changes in transmembrane potential (Goldensohn and Purpura 63). These shifts give rise to electric fields between 3-9 mVmm⁻¹ (Weiss et al 13) – sufficient to induce depolarisation in neurons. This could provide a mechanism for synchronising the firing of neurons into pathological sharp waves. Computer simulations have suggested that field effects could theoretically synchronise action potentials on a millisecond timescale (Traub et al 85), as would be required to produce high frequency activity. This is supported by more recent experimental data, which shows that pyramidal neurons in the neocortex have a decreased firing threshold during the negative phase of HFA, despite no change in transmembrane potential (Grenier et al 03). It is suggested that these findings demonstrate a role for local field effects in recruiting more neurons into an existing oscillation, thus increasing its power. This in turn would enable further neurons to be recruited in a positive feedback loop. Finally, the presence of HFA in the low calcium model, where synaptic transmission is impaired, combined with the observation that gap junctional coupling in the hippocampus is relatively sparse, suggests that electric fields play a role in the generation of high frequency activity (Dudek et al 98).

1.3 Models of temporal lobe epilepsy

1.3.1 General

As is apparent from section 1.2.4, HFA is a network phenomenon which arises from an intricate interplay between the cellular components of the oscillatory population. Therefore, experimental studies into the mechanisms of HFA require the use of invasive tools to record at the cellular level. Whilst it might be desirable to study the 'real' oscillation in the epileptic human brain, this is limited to the subset of clinical cases in which the implantation of depth electrodes is needed for diagnosis (Jefferys et al 12; Maris et al 11). As a result, basic scientific investigations into HFA require models of the phenomenon in a situation which is more permissive of electrophysiological recording techniques. To this end, both acute and chronic models can be used *in vitro* and *in vivo* (Jefferys et al 12).

1.3.2 The high potassium model

Epileptiform bursts can be induced acutely in brain slices by increasing the concentration of potassium (K^+) in the circulating aCSF (Jiruska et al 10a; Karlocai et al 14; Traynelis and Dingledine 88). This can be achieved by raising the K^+ concentration from ~ 3 mM, as in the normal aCSF, to $\sim 8-9$ mM (Traynelis and Dingledine 88). This increase in extracellular K^+ increases the equilibrium potential for K^+ to a more positive value, as calculated using the Nernst equation. Thus, following the Goldman equation, neuronal resting membrane potential increases towards the threshold for action potential firing. As a result, neurons become

hyperexcitable and spontaneous epileptiform bursts can be observed. These high K^+ -elicited bursts are a separate phenomenon from the spontaneous physiological SPW-Rs described in section 1.2.2, with differences in amplitude, duration and underlying multiunit activity between the two (Karlocai et al 14). Indeed, the elicited bursts resemble those recorded *in vivo* during tonic-clonic seizures in animal models of epilepsy (Traynelis and Dingledine 88).

1.3.3 *The tetanus neurotoxin model of epilepsy*

Whilst the acute high potassium model provides an adequate representation of pathological brain oscillations, it uses tissue in which neuronal networks remain physiologically interconnected, and have not undergone any of the changes described in section 1.1.3. It could thus be considered more realistic and desirable to use chronic models of epilepsy *in vivo*, where animals undergo epileptogenesis. This leads to a brain state which is capable of generating spontaneous seizures, and is thus a better model of human epilepsy. This can be achieved using the tetanus neurotoxin (TeNT) model of epilepsy.

TeNT is derived from the bacterium *Clostridium tetani* (Schiavo et al 00) and contains metalloproteases which specifically target neurons (Schiavo et al 00). Structurally, the toxin consists of three domains. The two domains which comprise the heavy chain permit neuronal specificity and confer the ability to internalise into neurons. Once inside the cell, the light chain can be activated by cleavage of a disulphide bond and then carries out protease activity (Schiavo et al 00). Specifically, TeNT targets Vesicle Associated Membrane Protein (VAMP)

(Ferecsko et al 14), which is a component of the SNARE complex that is responsible for the presynaptic release of neurotransmitters. Therefore, TeNT disrupts synaptic transmission between cells. It has been demonstrated in spinal cord neurons that this effect is limited to inhibitory transmission (Shin et al 12), thus increasing the excitability of neuronal networks by disinhibiting them. Peripherally, this causes spastic paralysis (Pellizzari et al 99). In the central nervous system, TeNT has also been shown to have an impact on excitatory transmission, but not to the same extent as that on inhibitory transmission – the latter being almost entirely abolished in the hippocampus at 8-16 days post injection with toxin (Ferecsko et al 14). This can explain why injection of TeNT into the central nervous system causes epilepsy (Mellanby et al 77). The toxin can be applied to the desired brain region using stereotaxic injection. Previously targeted structures include the motor cortex (Wykes et al 12) and the hippocampus (Jefferys 89; Jiruska et al 10b; Mellanby et al 77). Injection of TeNT into the rat hippocampus causes spontaneous seizures, which begin to occur at around one week post injection (Jiruska et al 10b), when VAMP levels are significantly decreased (Ferecsko et al 14). The seizures can be classified as complex partial seizures with secondary generalisation (Jiruska et al 10b) with the rats gaining remission in the majority of cases around 4-8 weeks post injection (Jefferys 89). The behavioural manifestations of the seizures and the underlying pathological brain activity are akin to that seen in the human condition (Mellanby et al 77), suggesting that this is a good model of temporal lobe epilepsy. Further, both ripple and fast ripple band HFA can be observed in the *in vivo* model (Jiruska et al

10b). The TeNT model has an advantage over other chronic models of TLE (cf. pilocarpine (Foffani et al 07)) because it is non-lesional and does not rely upon cell death and hippocampal sclerosis to cause epileptogenesis (Jiruska et al 10b). This means that the cellular components of oscillating networks remain intact, permitting the study of changes in their interconnections which may underlie the development of epilepsy and the associated fast ripples.

Whilst it is technically challenging to record from single cells, as desired for this study, using *in vivo* models (Jefferys et al 12), *ex vivo* brain slices prepared from TeNT injected rats can also generate comparable epileptic-like activity (Jefferys 89). In these slice preparations, spontaneous epileptiform bursts can be recorded in response to a modest elevation of K^+ (5mM, which is not sufficient to cause spontaneous bursting in healthy tissue). In approximately one third of cases, discharges were observed even with normal K^+ levels (Jefferys 89). Thus, *ex vivo* slice preparations facilitate the study of the behaviour of single cells during the chronic model.

The use of acute brain slices facilitates both high magnification imaging and patch clamp recording from single cells within the slice. However, previous uses of the high K^+ model have limitations which must be addressed for the current study. Firstly, 400 μm brain slices are thicker than is desirable for both patch clamp and imaging. Secondly, it is known that the ventral portion of the hippocampus is more susceptible to seizure-like events (Borck and Jefferys 99), so this could necessitate the use of horizontal, rather than sagittal, slice orientation, to give

access to the most ventral part. Finally, conventional submerged recording chambers do not support brain oscillations (Hajos and Mody 09). This can be overcome by using a novel recording chamber – the membrane chamber.

1.4 The membrane chamber

Conventional recording chambers for acute brain slices tend to fall into one of two categories: interface (Haas and Macdonald 99) or submerged (White et al 78).

Interface style chambers provide the advantage of having a greater availability of oxygen to the slice than that in submerged chambers (Hill and Greenfield 11). This is crucial for the modelling of brain oscillations, including HFA, where the slice has a high metabolic demand (Hajos et al 09). However, there are also several advantageous features which are unique to submerged chambers, including the use of water immersion objective lenses for high magnification imaging and for visually guided patch clamp (Hajos et al 09). Submerged chambers also permit higher flow rates, allowing for faster exchange of bath applied agents (Hill and Greenfield 11). For this work, in which both a realistic model of HFA and the capacity for visually guided patch clamp are required, neither conventional chamber is suitable.

The membrane chamber (Hill and Greenfield 11) is a modified submerged chamber, which aims to increase the supply of oxygen to the slice, whilst retaining the other experimental advantages of this style. In this recording chamber,

summarised in Figure 1.1, the slice rests on a semi-permeable membrane, which is mounted on a Perspex ring. ACSF flows in to the chamber at a high flow rate and first passes underneath the membrane and slice. The aCSF then passes, through an outlet at the opposite end of the chamber, into the larger recess above the membrane. Because this space is bigger, the aCSF passes over the slice at a slower speed than when it passed under the slice. This creates a Bernoulli effect, which has two advantages. Firstly, it creates mechanical stability by sucking the slice down on to the membrane. Secondly, it confers the property of 'active flow' where aCSF is sucked through the slice, thus permeating it with oxygen. Moreover, because the slice is suspended within the chamber, both surfaces are perfused with aCSF, further supporting physiological activity in the slice (Hajos and Mody 09). These properties, coupled with the fast flow rates that are supported (17 ml/min compared with ~4-6 ml/min in conventional submerged), confer greater availability of oxygen than conventional submerged chambers. As a result, the chamber can support consistent slice physiology (shown by recording evoked field potentials in CA1) for at least 16 hours (Hill and Greenfield 11).

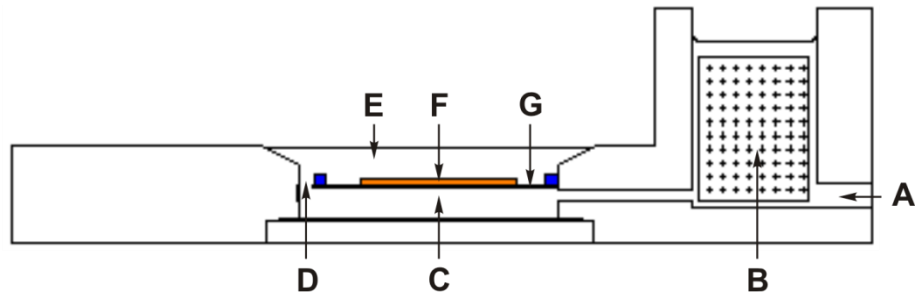


Figure 1.1 – Schematic diagram of the membrane chamber. *Perfusate flows into the chamber through the inlet (A) at high flow rate and the flow of the solution is smoothed by the buffer material (B). The perfusate flows quickly underneath the slice through the ‘infra-chamber’ (C) and through an outlet (D) into the ‘supra-chamber’ (E). Here, the solution flows, at a slower rate, back over the slice (F) which sits on a semi-permeable membrane (G). Solution then leaves the chamber via an outgoing perfusion line (not pictured).*

1.5 VGAT-Venus rats

VGAT-Venus is a strain of transgenic rat in which Venus, a yellow fluorescent protein (YFP), is co-expressed with the protein vesicular GABA transporter (VGAT) (Uematsu et al 08). Two strains, VGAT-Venus-A and VGAT-Venus-B, were generated in Wistar rats using bacterial artificial chromosome technology. In the hippocampus of VGAT-Venus A rats, Venus is expressed exclusively in non-pyramidal cells. In contrast, some CA1 pyramidal cells are also labelled in VGAT-Venus-B and thus the A strain is a more reliable marker for the study of hippocampal interneurons. Venus is around 20x brighter than conventional eGFP

markers, making it easier to detect using fluorescence microscopy. Whilst ordinary YFPs are sensitive to acidosis and Cl^- ions, mutations in the Venus protein confer resistance to these effects (Nagai et al 02). This could be crucial, as fast, synaptic inhibitory signalling in the hippocampus is mediated by chloride ions. Previous studies involving the visualisation of interneurons have used green fluorescent protein, under the control of the promoter for glutamate decarboxylase (GAD), in mice. Here, labelling was limited to a subset of interneurons and was not ubiquitous throughout the entire GABAergic population. For example, GIN mice (Oliva, Jr. et al 00) only express their fluorescent label in somatostatin expressing interneurons. Further, GAD67-GFP knock-in mice show reduced levels of GABA, owing to disruption of the GAD67 gene by the inserted genetic cassette (Tamamaki et al 03). As the Venus gene is much smaller than that for GAD67 (~5 kb compared with ~45 kb), there is less disruption to the intrinsic genome and so GABA levels remain at wildtype levels in VGAT-Venus rats (Uematsu et al 08), thus retaining the normal physiology of inhibitory signalling within neuronal circuits. Moreover, the use of rats is more compatible with previous *in vivo* studies (Csicsvari et al 99; Ylinen et al 95) and facilitates the use of the *in vivo* tetanus toxin model of temporal lobe epilepsy.

1.6 Aims and hypotheses

The first aim of this work was to establish a reliable, acute model of *in vitro* epilepsy in which simultaneous extracellular and fluorescently targeted interneuronal patch clamp recordings were possible. The hypothesis was that the membrane chamber would support epileptic-like pathophysiology, which was comparable to that seen in interface-style recordings, whilst also permitting Venus fluorescence imaging and patch-clamp recording.

With this achieved, the second aim was to use the chamber to characterise HFA elicited acutely by high potassium *in vitro*. Following this, the study aimed to determine the relationship, if any, between the firing of GABAergic interneurons and epileptic-like HFA in this model. The hypotheses were that the high potassium model would generate pathological-like HFA, and that interneuron firing would display a significant phase relationship with the field event.

Finally, with the role of interneurons in acutely induced HFA established, the study aimed to characterise pathological activity in the TeNT model using *ex vivo* tissue from chronically epileptic rats. It was hypothesised that the chronic model would exhibit fast ripple activity separately from ripple activity, comparable with the results from Bragin et al. (Bragin et al 99a; Bragin et al 04). The study then aimed to compare and contrast the phase relationships between interneurons and acutely induced field ripples, chronically induced field ripples and chronically induced fast ripples. The hypothesis was that interneurons would correlate with ripple events, but not with fast ripple activity.

2. METHODS

2.1 Breeding and maintenance of rat colony

All experimental procedures were carried out in accordance with the Animals (Scientific Procedures) Act 1986. VGAT-Venus transgenic rats (Uematsu et al 08) were generated by Drs. Y. Yanagawa, M. Hirabayashi and Y. Kawaguchi in National Institute for Physiological Sciences, Okazaki, Japan, using pCS2-Venus provided by Dr. A. Miyawaki. Founder rats were imported to the Biomedical Services Unit at the University of Birmingham. Rats were housed in pairs; food was available *ad libitum* and they were kept under a 12 hour light/dark cycle. Subsequent generations of rats were weaned at 3-4 weeks old, at which time they were genotyped using the polymerase chain reaction (see section 2.2). When required, new breeding pairs were selected from those animals which expressed the VGAT-Venus transgene.

2.2 Polymerase chain reaction (PCR)

Sample tissue was clipped from the ear of each rat at weaning. Tissue was digested overnight at 55 °C in 250 µl lysis buffer (100 mM Tris, 5 mM EDTA, 0.2% SDS, 200 mM NaCl) and 1 µl Proteinase K (Promega, Wisconsin, USA). Digested samples were centrifuged (Model 5415 C, Eppendorf UK Ltd., Stevenage, UK) for 5 minutes at approximately 14000 g at room temperature, to remove any hair and undigested tissue. 200 µl isopropanol (Thermo Fisher Scientific Inc.,

Loughborough, UK) was added to an equal volume of supernatant to precipitate the DNA. Samples were spun for a further 30 minutes at around 14000 g at room temperature. The supernatant was removed, taking care not to dislodge the precipitated DNA pellet. The pellet was washed with 100% ethanol, allowed to air dry at room temperature and then dissolved in 50 µl nucleotide –free PCR water (Promega) for five minutes at room temperature. DNA samples were kept at -20 °C for long term storage when necessary.

1 µl of dissolved DNA was added to 1 µl of each primer (primers held in 10 µM stock; Venus-F: 5'-ATGGTGAGCAAGGGCGAGGAGCTGT-3'; Venus-R: 5'-TTACTTGACAGCTCGTCCATGCCGA-3' (Uematsu et al 08); Sigma-Aldrich, Missouri, USA) , 10 µl GoTaq Hot Start Green Master Mix (Promega) and 7 µl PCR water (Promega) in a 0.2 ml PCR tube (Thermo Fisher Scientific Inc.). PCR was carried out in a DNA Engine Tetrad 2 (Bio-Rad, California, USA). The denaturing phase was 94 °C for 30 seconds, the annealing phase was 55 °C for 30 seconds and the extension phase was 72 °C for 30 seconds. This cycle was repeated 36 times before holding at 72 °C for 5 minutes. Previously confirmed negative and positive samples were used as controls for the PCR. Following PCR, 10 µl of each PCR reaction was electrophoresed for 60 minutes at 160 V using a 3% (w/v) agarose (Bioline Reagents Ltd, London, UK) gel in 1X Tris-Borate-EDTA (TBE) buffer (Thermo Fisher Scientific Inc.). 5 µl GeneRuler 100 bp DNA ladder (Thermo Fisher Scientific Inc.) was run alongside the samples. GelRed (VWR International Ltd., Lutterworth, UK) (0.5X, 1:60,000 dilution) was used to visualize DNA bands on a

Multigenius Bio Imaging System (Syngen, London, UK). Sample data is shown in Figure 2.1.

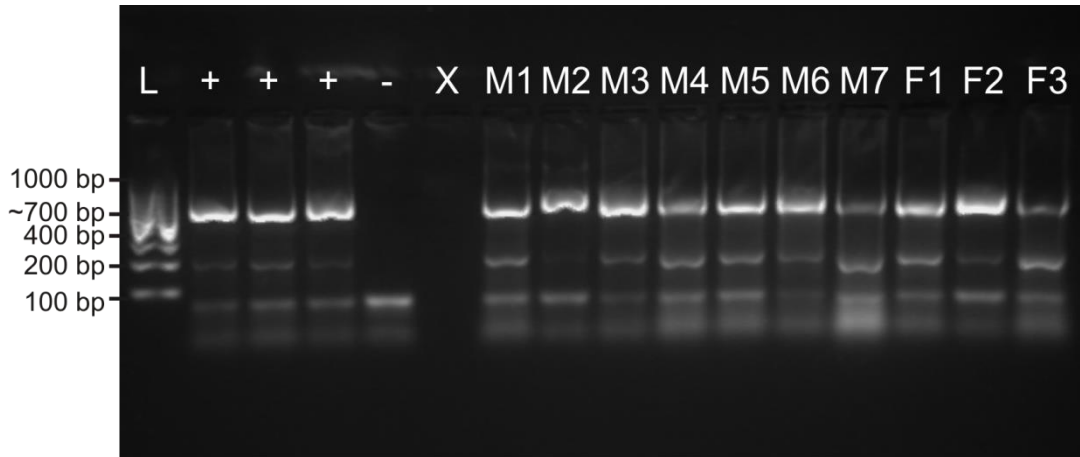


Figure 2.1 – Sample PCR Results. *Representative data for genotyping using PCR. (L) DNA ladder; (+) positive control; (-) negative control; (X) empty lane; (M1-7) males 1-7; (F1-3) females 1-3. The positive band for the VGAT-Venus transgene was seen at around 700 bp, though it was impossible to define accurately because the DNA ladder was blurred from 400-1000 bp.*

2.3 Slice preparation

Adult Venus rats were anaesthetised with a 0.24 mg/kg medetomidine and 58.2 mg/kg ketamine mixture, delivered using intraperitoneal injection. Anaesthetised rats were then perfused via cardiac puncture with ice cold oxygenated sucrose artificial cerebrospinal fluid (sucrose aCSF; 189 mM sucrose, 2.5 mM KCl, 26 mM NaHCO₃, 1.2 mM NaH₂PO₄·H₂O, 10 mM glucose, 5 mM MgCl₂, 0.1 mM CaCl₂) at a rate of 13.3 ml/min, controlled by a model 341A syringe pump (Sage Instruments, California, USA). Following perfusion, the skull was exposed and a cut made along the midline. The skull was peeled back to give access to the brain, which was quickly extracted into ice cold sucrose aCSF. Where horizontal slices were made, the brain was then turned upside down and glued using cyanoacrylate to the slicing stage of a 7000 smz Integraslice (Campden Instruments, Loughborough, UK). A cut was made through the midline of the brain using a single-edged razor blade, and excess tissue (cerebellum and frontal lobe) was removed using a razor blade and scalpel. For sagittal slice preparation, the brain was cut down the midline prior to gluing, and each hemisphere was mounted with the most medial part touching the stage. The brain was sliced into 300 or 400 micron slices where relevant. Horizontal slices were taken from a depth of approximately bregma -6.1 mm to -3.7 mm and sagittal slices from approximately 3.9 mm to 1.4 mm lateral to bregma. All slices were kept in a storage chamber on an interface between oxygenated aCSF (10 mM glucose, 125 mM NaCl, 3 mM KCl, 26 mM NaHCO₃, 1

mM MgCl₂, 1.25 mM NaH₂PO₄·H₂O and 2 mM CaCl₂) and air at room temperature (approximately 21 °C).

2.4 Data acquisition and experimental protocols

2.4.1 Refining a model of high frequency activity

Slices to be used for extracellular recordings were moved from the holding chamber to a Haas style recording chamber perfused with normal aCSF at 32 °C and left to equilibrate for one hour. After this time electrodes were placed. One directly-coupled (DC) electrode and one capacitive-coupled (or AC) electrode were placed in both the CA1 and CA3 regions of the hippocampus. Their positions were confirmed by recording the characteristic responses to stimulation of the Schaffer Collateral pathway (70 V for 0.1 ms, applied via a nickel/chromium wire (Advent Research Materials, Oxford, UK) using a DS2A stimulator (Digitimer, Welwyn Garden City, UK)). Electrode placement was guided using a Leica MZ 8 microscope (Leica, Wetzlar, Germany). DC recordings were made with glass electrodes (1-10 MΩ resistance), made from GC120F-10 borosilicate capillary tubes (Harvard Apparatus, MA, USA) in a P97 pipette puller (Sutter Instrument Co., California, USA). The electrodes were partially filled with normal aCSF and contained a silver chloride wire, connected to a HS-2A headstage (Molecular Devices, California, USA). The signal was amplified 10x using an Axoprobe-1A amplifier (Molecular Devices), then mains noise (usually on the level of several μV) was removed using

a HumBug (Quest Scientific, Vancouver, Canada) and the signal passed through a NL 106 NeuroLog AC-DC amplifier (Digitimer) at a further 10x amplification. AC recordings were made from 90% platinum/ 10% iridium wire (bare wire, \varnothing 0.025 mm, Advent Research Materials) connected to a NL 100 headstage (Digitimer), amplified at a gain of 500x by a NL 104 AC preamplifier (Digitimer) and band pass filtered at 2 Hz-2 kHz using NL 125 filters (Digitimer). Signal was then passed through a HumBug (Quest Scientific) to remove mains noise. All signals were digitised using a Power 1401 (Cambridge Electronic Design) and acquired at a sampling rate of 5 kHz using Spike 2 (Cambridge Electronic Design) software.

Following electrode placement, 5 minutes of baseline activity was recorded before the extracellular potassium concentration ($[K^+]_o$) was raised to 8 mM by application of potassium chloride (KCl) to the perfusing aCSF. If no seizure-like events (SLEs) were recorded within 30 minutes of KCl application, $[K^+]_o$ was further raised to 8.5 mM for 30 minutes and then, if necessary, 9 mM for 30 minutes. If this concentration did not elicit SLEs then the recording was ended and the slice discarded. Recording continued until at least 5 SLEs were acquired.

2.4.2 The role of interneurons in the high potassium (9mM) model of epilepsy

For submerged recordings made to target individual neurons, 300 μ m horizontal slices were made and stored as detailed earlier, with the exception that the holding chamber was covered with foil as a precaution to prevent photo-bleaching of the fluorescent Venus protein.

Submerged recordings were carried out using a membrane chamber (Scientific Systems Design, Ontario, Canada; Hill and Greenfield 11). A new membrane was made from SnakeSkin dialysis tubing (10,000 MWCO; Thermochemical, IL, USA) stretched over an MCR Perspex ring (Digitimer) and fitted at the start of each day of experiments. The chamber was perfused with normal aCSF at a flow rate of 13-14 ml/min and a temperature of 31-32 °C.

Slices were visualised using a BX51WI microscope or a standalone FV1000 confocal microscope (both Olympus UK Ltd., Southend on Sea, UK). Identification of hippocampal cell line and coarse electrode placement for extracellular recording was carried out using a 20x water immersion lens (Olympus UK Ltd.). Fine placement for patch clamp recordings used a 40x water immersion lens (Olympus UK Ltd.). BX51WI imaging used an Optoscan Monochromator (Cairn Research, Faversham, Kent, UK) and was acquired using an ExiAqua camera and Q capture software (Q imaging, BC, Canada). FV1000 imaging used the appropriate confocal laser and Olympus Fluoview (Olympus UK Ltd.). Venus fluorescence used 515 nm for excitation and 530-570 nm for emission.

Recording electrodes (resistance of 4-7 M Ω) were made from GC120F-10 borosilicate glass tubes (Harvard Apparatus, Kent, UK), pulled using a P-97 horizontal pipette puller (Sutter Instrument Company, California, USA) and filled with internal solution comprised of (in mM): 130 KMeSO₄, 8 NaCl, 10 HEPES, 2 Mg-ATP, 0.3 Na-GTP; pH 7.3 with KOH; osmolarity 280 mOsm) and 200 nM Alexa 647 hydrazide (Life Technologies, Paisley; visualised using excitation at 635 nm and

emission at 650-750 nm). Electrodes were connected via a silver chloride wire and a gold pin to a HS-2A headstage (gain = 0.1x; Molecular Devices, California, USA). Signal was amplified with a gain of 10x using an Axoprobe-1A amplifier (Molecular Devices). Both signals then passed through a NL 106 AC-DC Amplifier (Digitimer,) where the extracellular signal was amplified a further 100x and the patch clamp signal at 10x. Both signals were low pass filtered at 2 kHz using a NL 125 filter (Digitimer) and any remaining noise which was locked to the mains frequency (rarely occurring on the BX51WI set up and only occurring in the earlier FV1000 recordings) was removed using a HumBug . Signals were digitised using a Micro 1401 (Cambridge Electronic Design, Cambridge, UK) and recorded using Signal (version 3; Cambridge Electronic Design) at a sampling rate of 5 kHz.

Slices were allowed to equilibrate in the holding chamber for one hour after preparation, before transfer to the membrane chamber. The extracellular electrode was placed in the stratum pyramidale region of CA3b and the circulating potassium concentration was raised to 9 mM by adding KCl to the perfusate. The resulting epileptic-like activity was allowed to develop for 30 minutes, at which time a patch clamp recording was made from a visually identified interneuron. Once a sufficiently high quality (those where action potentials could be discerned using the designated thresholds) juxtacellular or whole cell recording was achieved, the extracellular and single-cell recordings were acquired for at least 10 minutes. This provided at least 100 sharp waves in order to give sufficient data for phase relationship analysis as described in section 2.5.6.

2.4.3 *The role of interneurons in the tetanus neurotoxin model*

Adult male VGAT-Venus A rats (20 control, 24 TeNT injected; weight range: 200-500 g) were anaesthetised initially with 5 % isoflurane in oxygen at a flow rate of 1 l/min and mounted in a stereotaxic frame (Stoelting, IL, USA). Anaesthesia was maintained with 1.5-2.5 % isoflurane as appropriate. Anaesthetic depth was monitored every 10-15 minutes using breathing rate and depth as well as absence of pedal reflex as markers. Rats were given 5 ml glucose/saline solution and 0.1 mg/kg buprenorphine, both subcutaneously, prior to beginning surgery. The skull was exposed using a midline incision in the scalp and a hole was drilled (230 VAC Drill, Microtorque II, Circuit Medic, USA) at 4.4 mm lateral to and 4.3 mm posterior to bregma. 1 μ l of either tetanus toxin (2.5 ng/ μ l in PBS; List Biological Laboratories Inc., California, USA) or bovine serum albumin (BSA; 2 % in PBS) was injected at a depth of 7.5 mm below the cortical surface, using the hole as a guide. Injections used a 1 μ l syringe (model no. 7001 KH, Hamilton Company, Nevada, USA), controlled by a microinjection pump (KDS 311CE, kd Scientific, RoYem Scientific Limited, UK) to give a rate of 0.2 μ l/min. The needle was left in place for five minutes following completion of the injection, in order to minimise backflow along the injection track. The wounds were then repaired and the rats were allowed to recover in separate cages for at least 24 hours. Each toxin injected rat was housed with either a BSA injected rat or an uninjected companion for video monitoring (Y-cam Solutions Ltd., Surrey, UK) over the following 3 weeks. Any seizures experienced by the animals were scored on a scale set out by Racine (Racine 72). The scale gives a measure of the severity of seizures based on their

motor manifestations as follows: 1) an absence of movement and purposeless chewing; 2) abnormal head bobbing; 3) disorganised clonic contractions of forelimbs; 4) postural rearing during seizures; 5) postural rearing and then falling during seizures. These rankings can be somewhat subjective and especially scales 1 and 2 are difficult to distinguish from each other in spontaneously seizing animals.

Rats were taken at 21 ± 3 days following surgery and 300 μm horizontal brain slices were prepared as detailed earlier. Slices which were closest to the likely injection site were used.

The protocol is identical to that detailed in 2.4.2 , with the exception that potassium concentration in the perfusing aCSF was raised to 5, 6 and 9 mM in turn, each for 30 minutes until HFA was elicited. For these experiments, the patch pipette internal solution also contained 0.2% w/v biocytin (Sigma, Dorset, UK). Experiments and analyses were performed blind to control or toxin injected experimental groups.

2.5 Data analysis

2.5.1 *Interictal periods*

In the case of discrete seizure-like events, the recording was subdivided into ictal and interictal periods. This was initially done by eye, with the start of the interictal period defined as the time point after which all discharges from the previous seizure had stopped. The transition from interictal to ictal period was defined as the point at which both amplitude and frequency of epileptic-like discharges rapidly increased (Figure 2.2). With the addition of DC recording electrodes, the ictal period was more accurately defined by its characteristic negative DC shift, likely caused by changing concentrations of extracellular potassium ions (Figure 2.2).

Where discrete seizure-like events were present, five successive cycles of interictal and ictal periods were selected for further analysis. The first cycle was excluded as it was part of the transition from normal to pathological state and so could differ from the steady-state epileptiform bursts which are the subject of this work. Ictal HFA was analysed by characterising HFA from the entire seizures following the selected interictal periods. Where the continuous bursting morphology was seen, HFA was characterised using ten minutes of the recording.

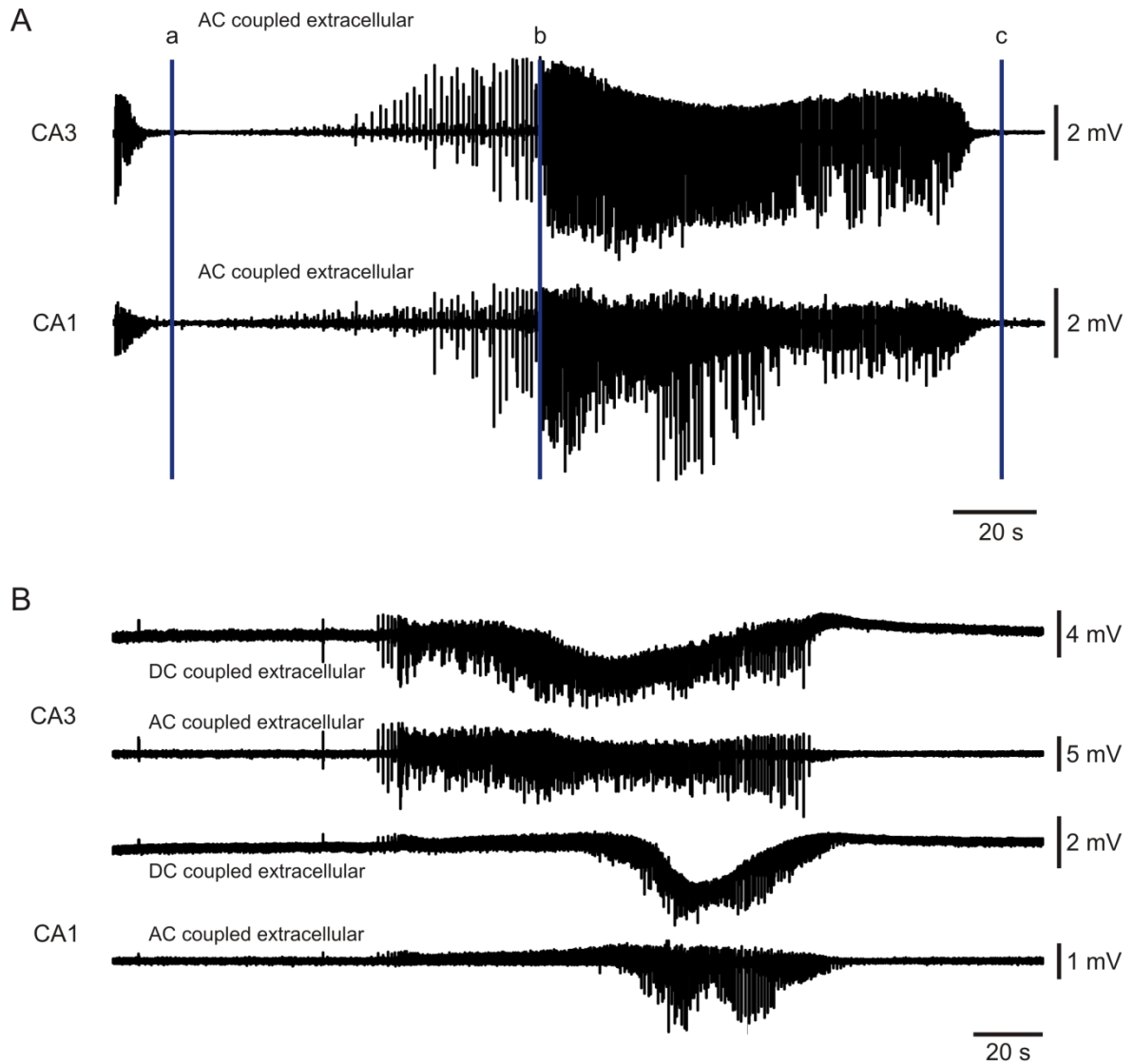


Figure 2.2 – Defining the interictal/ictal periods. (A) Raw traces representing one complete seizure-like event cycle. Cursors a-b show interictal period and b-c show ictal period, as defined by eye. (B) Paired DC (panels i and iii) and AC (panels ii and iv) coupled recordings, from a different slice to (A), to improve interictal period detection.

2.5.2 Power spectra

Raw signals were converted to the frequency domain using a fast Fourier transform (FFT size = 4096; Hanning window); the peak frequency of HFA was defined as the maximum peak on the power spectrum between 100 and 500 Hz, excluding any obvious artefacts such as harmonics of 50 Hz line noise. Ripple band power was measured as the summated power of all frequencies from 100–250 Hz and fast ripple band power was the total power between 250–500 Hz (Figure 2.3).

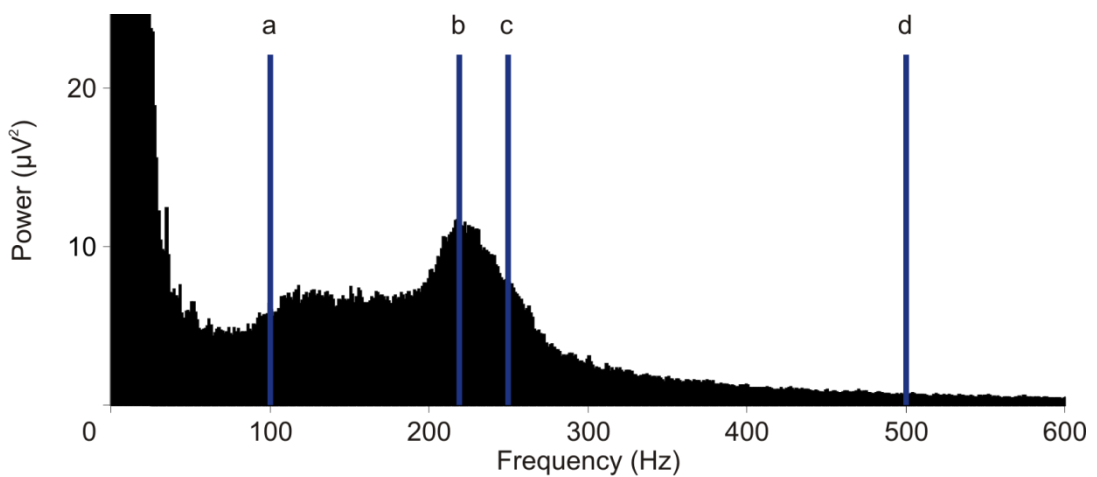


Figure 2.3 – Sample power spectrum. *Summated power from (a-c) gives ripple band power and from (c-d) gives fast ripple band power. (b) shows peak frequency.*

2.5.3 *Event detection*

For detection of HFA cycles, raw data were band pass filtered at 100-500 Hz (finite impulse response (FIR) filter; length: 679) using the built-in FIR filter feature in Spike 2. The standard deviation of the signal during an artefact-free quiet period of the filtered trace was measured and multiplied by seven to give a threshold for event detection. HFA events were defined as troughs greater than the threshold value on the filtered trace (Figure 2.4). The minimum time difference between detected events was set to 2 ms, to correspond to a maximum frequency of 500 Hz, as power spectra (see Figure 2.3) revealed that all recorded HFA was below this frequency. The same approach was used on a 25 Hz low-pass filtered extracellular trace for pathological sharp wave detection (Figure 2.4) and on the raw single-cell data for action potential detection (Figure 2.5). Following this automated detection, all events were confirmed visually.

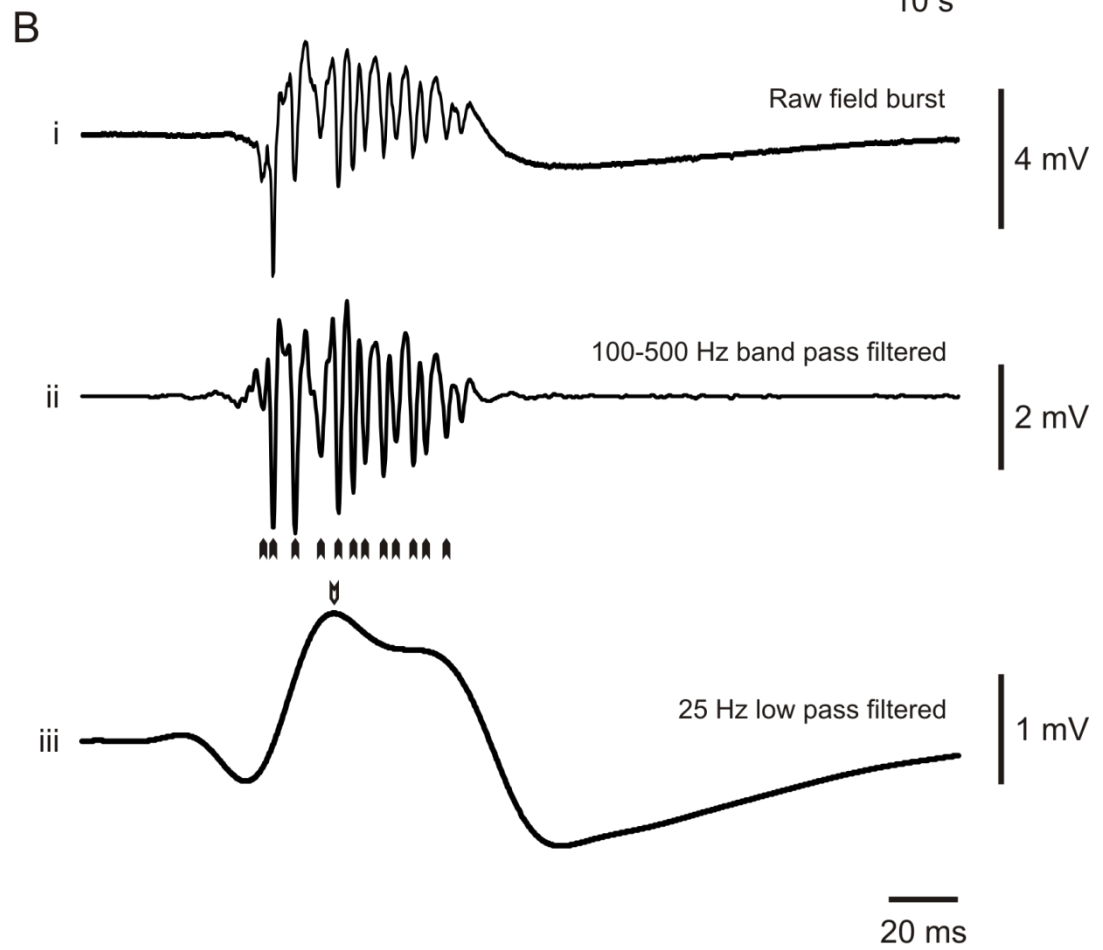
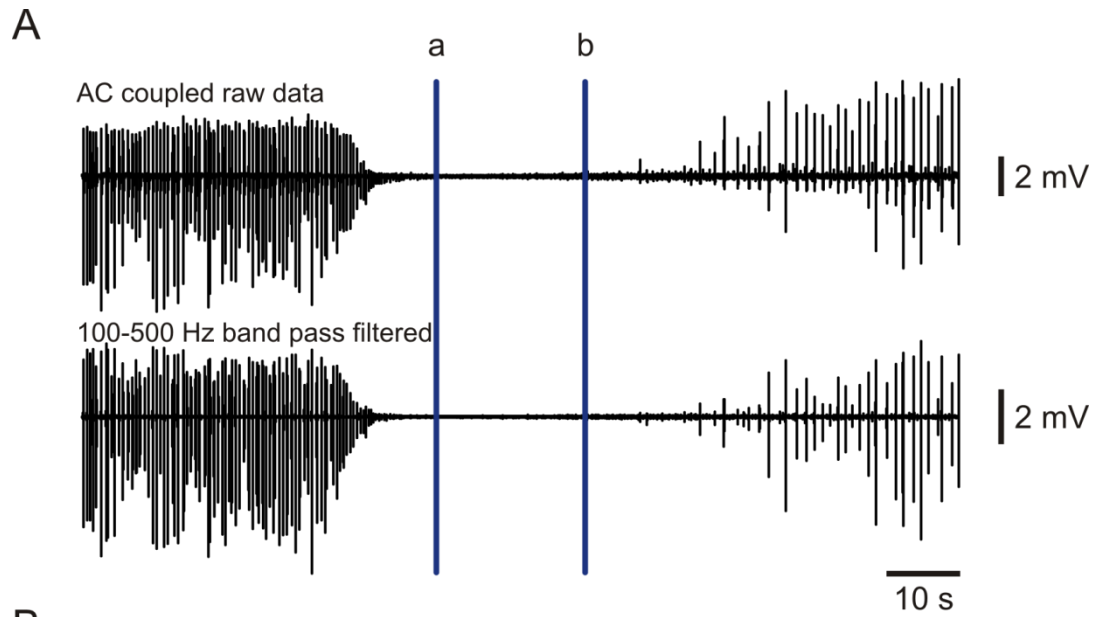


Figure 2.4 – HFA Event detection. (A) Raw (upper panel) and band pass filtered (100-500Hz, lower panel) data. a-b indicates the quiet period used for thresholding. (Bi) Raw high frequency oscillation. (Bii) Band pass filtered trace of (Bi), used for detection of HFA events (closed symbols). (Biii) Low pass filtered version of (Bi) for detection of pathological sharp waves (open symbol).

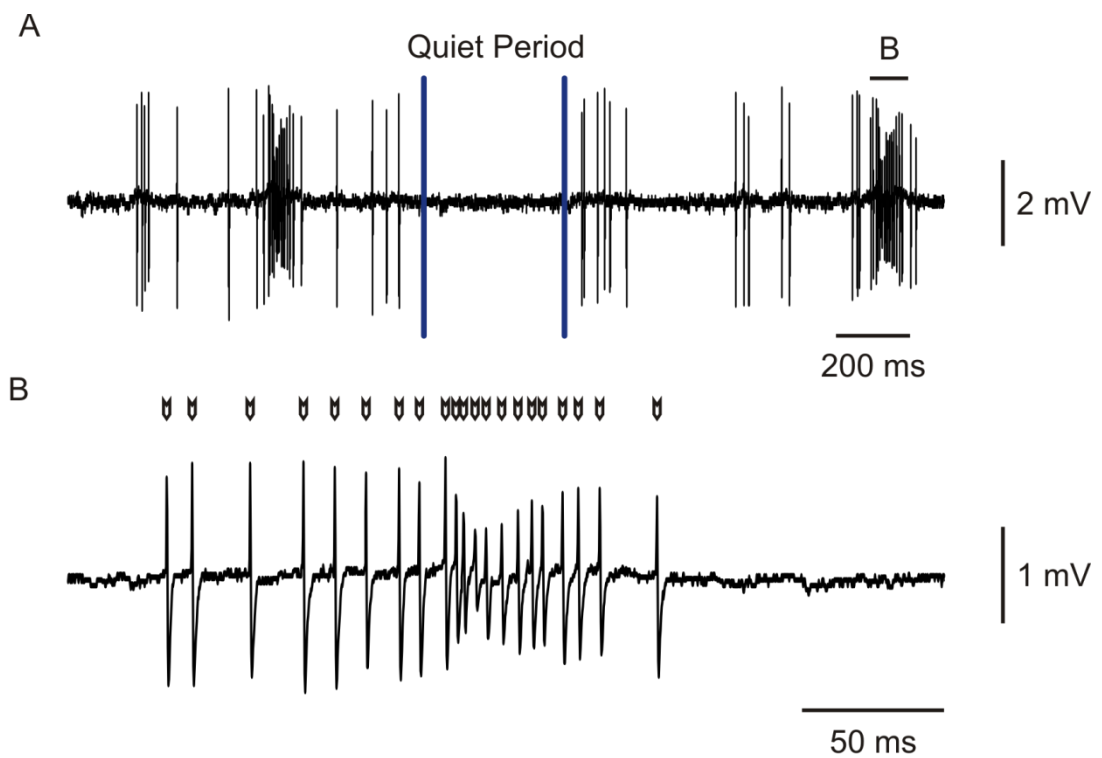


Figure 2.5 – Action potential detection. (A) Raw juxtacellular trace showing action potentials recorded from an interneuron. The cursors show the start and end of the quiet period used for thresholding. (B) Detected action potentials (open symbols) from an expanded time base of the highlighted portion of (A).

2.5.4 Average waveforms

Waveform averages were created for both raw and band pass filtered data using the detected HFA events as triggers. Generated waveforms were centred on the HFA and contained 25 ms preceding and 25 ms following the triggers. This trace allowed measurement of the average time length of one complete HFA cycle. The reciprocal of this time length gave a measure of average frequency.

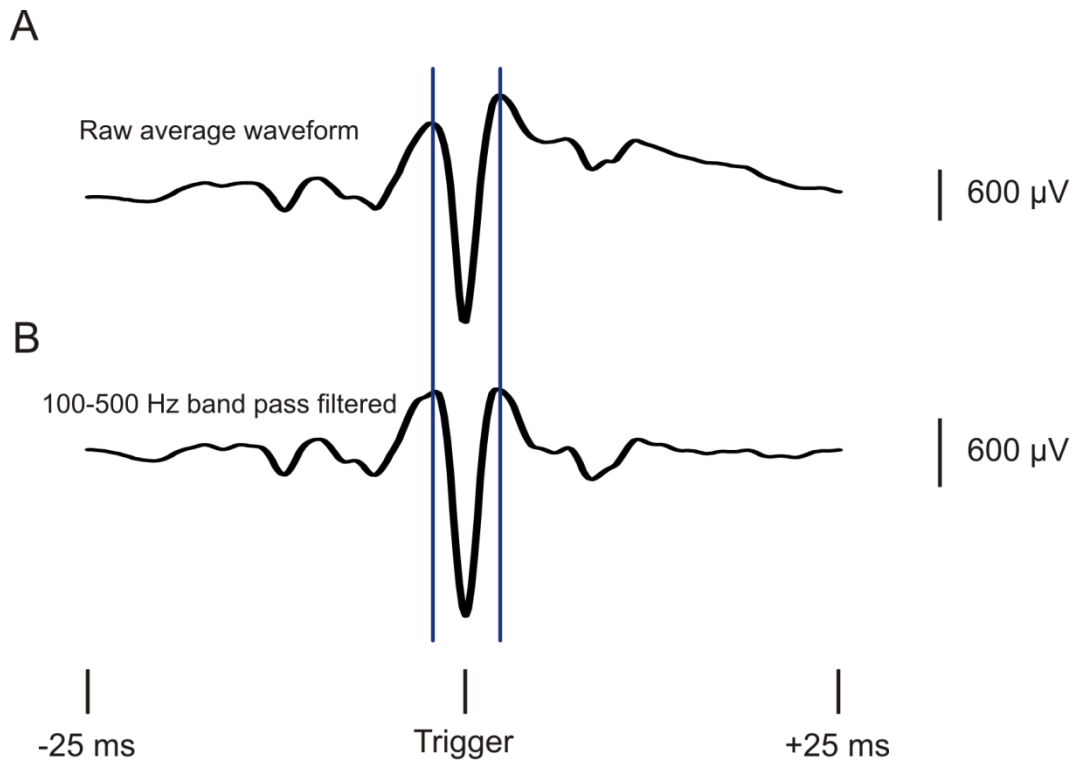


Figure 2.6 – Average waveforms for high frequency activity. (A) Raw average waveform 25 ms before and after an HFA event. (B) The same waveform, taken from a band pass filtered trace. The time difference measured between the two vertical cursors represents the length of one average HFA cycle.

2.5.5 Autocorrelation

Autocorrelation of detected HFA events was used to substantiate values for cycle length and frequency of the oscillations. The time difference between each HFA event and those occurring within 25ms of it was plotted onto a histogram (200 bins of 250 μ s, centred on 0 time difference) to build a profile of the periodicity of HFA cycles (Figure 2.7). The time difference from 0 to the first peak in either direction gave the time length of one cycle and the reciprocal of this was the frequency.

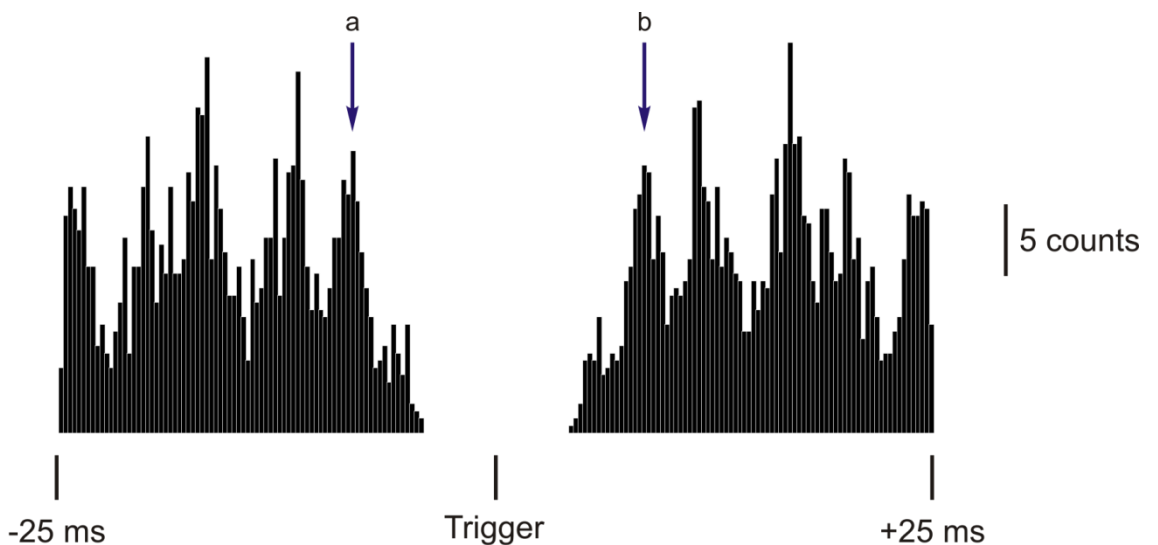


Figure 2.7 – Autocorrelation. Histograms (200 bins of 250 μ s) were created using event correlation in Spike 2. The artefact at 0 ms caused by events correlating to themselves is omitted. The time difference from trigger to the preceding (arrow a) and following (arrow b) peak represents the length of one HFA cycle. The reciprocal of this gives frequency.

2.5.6 Phase relationships using MatLab

Phase relationships were analysed using custom made scripts in MatLab (Mathworks, MA, USA). Detected event data for pathological sharp waves, HFA cycles and action potentials were imported from Spike 2. Phase relationships were calculated in two directions: one used HFA as the reference trigger and one used action potentials. To determine phase relationship, the time difference from each causative trigger to the next was considered to be a full 360° cycle. Cycles with a maximum time length of 10 ms (corresponding to 100 Hz) were considered. Where the other signal occurred within this time difference, their time lag from the initiating event was normalised as a fraction of the current full 360° cycle. This could then be expressed in degrees as a fraction of the full cycle. Only HFA and action potentials within 40 ms of pathological sharp waves were analysed. Phase differences were displayed in a rose plot. The distribution of phase difference was tested for significant difference from a uniform value using the Rayleigh test (Fisher 95; Babiloni et al 02). The x and y components of the mean vector, \bar{S} and \bar{C} , are obtained using the equations:

$$\bar{S} = \frac{1}{n} \sum_{i=1}^n \sin(\alpha_i) = \frac{1}{n} [\sin(\alpha_1) + \sin(\alpha_2) + \sin(\alpha_3) + \dots + \sin(\alpha_n)]$$

$$\bar{C} = \frac{1}{n} \sum_{i=1}^n \cos(\alpha_i) = \frac{1}{n} [\cos(\alpha_1) + \cos(\alpha_2) + \cos(\alpha_3) + \dots + \cos(\alpha_n)]$$

α_1 to α_n are all of the measured phase differences. The magnitude, R, of the mean vector is calculated by:

$$R = \sqrt{\bar{x}^2 + \bar{y}^2}$$

The Rayleigh test Z value is calculated by:

$$Z = nR^2$$

n is the number of recorded phase differences. The equation

$$p = \exp(-Z)$$

gives an adequate approximation of p, given that $n > 50$ (Fisher 95).

2.5.7 Cell visualisation

For the tetanus neurotoxin model experiments and for the latter part of the high potassium model experiments, the recording micropipette contained 0.2% w/v biocytin. Following whole cell recordings, the patch electrode was carefully removed and slices were left in the membrane chamber for ~10 minutes, in order to remove extracellular biocytin. Slices were then fixed in 4% paraformaldehyde in 0.1M phosphate buffer (PB) at pH 7.4 for 24 hours (at 4°C) before washing 3 times for 10 minutes in 0.1M PB. Washed slices were stored in 0.1M PB with 1:1000 thimerosal at 4°C.

Slices were washed for 1 hour in TBS/triton to permeabilise cells for biocytin entry and then incubated with avidin/biotinylated complex (ABC) peroxidase system (1:200 dilution; Vector Laboratories; Peterborough, UK) for 4 hours. Slices were then washed 3 times in TBS for 15 minutes each before being exposed to DAB-Ni solution (in mM: 10 PB, 2.5 NiNH₄SO₄, 6.9 NH₄Cl, 1.4 DABN) for 20 minutes. H₂O₂

was then added to begin the staining reaction, which was allowed to continue for 15 minutes. Slices were then washed twice in PBS for 10 minutes. Slices containing visualised cells were mounted on a coverslip and brightfield images were photographed at 10x using an FV1000 confocal microscope.

3. RESULTS – DESIGNING A PROTOCOL

This study required simultaneous extracellular and single-cell recording from visualised neurons in acute brain slices during an *in vitro* model of epilepsy. These techniques are individually technically challenging and, for reasons outlined in section 1.4, cannot be carried out simultaneously using conventional recording chambers. Therefore, the optimum brain slice parameters were investigated in an interface-style chamber and then a novel recording apparatus, the membrane chamber, was trialled.

3.1 Slice parameters

3.1.1 *Slice orientation – Horizontal vs Sagittal*

A previous study from this lab (Jiruska et al 10a) demonstrated that the high potassium model of epilepsy elicits field bursts which feature superimposed HFA. This work used 400 µm thick brain slices in the sagittal orientation, thus targeting the dorsal hippocampus. However, another study suggested that the ventral hippocampus is more prone to epileptic activity than the dorsal region (Borck and Jefferys 99). Therefore, it was necessary to compare the two slice orientations, in order to maximise the experimental yield.

For this comparison, 10 recordings were made for each orientation. In horizontal sections, 8 slices exhibited seizure-like events and 2 slices did not. In comparison, 1 sagittal slice exhibited seizure-like activity in the presence of 8-9 mM potassium,

while the remaining 9 did not (Figure 3.1). Therefore, horizontal slices were significantly more likely than sagittal sections to generate seizure-like events in response to high potassium (Fisher's exact test, $p < 0.01$).

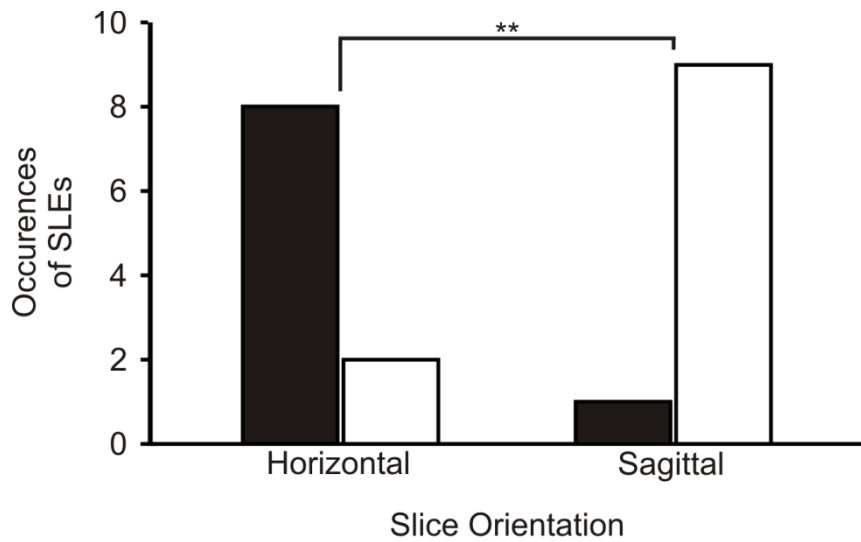


Figure 3.1 – Horizontal slices are more prone than sagittal slices to seizure-like events. Bars show the number of slices which generated seizure-like events (closed bars) and which did not (open bars) in response to high potassium.

3.1.2 Region of interest – CA3 vs CA1

Having established that horizontal slices were more likely to exhibit epileptic seizure-like events, the next step was to determine a specific region of interest within the hippocampus for this study. Thus, a comparison was made between the HFA generated in the CA1 and CA3 subregions, in horizontal slices, in order to find which featured more robust HFA.

For this experiment, the data from horizontal slices in 3.1.1 was supplemented with 30 more recordings, taking the total number of horizontal slices to 40. Of these slices, 11 generated HFA in both subregions under high potassium; 13 showed HFA only in CA3 and 0 showed HFA only in CA1. The remainder (16 out of 40 slices) did not generate HFA at all. These observations suggested that CA3 was more likely to generate HFA than CA1 and so would be the most appropriate region to study HFA.

For the 11 recordings in which HFA was seen in both subregions, direct comparisons were made between the two. Epileptiform bursts in CA3 were followed ~ 2 ms later by a burst in CA1, suggesting that CA3 was responsible for generating these events (Figure 3.2). In CA3, the power of recorded HFA was significantly higher than it was in CA1 ($34620 \pm 12753 \mu\text{V}^2$ compared with $1904 \pm 791 \mu\text{V}^2$; paired t -test, $p < 0.05$). This is illustrated in Figure 3.3. There was no significant difference in peak frequency of HFA between the two regions (166 ± 33 Hz in CA1 and 197 ± 22 Hz in CA3; paired t -test, $p > 0.05$). Therefore, CA3 was the better region to study because epileptiform bursts originated there and the superimposed HFA was more powerful.

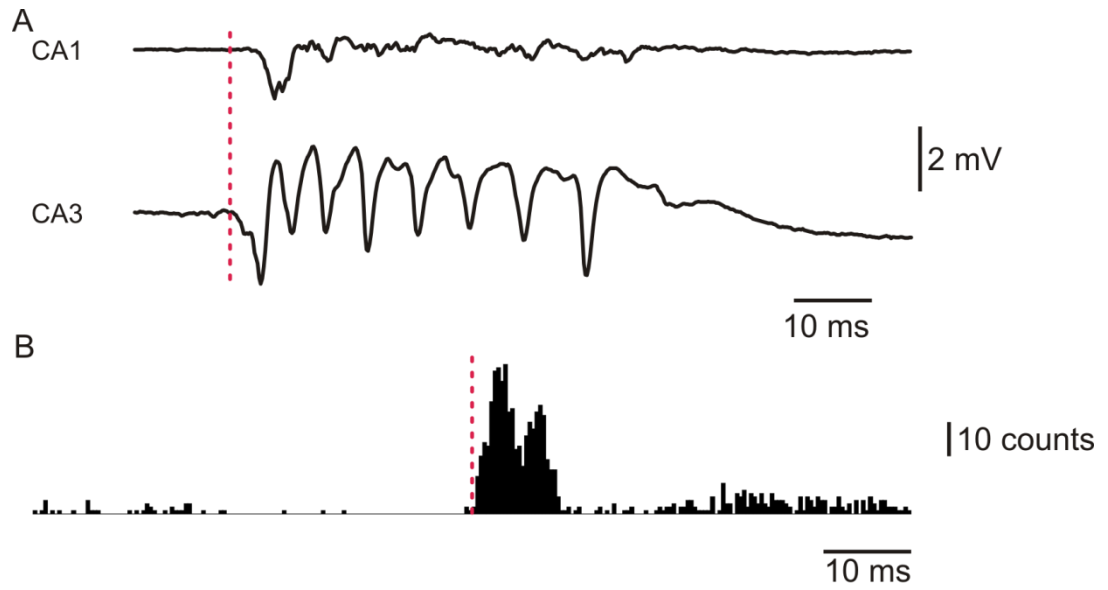


Figure 3.2 – Epileptiform bursts in CA3 precede those in CA1. Examination of raw traces (A) showed that burst onset (indicated by red dotted lines) occurred first in CA3. Event correlation (B) between epileptiform bursts in CA1 (black histogram) and CA3 (trigger event – red dotted line) showed that bursts occurred in CA1 ~2ms later than in CA3. Data taken from one representative slice recording.

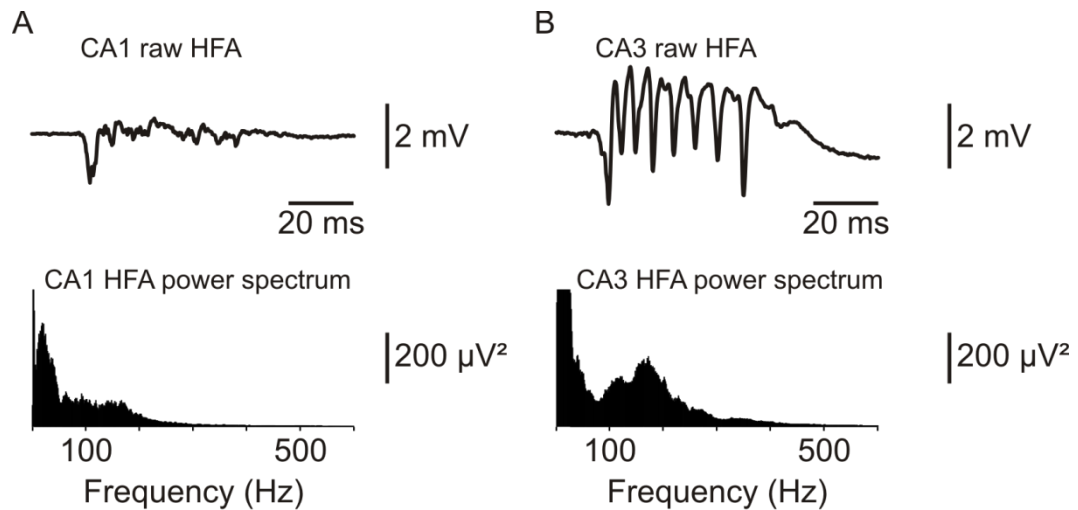


Figure 3.3 – HFA in CA3 has greater power than that in CA1. *Representative traces of HFA and corresponding power spectra in CA1 (A) and CA3 (B) taken from the same epileptiform burst in the same slice and presented on the same scales.*

3.1.3 Slice thickness – 300 μm vs 400 μm

The first two experiments showed that horizontal slices maximised the yield of experimental data and studying the CA3 region maximised the quality of elicited HFA. However, 400 μm slices were considered to be too thick to facilitate single-cell recording (Standen 94). Therefore, HFA in a sub-set of 300 μm slices ($n = 7$; data acquired and analysed by Dr. Andrew Powell) was compared with that in 400 μm thick sections in order to see whether it still provided a robust model for this study.

Peak HFA frequency remained comparable between the two thicknesses: 177 ± 11 Hz for 300 μm sections and 199 ± 12 Hz for 400 μm sections. This difference was

not significant (t -test, $p > 0.05$) and suggested that the two thicknesses produced qualitatively similar HFA. In contrast, there was a significant difference in power between the two thicknesses ($131 \pm 40 \mu\text{V}^2$ in 300 μm slices and $22111 \pm 6450 \mu\text{V}^2$ in 400 μm slices; t -test, $p < 0.01$). This was to be expected because the thinner slices had a smaller population of neurons within them and so generated less powerful oscillations. As they had been shown to have a similar frequency, this was taken as sufficient evidence to continue with 300 μm slices.

3.2 The membrane chamber

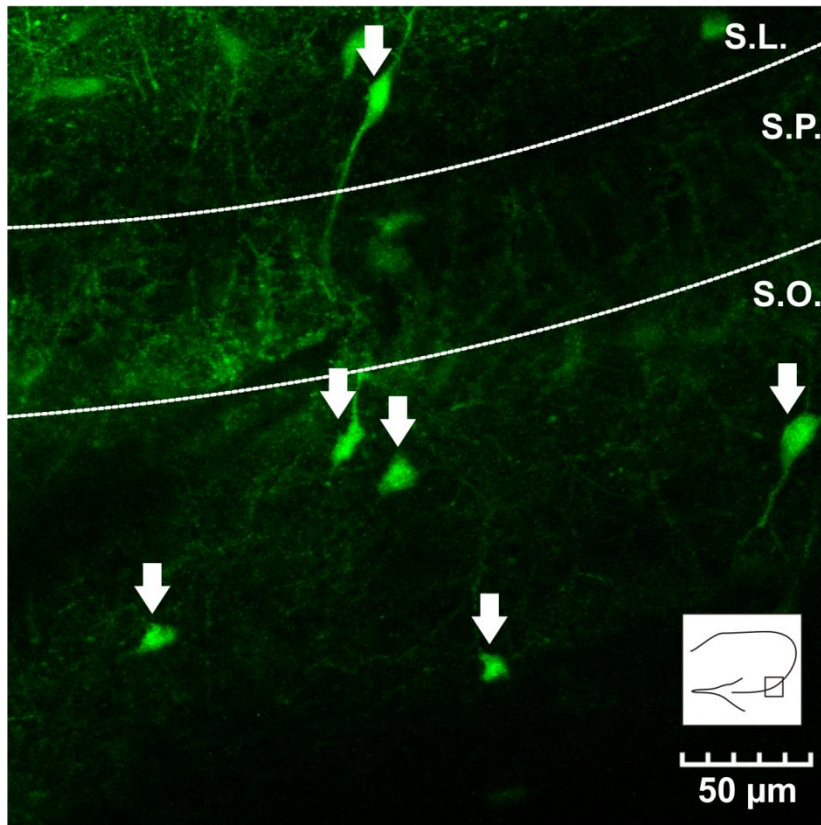
With optimal slice parameters established, the membrane chamber was then trialled to ascertain whether it could support fluorescence imaging, single-cell recording and *in vitro* epilepsy, as was necessary for this study.

3.2.1 Imaging

In order to permit the identification of interneurons in brain slices from VGAT-Venus A rats, the chamber needed to support visualisation of the fluorescent Venus marker.

Confocal fluorescence microscopy showed individual Venus-expressing interneurons (Figure 3.4). In most cases, the somata and any large projections, such as dendrites, were easily identified in this way. Finer projections, including axons, were difficult or impossible to discern from background fluorescence. Further, the axons of perisomatic-targeting interneurons caused dense perisomatic staining within the pyramidal layer, making them impossible to distinguish from each other.

A Confocal 40x Excitation: 515 nm Emission: 530-570 nm



B Confocal 40x Brightfield

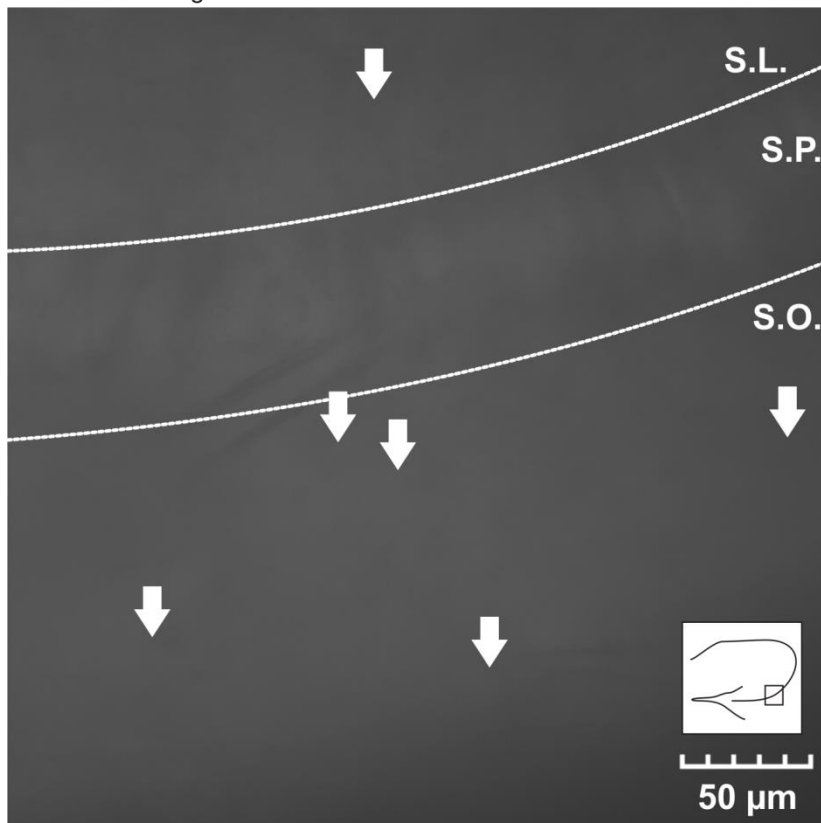


Figure 3.4 – Interneurons expressing VGAT-Venus can be visualised in the membrane chamber. *The CA3b region of a 300 μm thick horizontal brain slice from a VGAT Venus A rat (Uematsu et al 08) imaged using fluorescence (A) and bright field (B) microscopy. Interneurons (white arrows) were clearly identifiable by expression of Venus. White dotted lines denote rough boundaries in the laminar structure of the hippocampus. Insets show the rough location of the image within the hippocampus.*

3.2.2 Single-cell recording

Once interneurons had been successfully visualised, the next step was to obtain single-cell recordings from the fluorescing cells. This meant that the chamber needed to provide mechanical and slice stability as well as electrode access whilst the microscope's objective lens was in place (see Figure 3.5 for illustration).

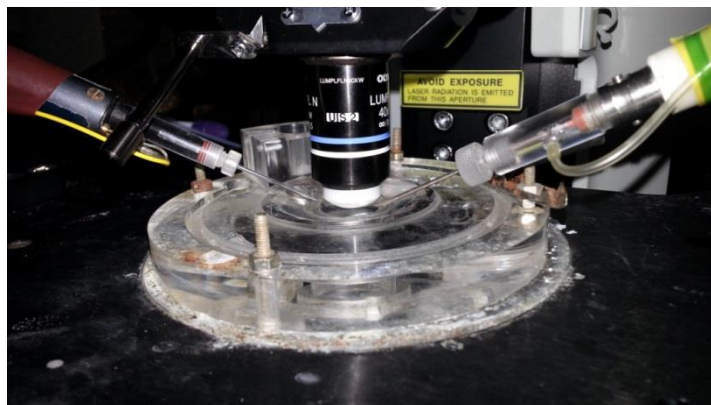
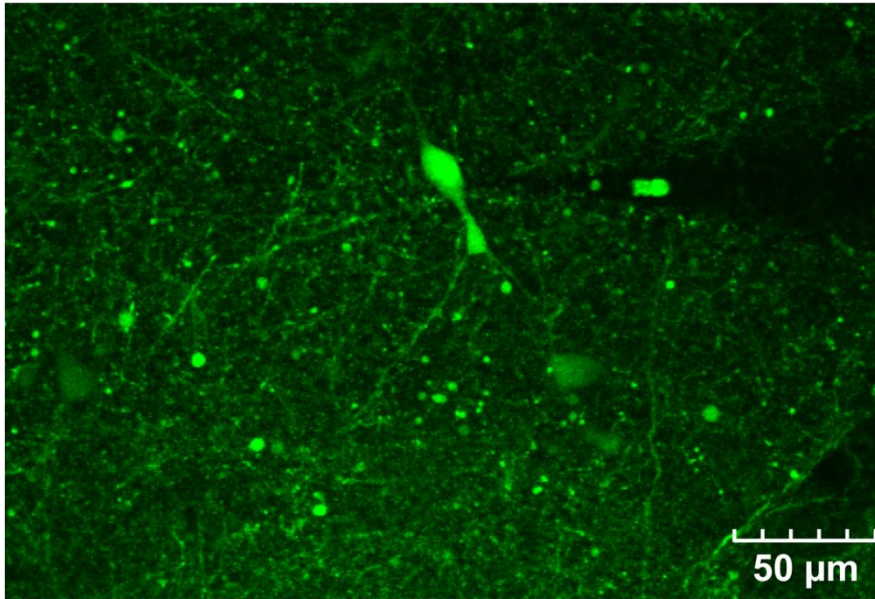


Figure 3.5 – Photograph illustrating the use of the membrane chamber. *The membrane chamber permitted access to the slice for multiple microelectrodes whilst using water-immersion objective lenses.*

Single-cell recordings were obtained in both juxtacellular and whole-cell configurations. Where whole cell patch clamp was obtained, cells could be filled with fluorescent tracers, such as Alexa 647. This enhanced the visualisation of interneurons by providing a difference wavelength of emitted light from the background Venus (Figure 3.6).

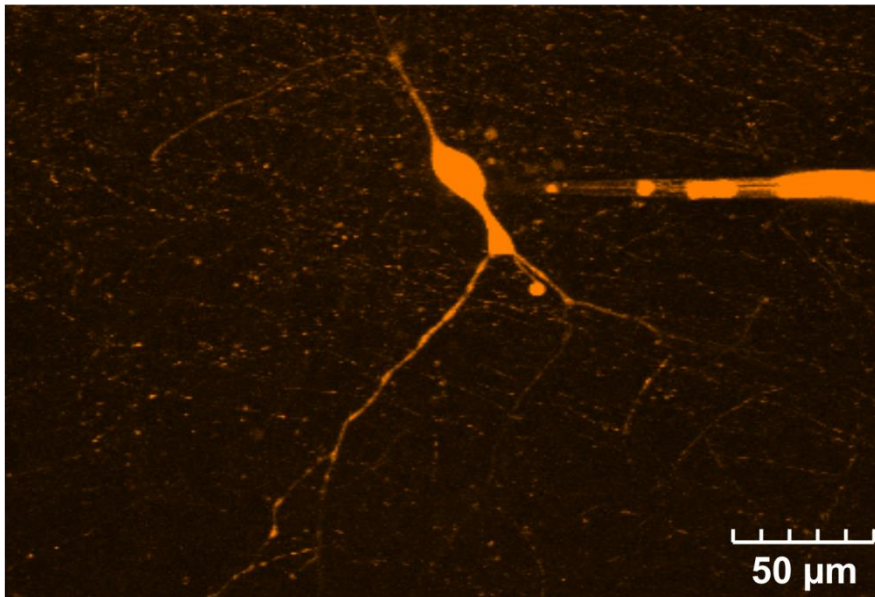
A

Confocal 40x Venus - Excitation: 515 nm Emission: 530-570 nm



B

Confocal 40x Alexa 647 - Excitation: 635 nm Emission: 650-750 nm



C

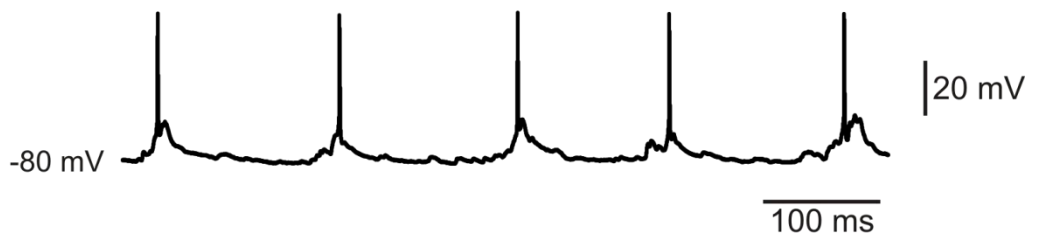
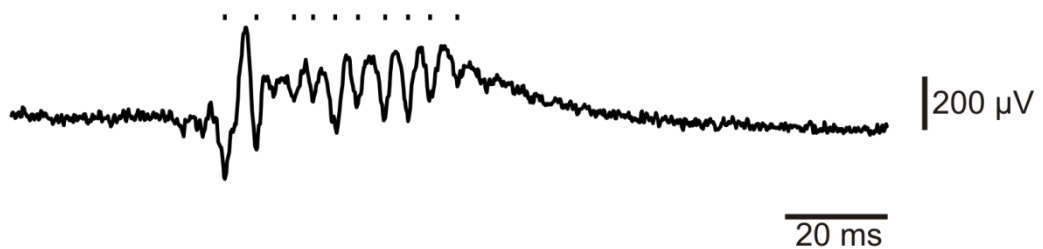


Figure 3.6 – Single-cell recording and imaging in the membrane chamber. An interneuron was identified using the VGAT-Venus fluorescent transgene (A). The cell was recorded in whole-cell patch clamp configuration and filled with Alexa 647 from the patch pipette (B). EPSPs and action potentials in the interneuron were recorded in current clamp (C).

3.2.3 High potassium recordings

As the chamber supported both imaging and single-cell recordings, it remained to demonstrate that epileptic-like activity, including HFA, could be observed in the membrane chamber. To show this, field recordings were made from the CA3 region in 300 μm thick horizontal slices (see 3.1) in the presence of 9 mM potassium.

A Raw extracellular HFA



B Raw juxtacellular action potentials

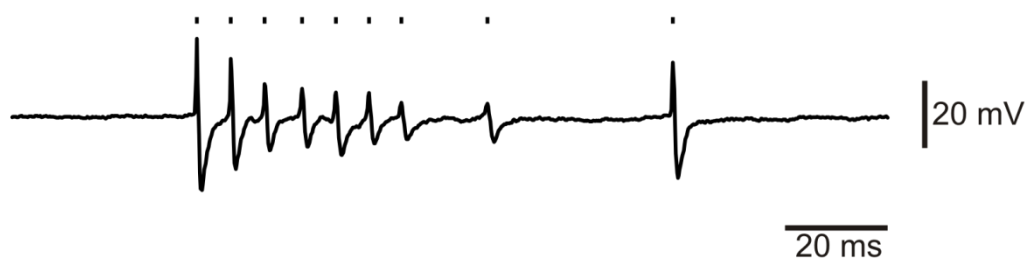


Figure 3.7 – Extracellular HFA can be recorded simultaneously with single-cell activity in 9 mM K⁺ in the membrane chamber. A sample extracellular trace (A) with HFA (denoted by tick marks) was obtained simultaneously with a juxtacellular recording from a targeted interneuron (B, tick marks denote action potentials).

4. RESULTS – THE HIGH POTASSIUM MODEL OF EPILEPSY

4.1 Characterising HFA induced by high potassium in the membrane chamber

4.1.1 *Epileptic-like activity is induced by high potassium*

The results presented in this chapter were taken from the 36 recordings where single-cell data of sufficient quality to distinguish action potentials was acquired simultaneously with robust extracellular HFA. Epileptic-like hyperactivity was induced by superfusion with 9 mM K^+ , using the protocol established in chapter 3. This activity followed one of two gross patterns (Figure 4.1). One pattern consisted of a continuous series of epileptiform bursts (n=34; Figure 4.1 A-C). In this case, each of the individual bursts had similar amplitude and patterns of superimposed high frequency activity. The second, less common, pattern displayed hyperactivity which was segregated into discrete seizure-like events, separated by quiet, interictal-like, periods (n=2; Figure 4.1 D-H). In this pattern, the seizure-like events had three distinct sections. The first, interictal-like, section contained positive field potentials of increasing amplitude, with little or no superimposed HFA. At the transition into the second, tonic ictal-like, state, the field bursts increased in both amplitude and frequency. At this point, HFA was

superimposed on the pathological sharp waves² and could be seen as a series of large negative field potentials occurring at a frequency of 100 Hz or above. In the final, clonic-ictal like state, pathological sharp waves decreased slightly in amplitude and frequency, but still had superimposed HFA. The characteristics of the induced fields are summarised in Table 4.1.

² Throughout this chapter and the next, 'pathological sharp waves' and 'sharp waves' will be used interchangeably and both refer to the slow component of an epileptiform burst.

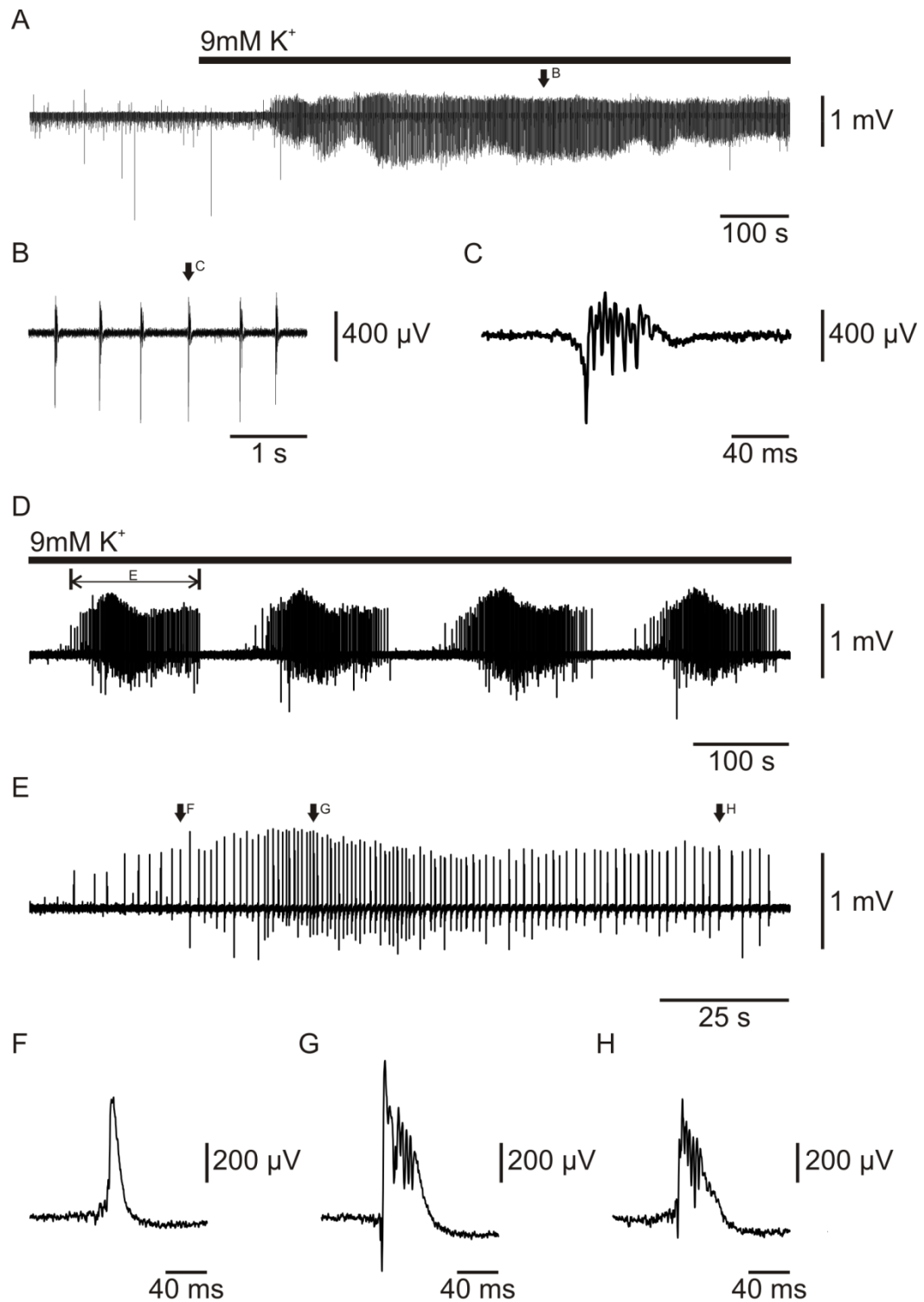


Figure 4.1 - High potassium induces epileptic-like activity, including HFA, in brain slices. *The induced activity followed either continuous (A) or discrete (D) patterns of hyperactivity. The continuous pattern consisted of a series of epileptiform bursts*

(B, magnified from A). HFA was superimposed on the pathological sharp waves (C, magnified from B). The discrete pattern consisted of individual seizure-like events (E, magnified from D), separated by quiet periods of relative inactivity. Each seizure-like event in the discrete pattern comprised interictal-like spikes (F), tonic ictal-like bursts (G) and clonic ictal-like bursts (H).

Time between field bursts	1.0 ± 0.03 s
HFA Peak Frequency	214 ± 5 Hz
HFA Power	564 ± 92 μV^2

Table 4.1 – Summary characteristics of continuous epileptic-like bursts induced by 9mM potassium. N = 34 slices.

4.1.2 High potassium induces HFA superimposed on pathological sharp waves

Examination of the raw extracellular data suggested that the HFA caused by high potassium was superimposed on pathological sharp wave field discharges. This was confirmed by average waveform analysis of the detected HFA events (Figure 4.2). The average HFA cycle occurred midway through the rising phase of a typical sharp wave event and was part of a longer oscillation which spanned the rising phase of the sharp wave. Event correlation of HFA events with reference to sharp waves (Figure 4.2 C) showed that HFA events were highly coincident with the

rising phase of the sharp wave, with a small number of events occurring shortly after this, as the excitatory wave diminished towards baseline.

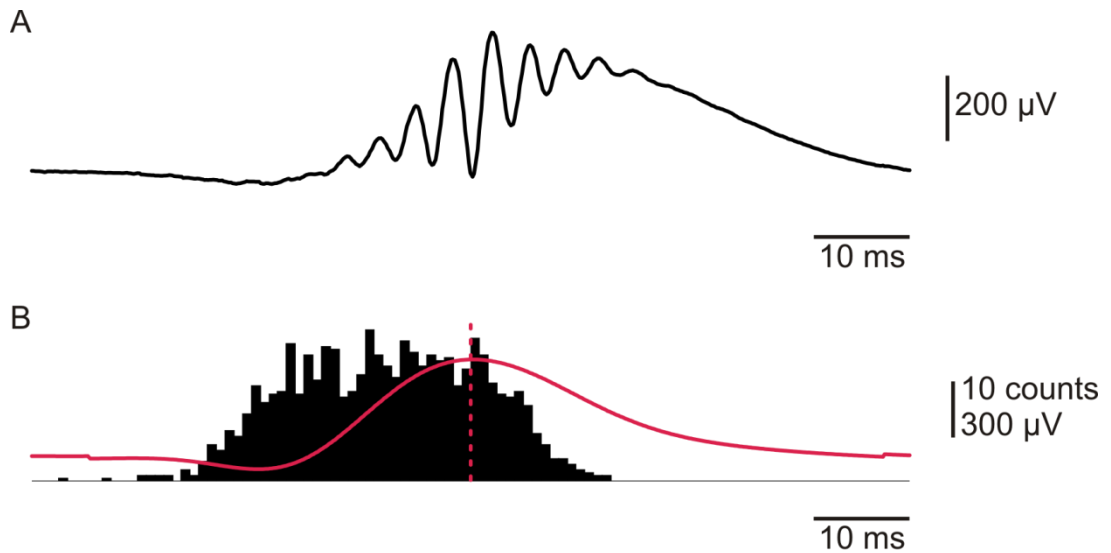


Figure 4.2 - High frequency activity occurs primarily on the rising phase of pathological sharp waves. Average waveform analysis (A) of 100 pathological sharp waves from one recording showed that HFA was typically superimposed on the rising phase of sharp wave events. Event relationships (B) between sharp waves (pink dotted line at zero point) and HFA events (black histogram) revealed no precise temporal relationship between the two.

4.1.3 The induced HFA spans both the ripple and fast ripple frequency bands

Fast Fourier transforms and average waveform analyses were used to determine the dominant (peak) frequency of each recording. Traces were then divided into ripple and fast ripple categories, according to conventional frequency cut-offs (100-250 Hz for ripples and 250-600 Hz for fast ripples (Jiruska et al 10a)). 34

recordings contained HFA in the ripple band (Figure 4.3) and the remaining 2 were in the fast ripple band (Figure 4.4). In each case, the HFA had a similar appearance on the raw trace – it was superimposed on the rising phase of sharp waves and appeared to contain a high frequency train of population spikes. The peak frequencies of all recordings were plotted in a histogram (Figure 4.5). This showed that the HFA frequencies followed a normal distribution (Kolmogorov-Smirnov test, $p > 0.05$) with a mean value of 214 ± 5 Hz. These results showed that, in the high potassium model, the classic frequency definitions of ripples and fast ripples are not valid. On the contrary, the normal distribution of the data suggested that the elicited HFA was actually one single phenomenon, ranging from 100-300 Hz, across both of the previously assumed HFA bands.

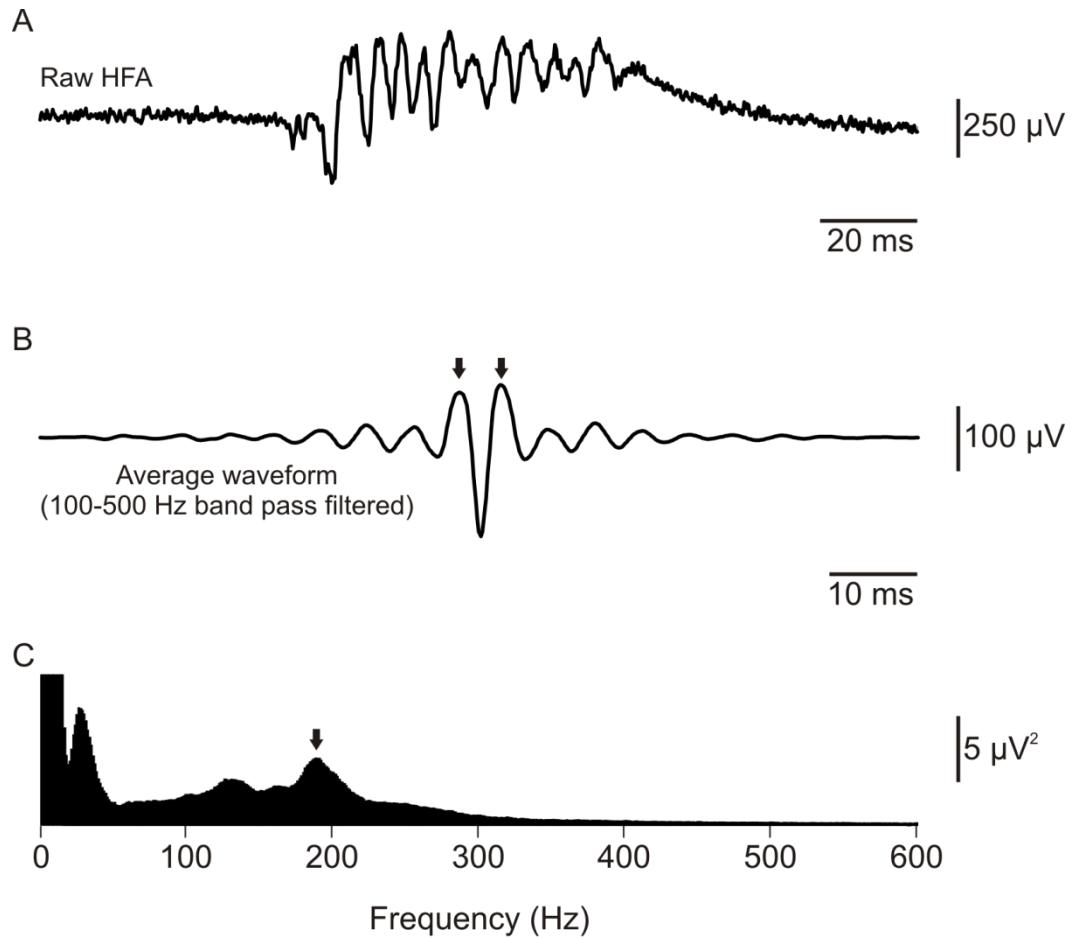


Figure 4.3 –‘Ripple band’ high frequency activity induced by high potassium.

High frequency activity in the ripple band was observed on raw extracellular recordings (A). The time difference from peak to peak of the average high frequency activity waveform (B; taken from a 100-500 Hz band pass filtered trace, see Figure 2.6) revealed a sub-250 Hz frequency. This was corroborated by fast Fourier analysis (C), which showed a peak frequency of ~ 190 Hz. The FFT peak at ~ 25 Hz reflects sharp wave activity.

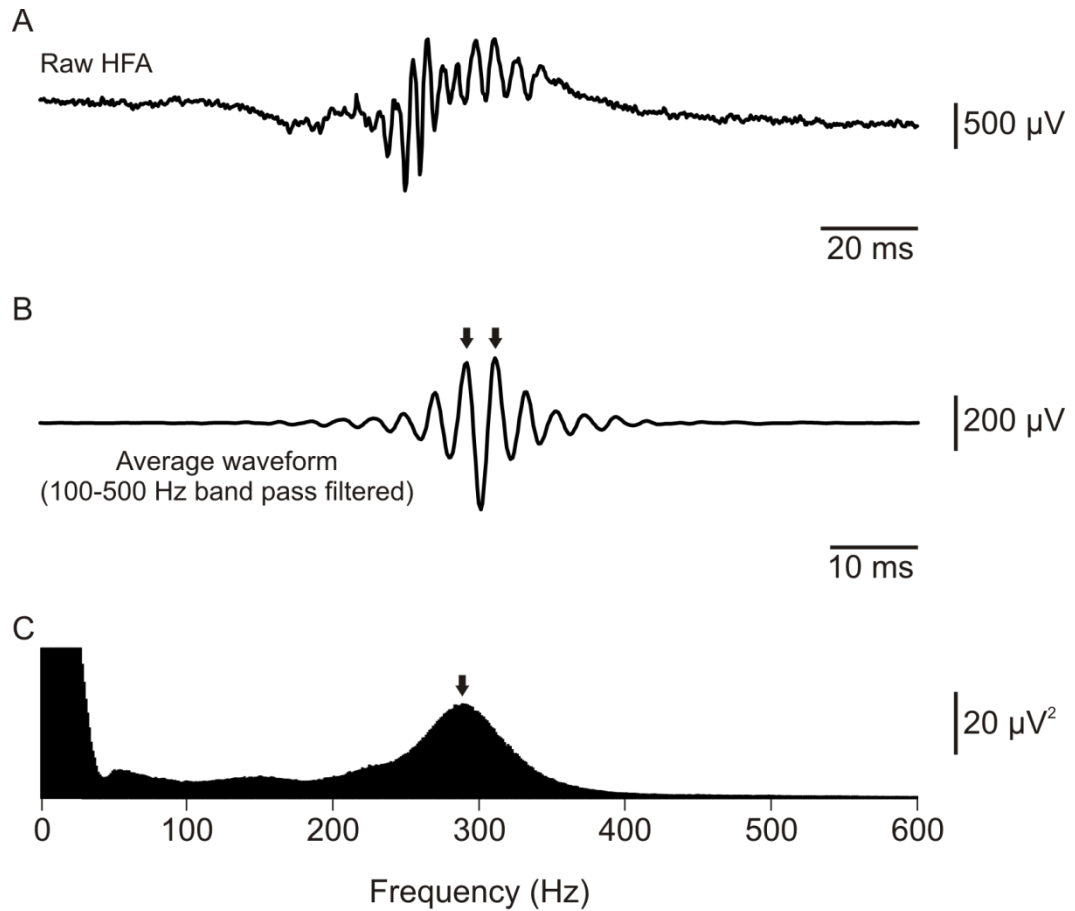


Figure 4.4 – ‘Fast ripple band’ activity induced by high potassium. *Raw extracellular traces could feature HFA in the fast ripple band (A). Peak to peak time difference of the average oscillation (B; see Figure 2.6) corresponded to activity faster than 250 Hz. This was in accordance with fast Fourier analysis (C), which revealed a peak frequency of ~290 Hz.*

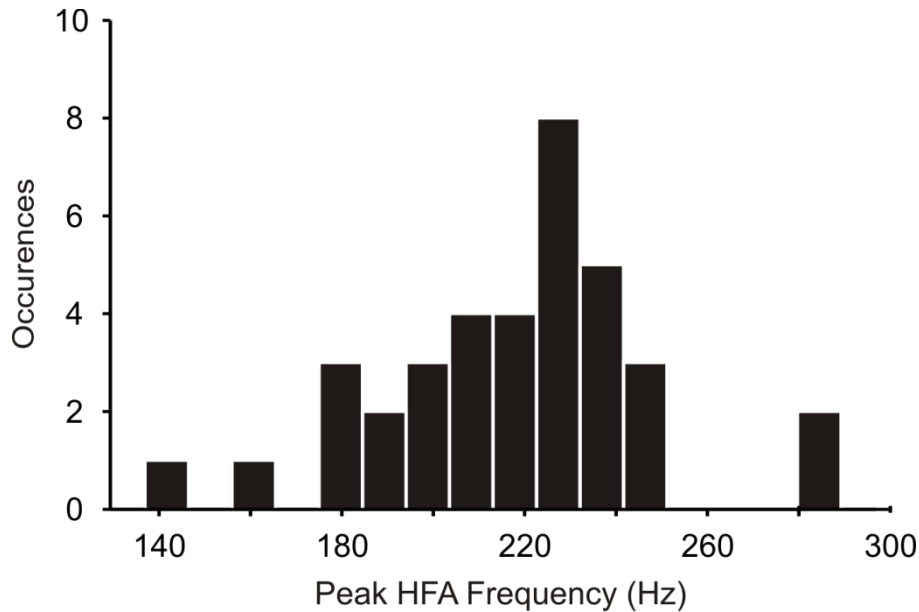


Figure 4.5 – The peak frequencies of induced HFA were normally distributed and spanned both the ripple and fast ripple bands. A histogram of the peak frequency from each of the analysed recordings showed a normal distribution ($n=36$, Kolmogorov-Smirnov test, $p>0.05$) spanning from ~ 140 to ~ 290 Hz. Bin size = 10 Hz.

4.2 Investigating the behaviour of interneurons during epileptiform bursts

Most interneurons fired action potentials both during and at different times to epileptiform bursts. Several changes in the behaviour of interneurons were seen during field bursts and may reflect the cells' involvement in this event, as well as in the superimposed HFA.

4.2.1 *Interneuron firing frequency is increased during pathological sharp waves*

One significant change was an increased firing frequency of interneurons during epileptiform bursts (Figure 4.6). Instantaneous frequency of recorded interneurons was significantly higher during these field bursts (155 ± 13 Hz) than it was in the quiet periods between extracellular discharges (52 ± 8 Hz; $n=34$ interneurons; paired Student's *t*-test, $p<0.001$). This change was seen in all interneurons which fired during sharp wave events ($n=36$). Of these, 2 interneurons did not fire action potentials at all outside of sharp wave events and so could not be included in the above comparison, as any increase in firing frequency could effectively be considered infinite.

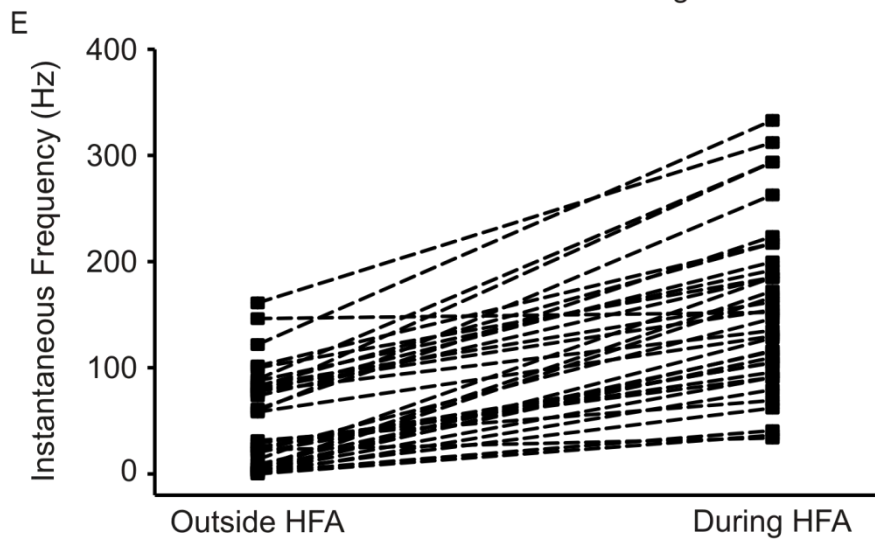
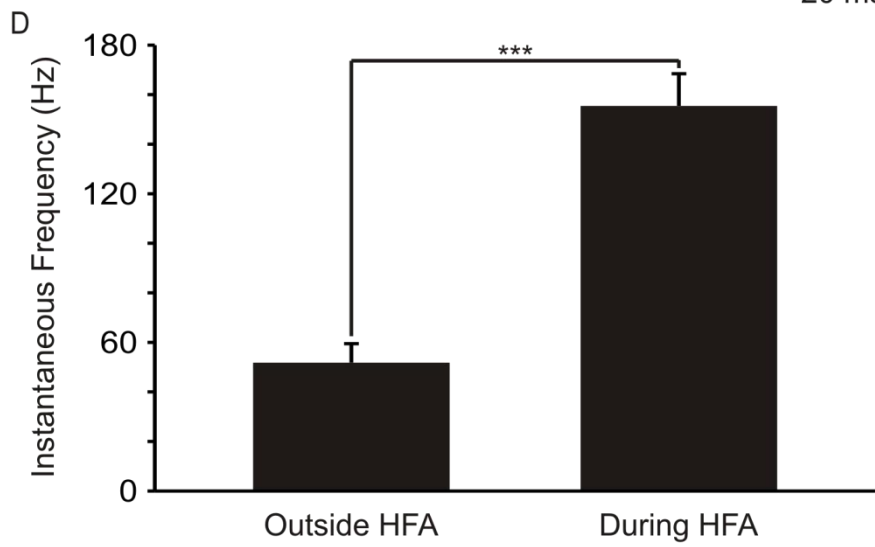
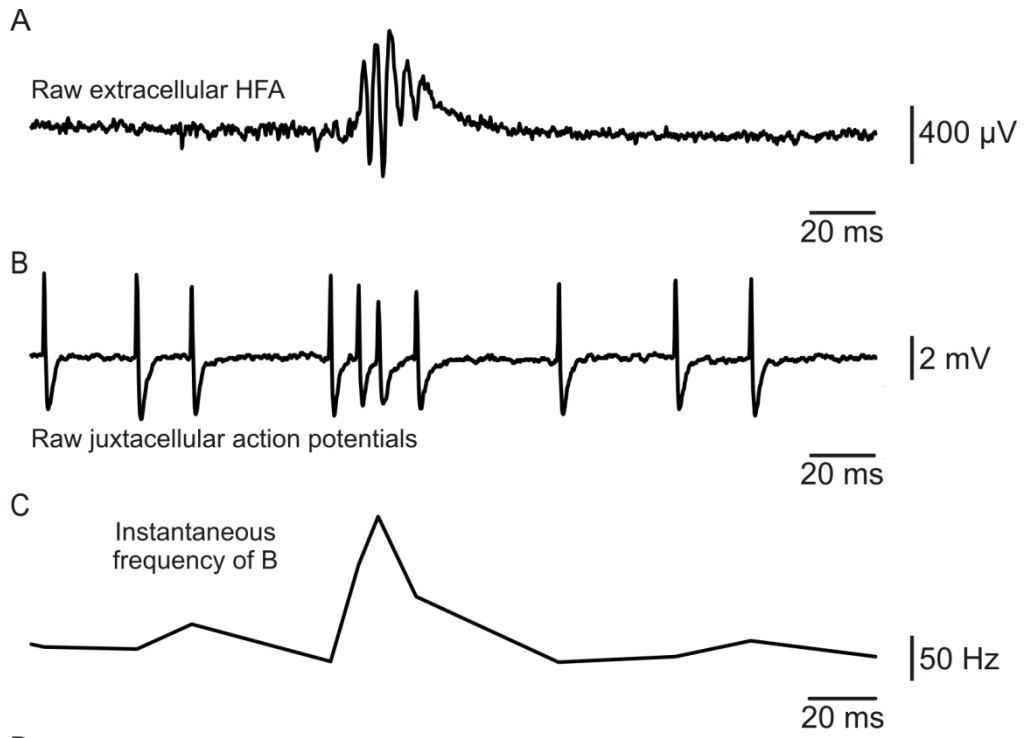


Figure 4.6 – Action potential firing frequency increases during epileptiform bursts. Comparison of the extracellular recording (A) with the single-cell recording from an interneuron (B) shows an increased firing frequency of the interneuron during the epileptiform burst. This can be visualised by plotting instantaneous firing frequency (C) of the cell. Mean data shows a significant difference between firing outside of and during epileptiform bursts (D; n=34 cells; paired student's t-test, $p < 0.001$). (E) shows frequency values for individual interneurons.

4.2.2 Interneuron action potential amplitude is decreased during HFA

Another change in the firing properties of interneurons in relation to epileptiform bursts was a decrease in action potential amplitude during the field discharge (Figure 4.7). All interneurons which fired during epileptiform bursts showed some reduction in amplitude (n=34). 2 interneurons did not fire action potentials outside of epileptiform bursts and so could not be included in this comparison as there was no baseline to compare with. Because some recordings were in whole cell and some in juxtacellular configurations, action potential amplitudes were normalised to their values outside of field discharges, so the reduction during bursts was expressed as a percentage of the initial value. During epileptiform bursts, interneuron action potential amplitude decreased to 54 ± 4 % of the baseline value recorded outside of epileptiform bursts (paired t-test, $p < 0.01$).

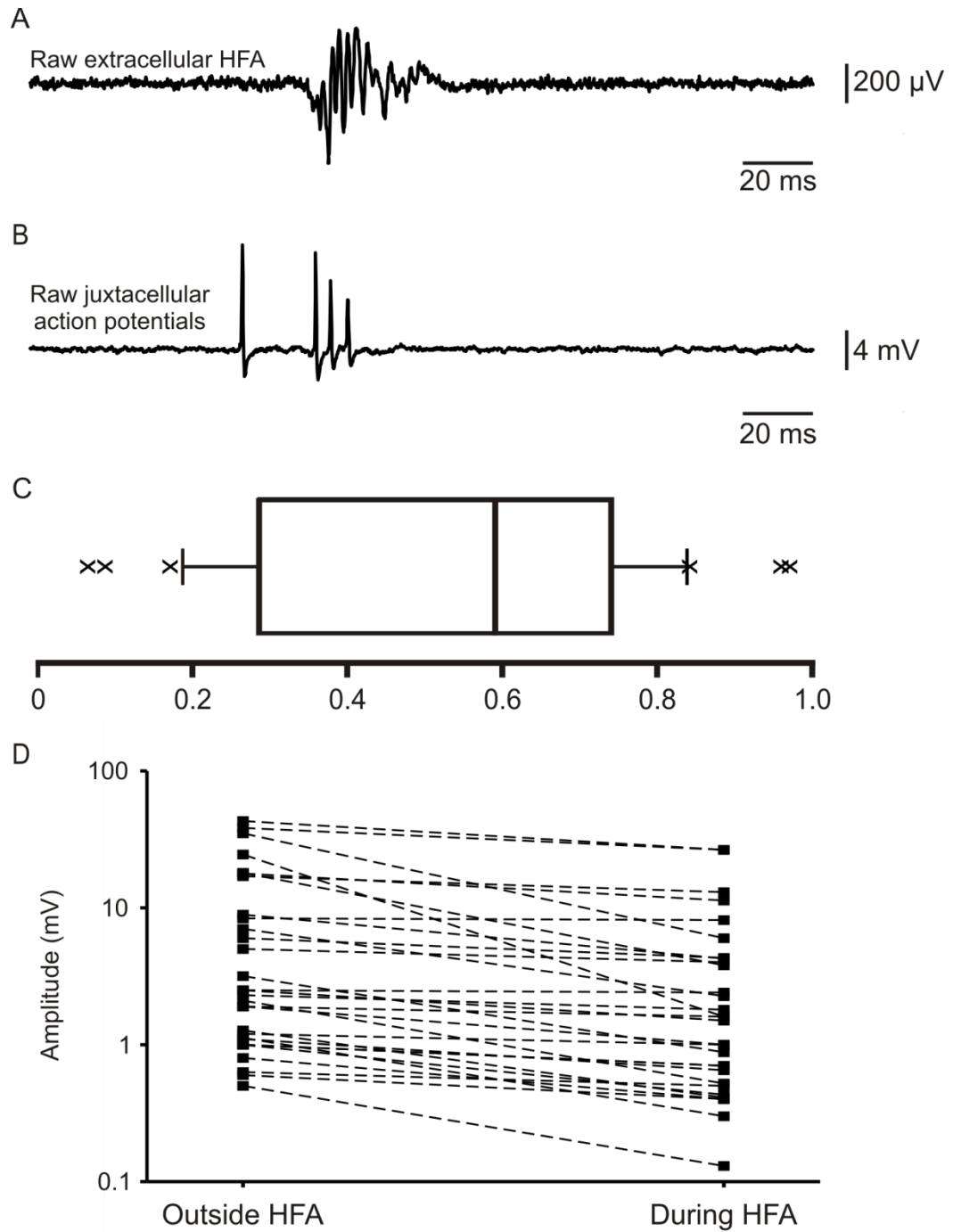


Figure 4.7 – The amplitude of action potentials recorded from interneurons decreased during epileptiform bursts. *Comparison of the raw extracellular trace (A) with the single-cell recording from an interneuron (B) showed a decrease in the*

amplitude of recorded action potentials during the epileptiform burst. Panel (C) shows a box and whisker plot of the normalised spike amplitude during field burst (n=33 cells). Panel (D) shows the paired values of action potential outside of and during field burst for all interneurons, plotted on a log scale.

4.2.3 Interneurons show a variety of firing patterns during HFA

Interneurons were first classified by their firing characteristics during epileptiform bursts. The cells were divided into four groups (Figure 4.8).

The first group (n=13) fired high frequency bursts of action potentials, of varying lengths, which overlapped temporally with the field discharge. Cells in this group fired bursts of at least three action potentials at a frequency in excess of 100 Hz. The high firing rate of these interneurons was compatible with pacing HFA and made them candidates to do so.

The second group (n=18) fired multiple action potentials during each field discharge. These action potentials were at a higher frequency than that occurring in the quiet background between field bursts, but still not at sufficient frequency to pace HFA.

The third group (n=1) contained an interneuron which fired one single action potential during each field discharge not at all between discharges.

The final group (n=4) contained cells in which action potential firing stopped for all or part of the epileptiform burst.

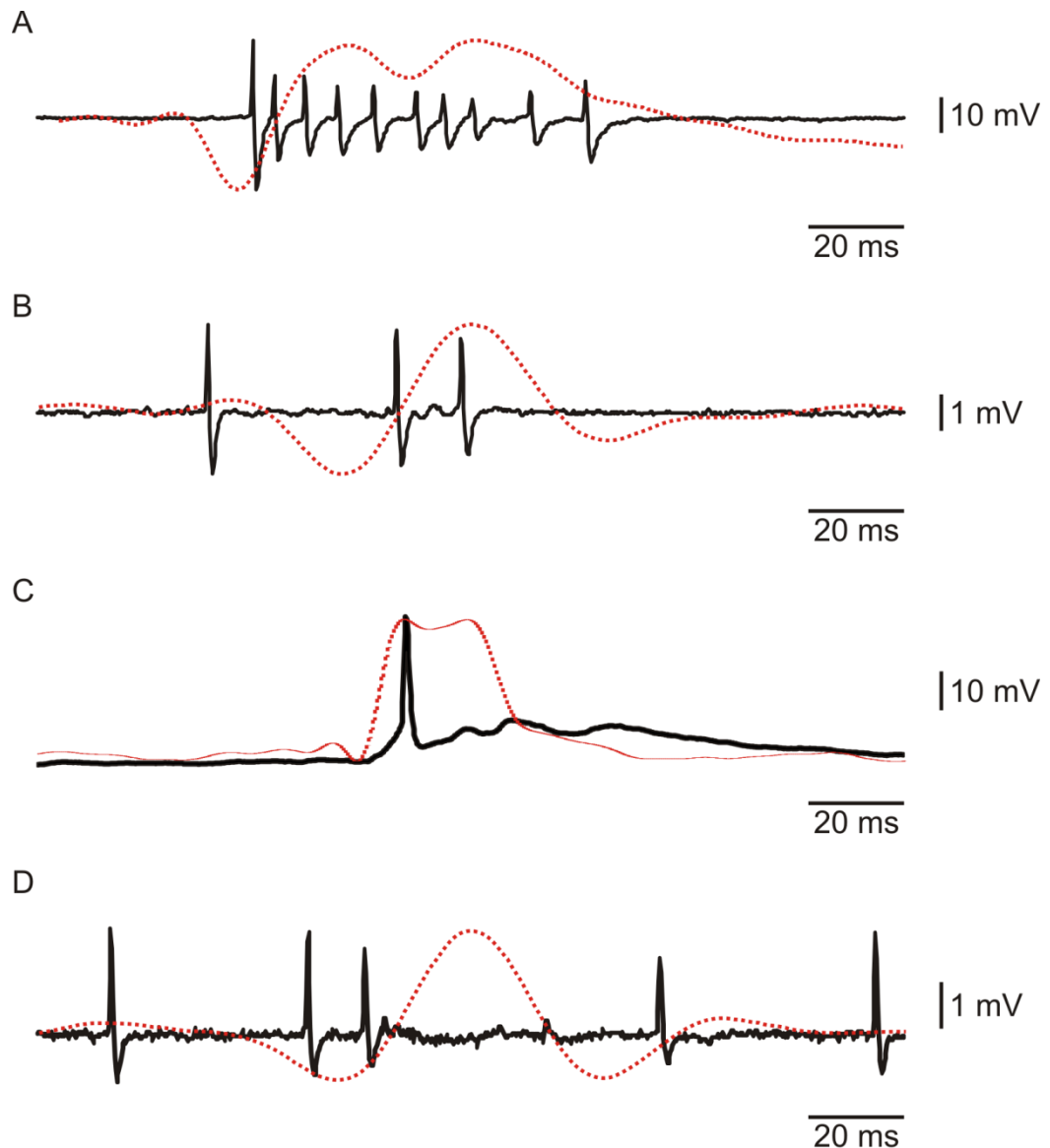


Figure 4.8 – Different firing patterns of interneurons during epileptiform bursts.

Each interneuron had a specific firing behaviour during epileptiform bursts, which was characterised into one of four groups: (A) – High frequency burst firing throughout the field activity; (B) – Firing multiple action potentials at lower frequency during field bursts and sporadically outside of field bursts; (C) – Firing single action potentials during field bursts and not at all outside of field bursts; (D) – Firing sporadically outside of field bursts and not at all during field bursts. In

each trace, the red dotted line indicates the timing of a typical sharp wave. The sharp wave amplitudes are normalised to action potential amplitude and are not representative.

4.3 Examining the relationship between interneuronal firing and HFA cycles

4.3.1 HFA cycles and action potentials both occur primarily during epileptiform bursts

As shown in Figure 4.2, high frequency activity cycles were most likely to occur superimposed on pathological sharp wave field discharges. Similarly, as shown in Figure 4.6, interneurons fired more action potentials during field discharges. At this stage, it remained unclear whether interneuron firing and HFA cycles were linked on a millisecond timescale, or simply both were caused independently by strong excitatory sharp waves. Thus, the next step was to characterise the relationship between field HFA cycles and interneuron action potential firing for each cell. HFA events were not subdivided into ripples and fast ripples because, as suggested by Figure 4.5, they were likely to be the same phenomenon, ranging from 100-300 Hz, in concordance with some estimates of the ripple band (Foffani et al 07).

4.3.2 Phase-domain correlations using HFA cycles as the trigger

Correlations between the two signals were calculated in the phase domain, in order to normalise the variable cycle length within some high frequency oscillations, using the method set out in section 2.5.6. 14 cells showed a significant relationship between field HFA cycles and interneuron action potentials, when using HFA cycles as the reference trigger. Therefore, in these cases, field events were a predictor for interneuron activity, suggesting a mechanistic link between the two. The remaining 22 cells did not show a correlation significantly different from a random distribution.

4.3.3 Phase-domain correlations using interneuron firing as the trigger

The same analysis was repeated using action potentials as the reference trigger, to begin to establish causality. In this case, the firing of 11 interneurons predicted HFA events significantly better than a random distribution. This included interneurons from firing pattern groups 1, 2 and 4 (see Figure 4.8) and from all tested layers of the hippocampus (Figure 4.11). Of these interneurons, 8 (represented in Figure 4.9) were also correlated in section 4.3.2, when the triggers were reversed. These findings hinted at a potential causative link between these 11 interneurons and the field HFA cycles. Further, the apparent cyclical relationship seen in 8 interneurons was consistent with the hypothesis that HFA arises from synaptic inhibition of pyramidal cells.

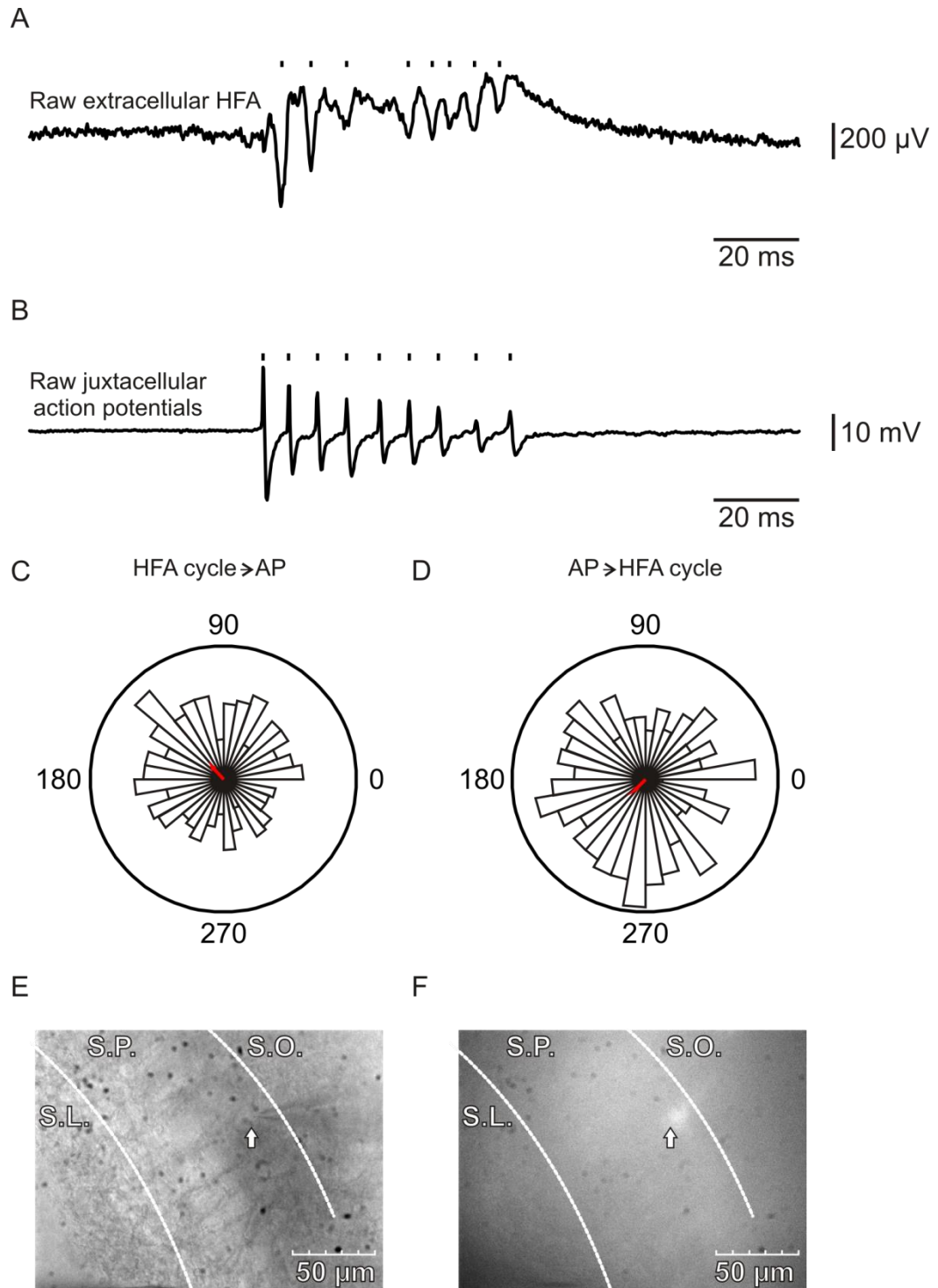


Figure 4.9 – A significantly correlated interneuron. Raw field data (A) containing HFA was correlated with action potentials recorded from an interneuron in juxtacellular configuration (B). In (A) and (B), tick marks denote detected events.

These events were processed to produce two rose plots: one using HFA as a reference trigger (C) and one with action potentials as a causative trigger (D). Both plots show a significant relationship (Rayleigh statistic, $p < 0.001$). The interneuron was in stratum pyramidale (E) and Venus fluorescence signal confirmed that it was an interneuron (F).

4.3.3.1 Interneuron firing was more likely to predict slower oscillations

When using action potentials as the causative trigger, field oscillations which correlated to the firing (197 ± 12 Hz; $n = 11$; Figure 4.10) were slower than oscillations which did not (221 ± 5 Hz, $n = 25$). This effect was statistically significant (Student's *t*-test, $p < 0.05$). This result hinted towards a modulatory role for interneurons in HFA, whereby their input lowers the frequency of existing oscillations.

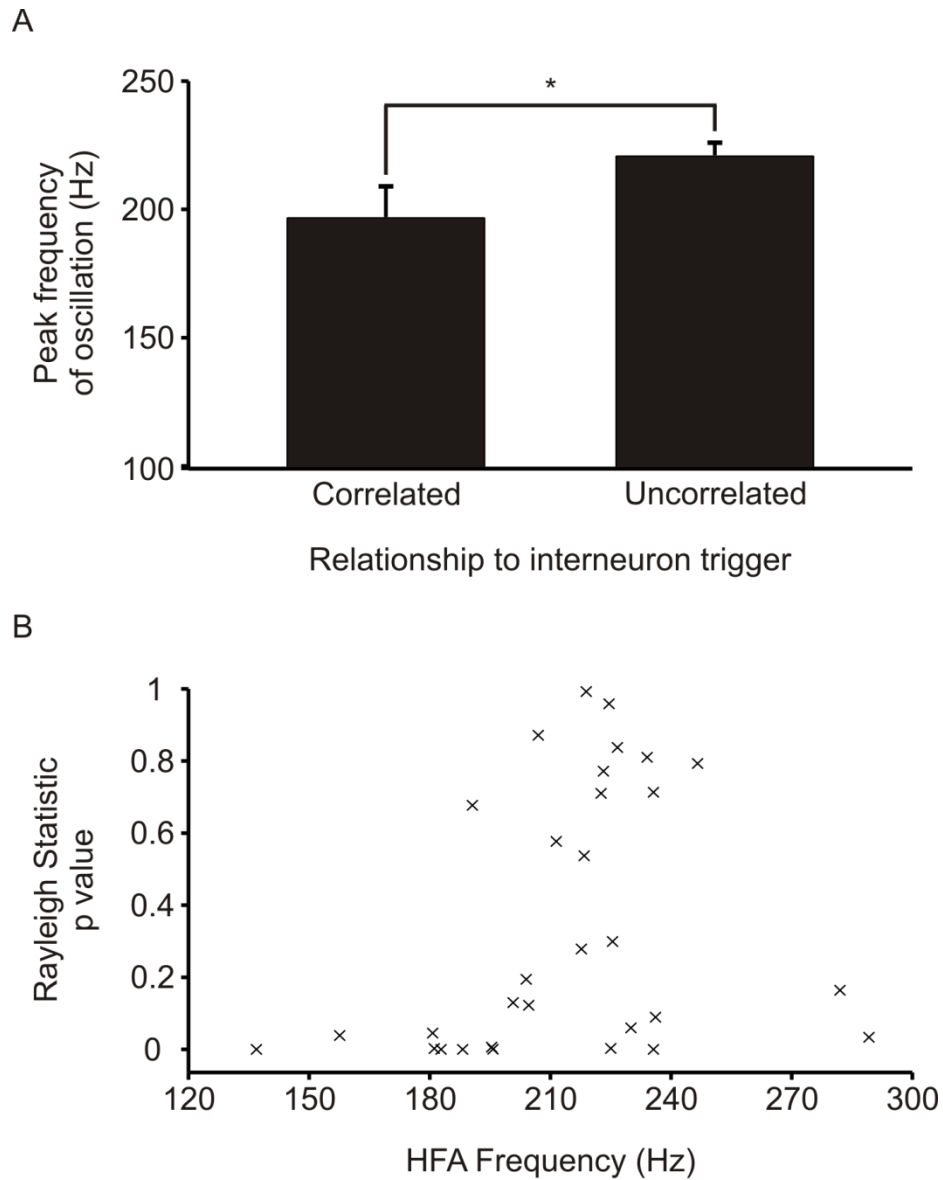


Figure 4.10 – Oscillations which correlated to interneuron firing were slower. (A) Bars show the mean frequency \pm S.E.M. of oscillations which were correlated and uncorrelated with interneuron firing, according to Rayleigh statistics – a measure of significant phase relationships between two signals. Student’s t-test, $*=p<0.05$. (B) Scatterplot showing the Rayleigh statistic p value, when using interneuron firing as the causative trigger, plotted against the frequency of the field oscillation.

Each symbol represents one experiment (n = 29 slices where Rayleigh analysis in this direction could be performed).

4.3.4 Laminar distribution of correlated interneurons

Interneurons which were correlated using both triggers for causality were found in all tested layers of the hippocampus (Figure 4.11). Interneurons which correlated when using only one trigger and those which were entirely uncorrelated were also found throughout the layers. Therefore the role of interneurons in HFA was not layer specific. The properties of the significant phase relationships are summarised in Table 4.2.

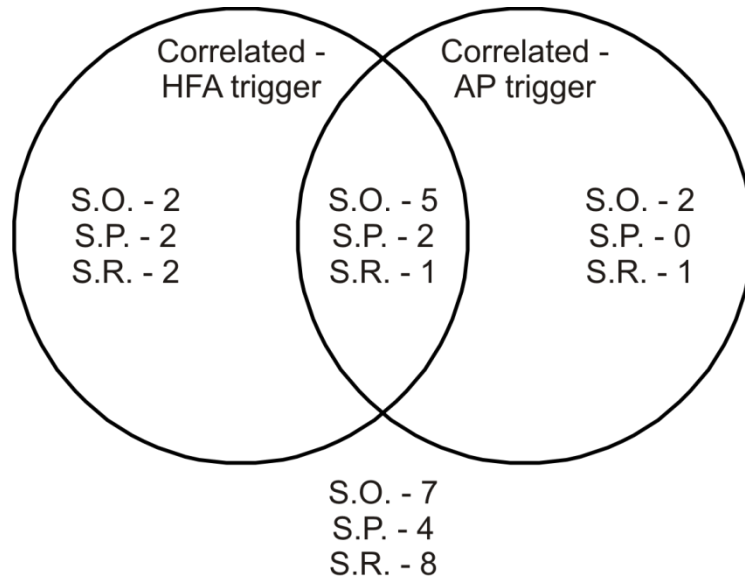


Figure 4.11 – Laminar distribution of correlated and uncorrelated interneurons.

The Venn diagram shows how interneurons which correlated with each trigger were distributed throughout the layers of the hippocampus.

Correlated by	Phase angle (HFA cycle trigger)	Circular S.D. (HFA cycle trigger)	Phase angle (AP trigger)	Circular S.D. (AP trigger)
Both triggers (n=8)	156 ± 22°	97 ± 5°	197 ± 22°	99 ± 8°
Only HFA cycle (n=6)	194 ± 32°	106 ± 5°	Uncorrelated	Uncorrelated
Only AP (n=3)	Uncorrelated	Uncorrelated	247 ± 31°	112 ± 13°
Overall (n=17)	187 ± 21°	101 ± 3°	224 ± 18°	102 ± 6°

Table 4.2 – Properties of significant phase relationships. *The table summarises the average phase angles and circular standard deviations of interneurons, subdivided by which phase relationships were significant.*

5. RESULTS – THE TETANUS TOXIN MODEL OF EPILEPSY

5.1 Response to tetanus toxin injection *in vivo*

5.1.1 *Time course of seizures*

Surgery (see section 2.4.3) was carried out on a total of 44 rats; 24 were injected with TeNT and 20 were vehicle controls. Two TeNT animals and two control animals were excluded due to technical error during surgery and two TeNT injected animals were killed prematurely by cervical dislocation due to the severity of their epileptic response. Thus 20 TeNT injected rats and 18 control rats remained for experimentation. Welfare records kept by technicians over the period between surgery and slice preparation indicated that 18 of the 20 TeNT treated rats experienced epileptic seizures during this time. The other two TeNT injected rats were not included in the results presented in this chapter. No seizures were observed in vehicle controls in response to surgery. It was technically difficult to identify all seizures using video recording alone and so the exact time course of all seizures experienced by these rats could not be produced. Comparable data from another study was supplied by Prof. John Jefferys and Alexander Ashby-Lumsden.

Figure 5.1 shows the time course and Racine scale classification of seizures experienced by a Wistar rat in response to injection of 2.5 ng TeNT (J. Jefferys and A. Ashby-Lumsden, unpublished data) from the same batch as used in this study) into the ventral hippocampus, using the same stereotaxic co-ordinates as this

work. The data in the figure was created using EEG recording to accurately identify epileptic brain activity. This was complemented with video recording which facilitated the classification of seizures on the Racine scale. EEG recording for this animal was made using dual biopotential radiotelemeters (TR50BB, Millar Instruments, US) implanted by Prof. John Jefferys. TeNT injection and data acquisition, analysis and presentation were carried out by Alexander Ashby-Lumsden.

Rats typically began to experience seizures at around 4-5 days post injection, followed by around one day in which few or no seizures were seen. Seizure activity peaked at around 8-10 days post injection. The occurrence of seizures then decreased for 1-2 days. Finally, seizures returned, at a lower frequency, at around day 12 and persisted until day 17. At this point, rats appeared to gain remission from seizures, although abnormal interictal-like activity persisted until day 20. *Ex vivo* brain slices were prepared from these animals at 21 ± 3 days post injection.

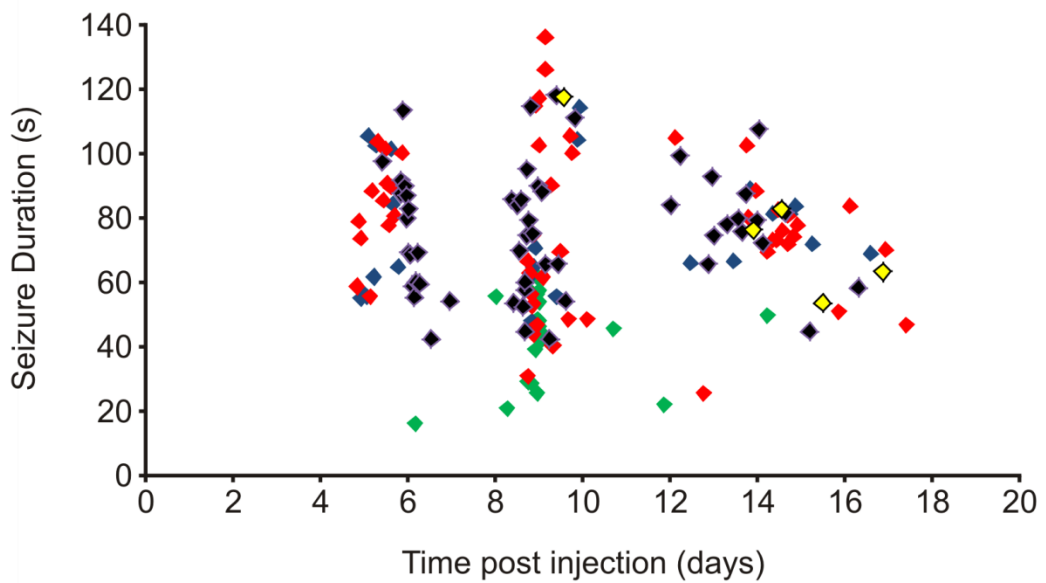


Figure 5.1 – Time course of epileptic response to TeNT injection. *The scatterplot shows the time course, Racine scale classification and duration of seizures in a Wistar rat injected with 2.5ng TeNT into the ventral hippocampus. The colour of markers denotes seizure severity, measured using the Racine scale classification: green – 2 (abnormal head bobbing), light blue – 3 (disorganised forelimb contraction), red – 4 (postural rearing), dark blue – 5 (postural rearing and falling), yellow - unclassified. Figure was adapted from a plot generated by Alexander Ashby-Lumsden.*

5.2 Characterising the HFA seen *ex vivo* after TeNT injection

5.2.1 *Potassium thresholds for the induction of HFA*

Brain slices in which simultaneous field HFA and interneuron action potentials were recorded were analysed further. Slices taken from TeNT treated rats did not exhibit spontaneous epileptic activity, or any HFA, when perfused with normal aCSF, perhaps because slices were made after rats had typically gained remission from seizures (see section 6.4.3). Therefore, the extracellular potassium concentration was raised in steps of 1 mM until epileptiform bursts were observed. 9 out of 13 TeNT treated slices generated epileptic-like activity in response to 6mM potassium, while the rest had a threshold of 9mM. In comparison, 1 out of 5 control slices responded to 6 mM and the remaining 4 to 9mM K⁺. This difference is not statistically significant (Fisher's exact test, $p > 0.05$), though the small dataset precludes the use of the more powerful Chi-Square test.

5.2.2 *Time course of seizure activity*

Similarly to the high potassium model, brain slices taken from TeNT treated rats exhibited two distinct profiles of epileptic-like activity (Figure 5.2). A continuous pattern, consisting of a prolonged series of epileptiform bursts, with superimposed HFA, was seen in 10 slices. The remaining 3 slices generated epileptic-like activity which was divided into discrete seizure-like bursts of field activity. The concentration of extracellular potassium needed to elicit field activity had no relationship with the seizure profile observed.

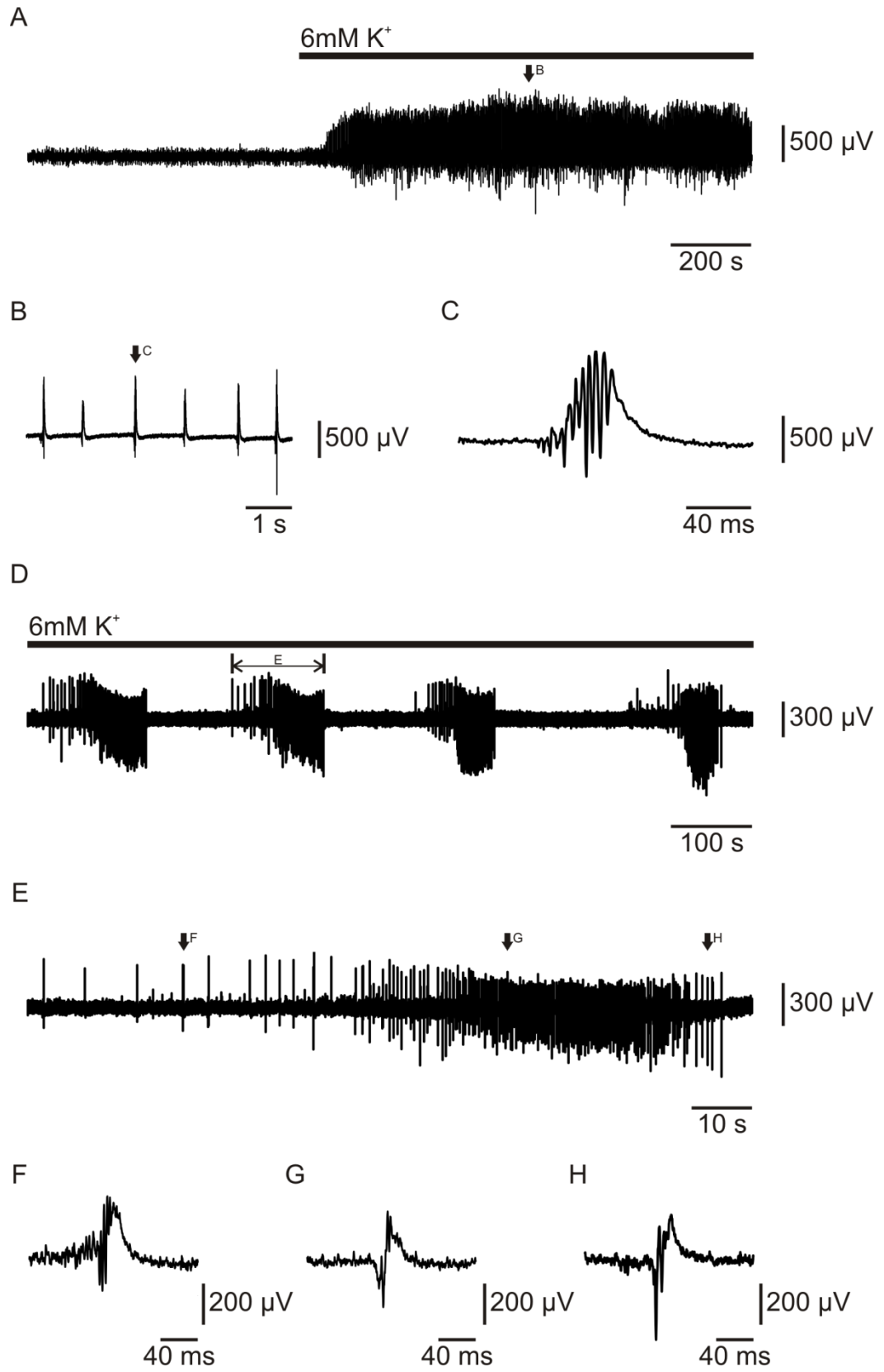


Figure 5.2 – Continuous and discrete patterns of epileptic-like activity in *ex vivo* TeNT treated slices. *10 out of 13 slices generated continuous epileptic-like discharges (A, magnified in B). On a millisecond timescale, HFA was superimposed on the field bursts (C, magnified from B). In the 3 remaining slices, field activity was organised into discrete seizure-like events (D). Each SLE (E, magnified from D)) roughly consisted of interictal-like discharges (F) followed by a tonic-like onset (G) and finally clonic-like discharges (H).*

5.2.3 Ripples (100-300 Hz)

Field HFA was first classified by its peak frequency and summated power between 100 and 500 Hz. Slices from tetanus toxin treated rats (n=13 slices) generated HFA with a frequency of 183 ± 13 Hz (210 ± 7 Hz for vehicle controls, n=5) and a power of $273 \pm 54 \mu\text{V}^2$ ($490 \pm 253 \mu\text{V}^2$). Neither measure was statistically different from control values (Student's *t*-test, $p > 0.05$). Peak frequency values for TeNT treated slices were not significantly different from normal distribution and ranged from 117 Hz to 269 Hz, consistent with the ripple band seen in the high potassium model (section 4.1.3).

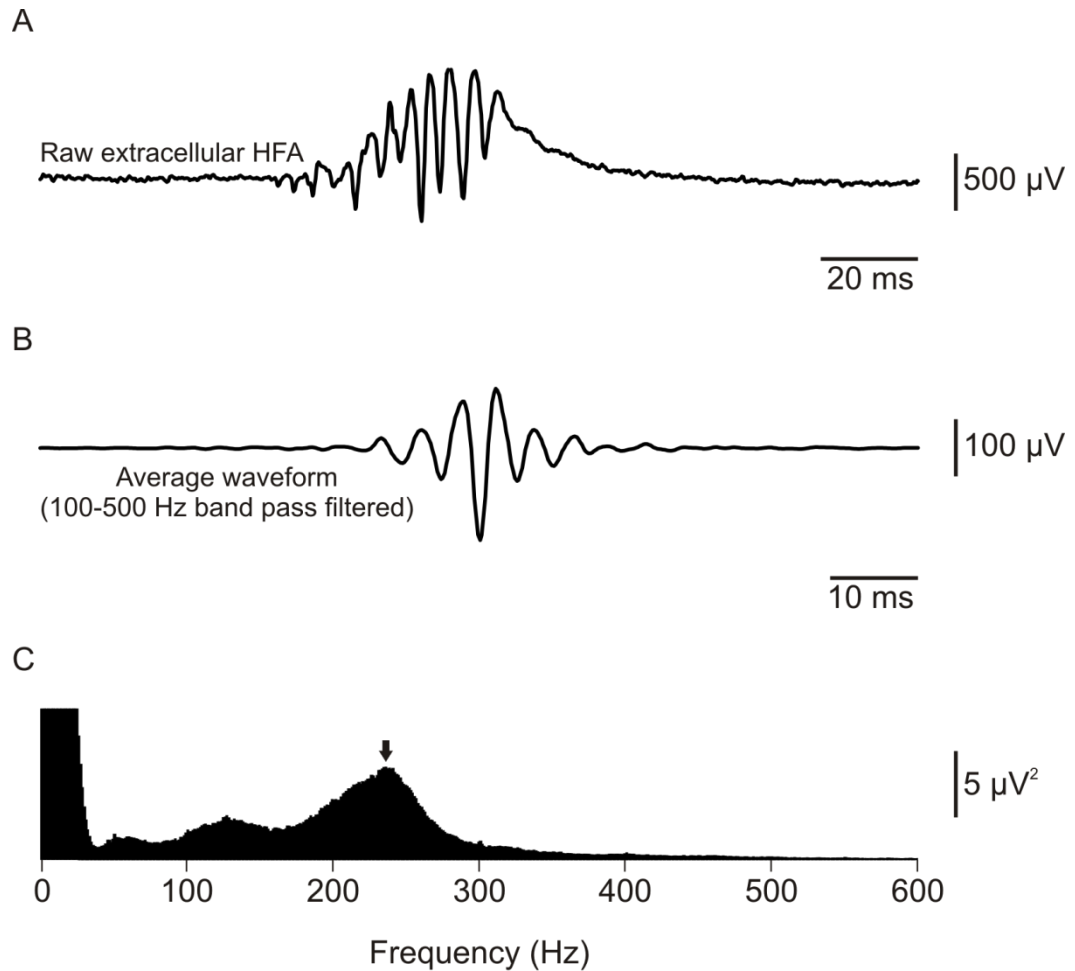


Figure 5.3 – Ripple band (100-300 Hz) HFA is dominant in the TeNT model.

Representative data from one slice with ripple band HFA. A typical field burst in slices taken from TeNT treated rats consisted of strong HFA superimposed on a pathological sharp wave (A). Average waveform (B) and fast Fourier transform (C) analyses showed that the dominant HFA fell within the ripple band (100-300 Hz).

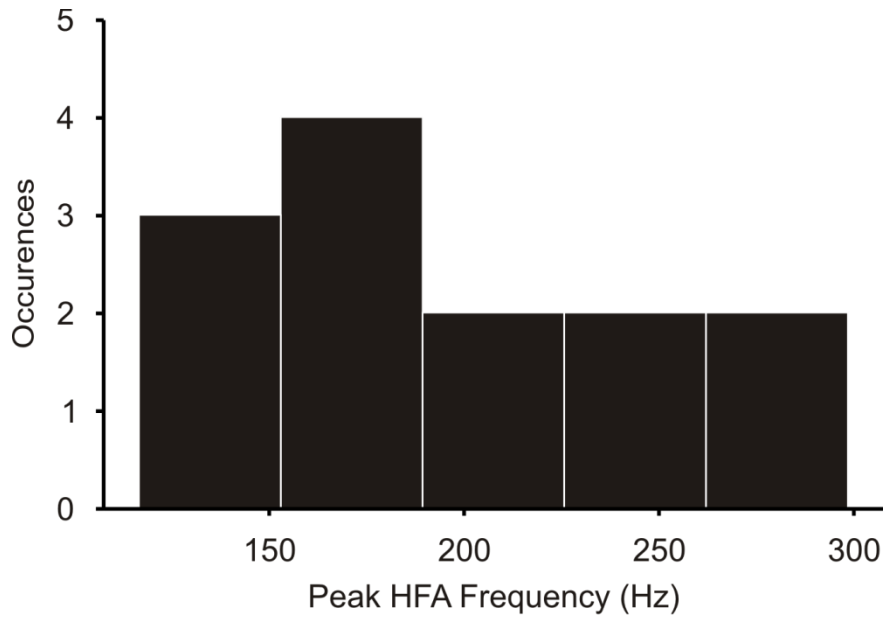


Figure 5.4 – Peak HFA frequencies from all slices. *The histogram shows the peak frequency of HFA taken from each of the 13 slices.*

5.2.4 Fast ripples (300-500 Hz)

Figure 5.4 showed that the dominant HFA generated by TeNT treated slices was likely to be a single phenomenon, ranging from 117 – 269 Hz. However, in 4 out of the 13 slices, a bimodal power spectrum, with a secondary peak in the fast ripple band, was seen (Figure 5.5). This indicated a second phenomenon, which was not seen in the acute high potassium model, occurring at the same time as the ‘ripple’ oscillation and at a frequency of 347 ± 28 Hz. These ‘fast ripples’ had a lower amplitude than the ripples. Both HFA phenomena occurred primarily during pathological sharp wave events (Figure 5.6), but there was no correlation between the two (Figure 5.7).

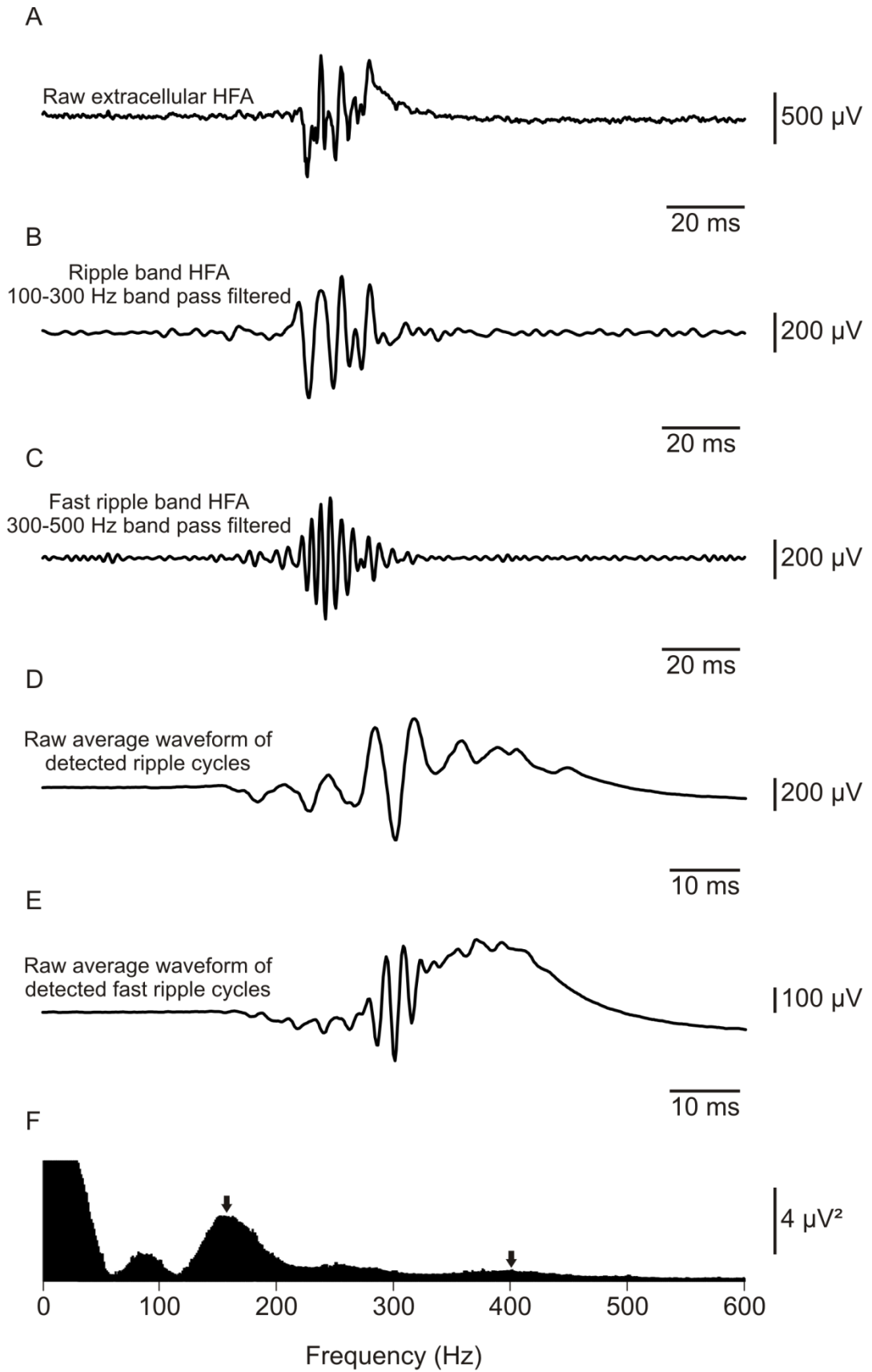


Figure 5.5 – The TeNT model featured both ripples and fast ripples. *Raw field bursts (A) were band pass filtered at 100-300 Hz (ripple band, B) and 300-500 Hz (fast ripple band, C). The relevant events in these filtered traces were detected as troughs and used to compute average waveforms for ripples (D) and fast ripples (E). The power spectrum (F) contained multiple peaks, which corresponded to the frequencies obtained from (D) and (E). This was seen in n=4 slices.*

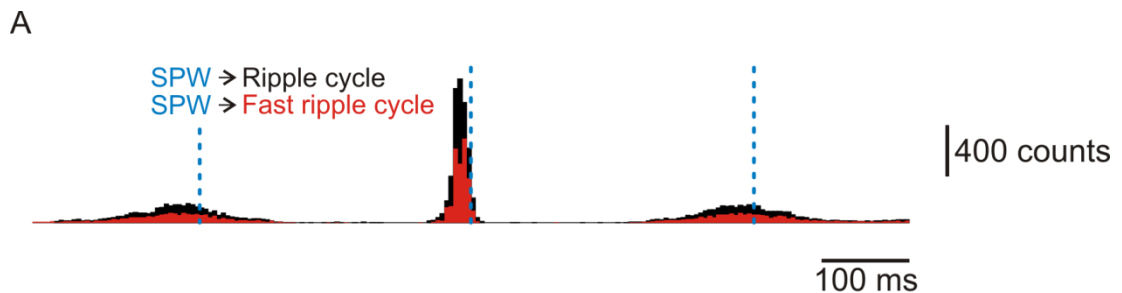


Figure 5.6 – Ripples and fast ripples occurred primarily during pathological sharp waves. *Event correlation (A) between a sharp wave reference point (centre red dotted line) and ripples (black) and fast ripples (red) showed a relationship between sharp waves and both HFA phenomena. Comparison with a sharp wave autocorrelation (B) showed that both ripples and fast ripples were most likely to occur just before the sharp wave peaks (dotted blue lines).*



Figure 5.7 – The timing of ripple and fast ripple cycles was not correlated. *Event correlation for fast ripple events (histogram) with reference to the trough of ripple cycles (red dotted line) revealed no temporal relationship between the two phenomena. See Figure 5.5 for raw data.*

5.3 The behaviour of interneurons in the tetanus toxin

model

5.3.1 Firing frequencies

As in the high potassium model (see section 4.2.1), interneuron firing frequency increased during epileptiform bursts elicited in tetanus neurotoxin treated slices (Figure 5.8). Mean firing frequency measured from all interneurons was 36 ± 15 Hz when there was no temporal overlap with field activity. During epileptiform bursts, this increased to 107 ± 15 Hz.

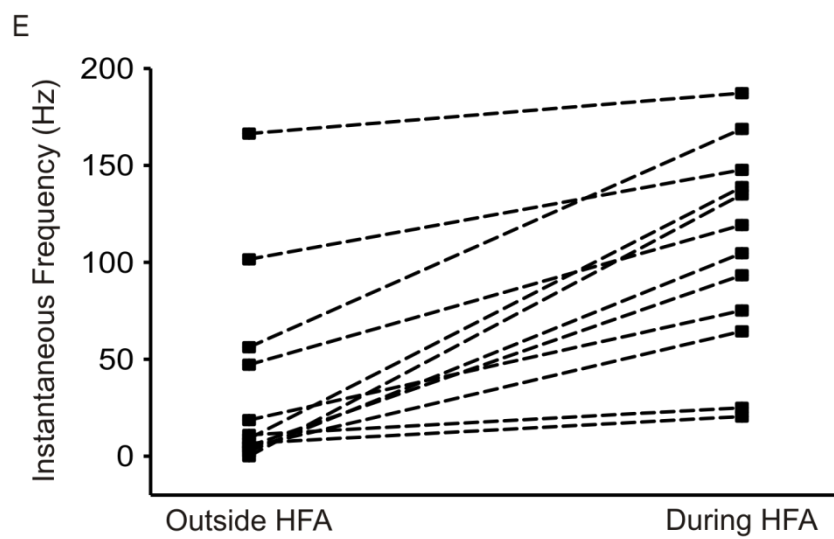
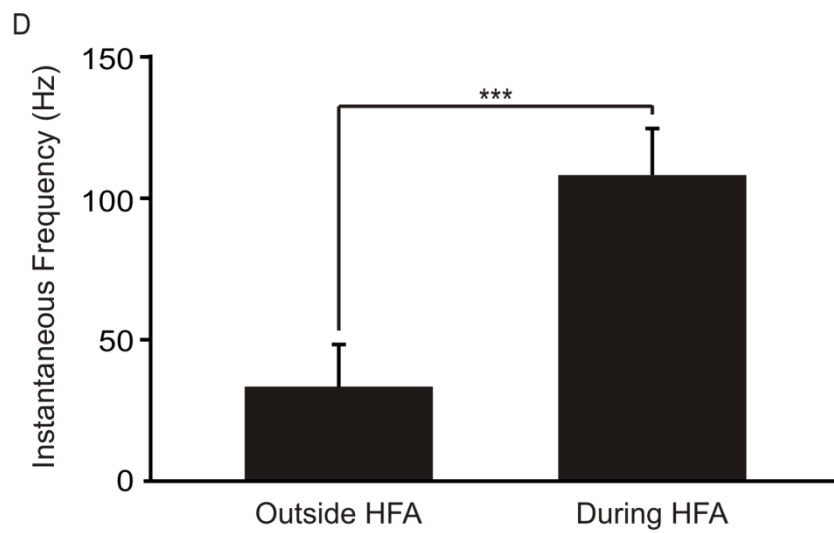
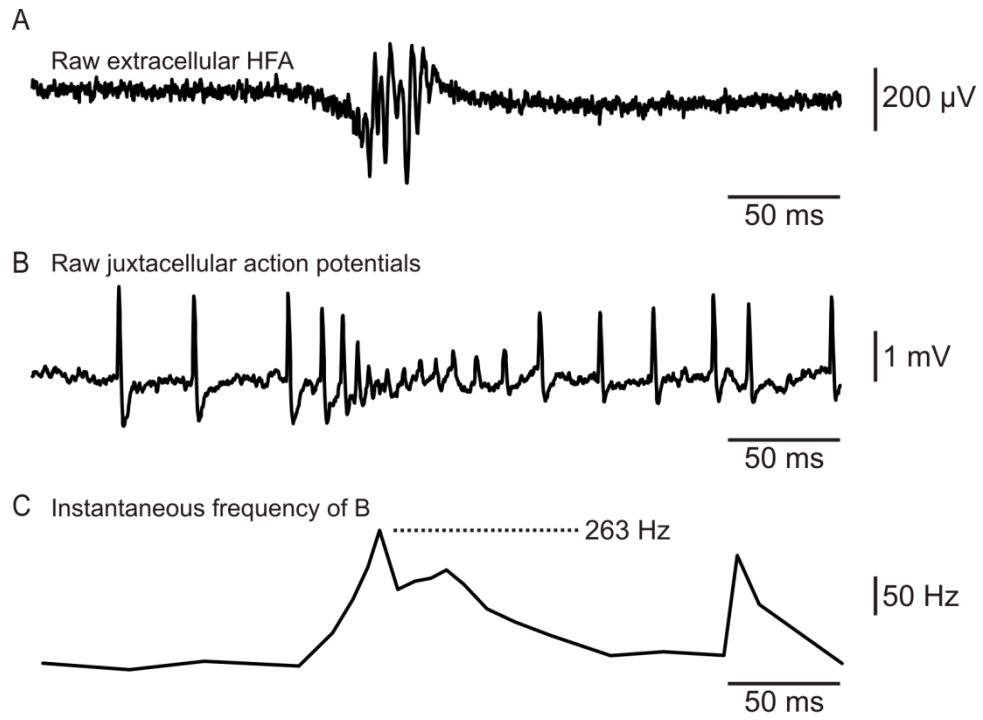


Figure 5.8 – Interneurons fire action potentials at higher frequency during epileptiform bursts in the TeNT model. *Comparison of raw field data (A) with the single-cell recording of interneuron activity (B) revealed an increase in firing frequency during epileptiform bursts. This was visualised using instantaneous frequency (C). This effect was statistically significant when examining all interneurons which fire during epileptiform bursts (D; n = 11 interneurons; paired t-test, $p < 0.001$). (E) shows the frequency values for all interneurons.*

5.3.2 Action potential amplitude

The amplitude of action potentials fired by interneurons decreased during epileptiform bursts (Figure 5.9) and, again, this was similar to the effect seen in the high potassium model (see section 4.2.2). Due to the variation in detected amplitudes between the single-cell recording configurations obtained, action potential amplitudes were normalised to give a mean value for the decrease, with amplitude falling during epileptiform bursts to $64 \pm 9\%$ of its baseline value.

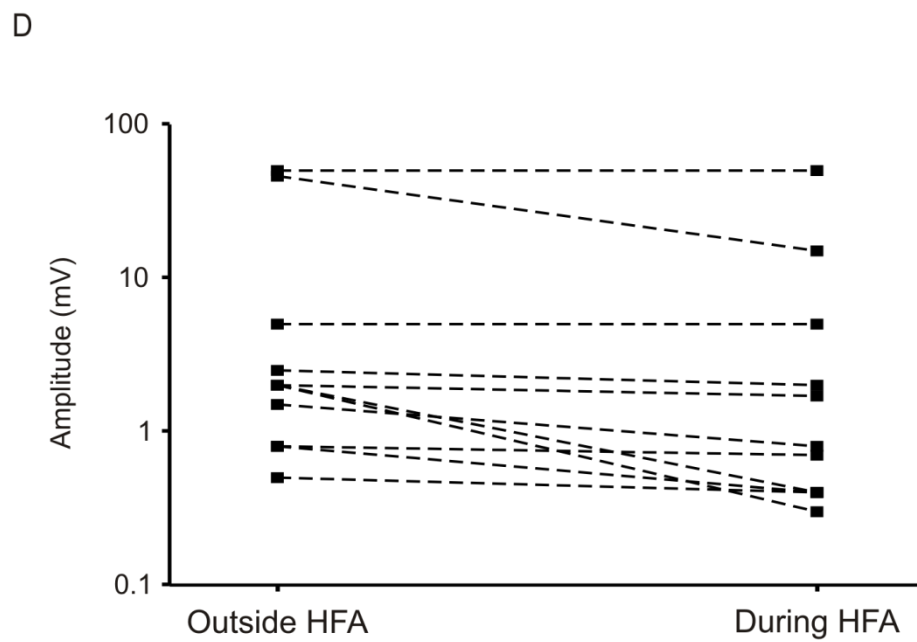
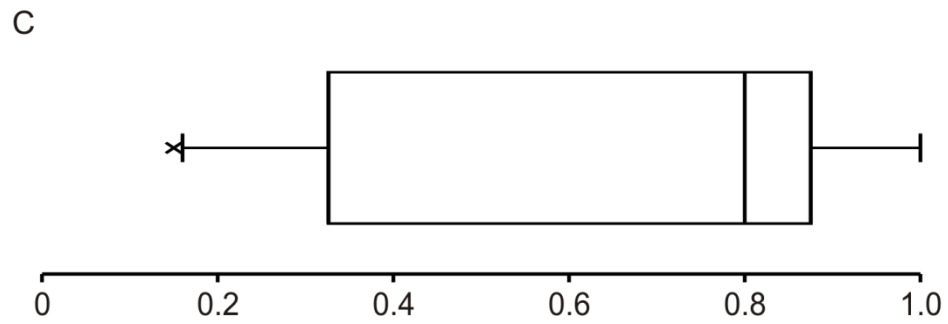
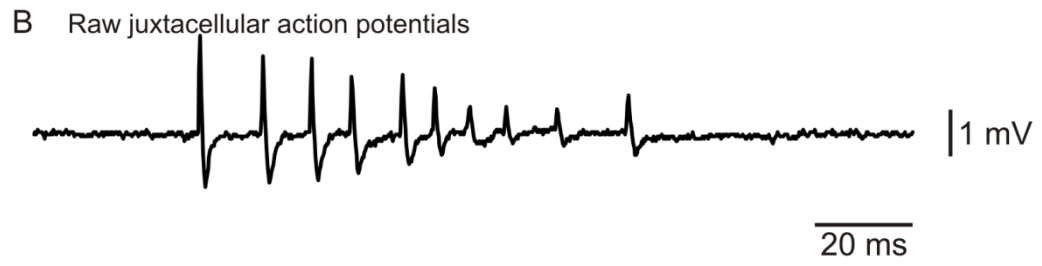
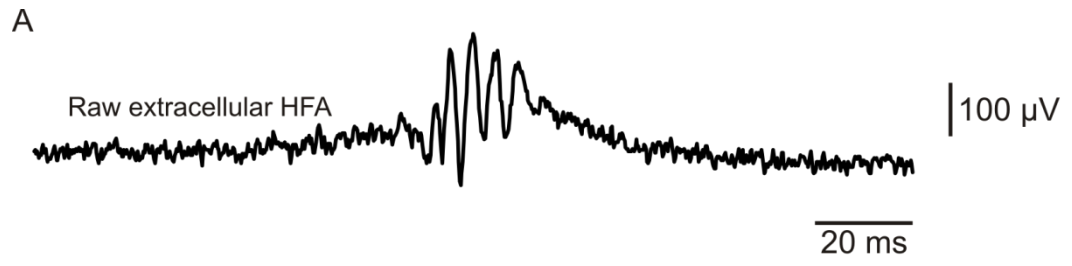


Figure 5.9 – Interneuron action potential amplitude decreased during epileptiform bursts. *Comparison of raw field data (A) with interneuron firing data (B) showed a reduction of action potential amplitude during epileptiform bursts. The box plot in (C) shows the normalised reduction in amplitude compared to maximal amplitude outside of field discharges. (D) shows the paired raw amplitude values, plotted on a log scale.*

5.3.3 Firing patterns

Interneurons in TeNT treated slices showed the same groupings as those in the high potassium model and so were grouped in the same way (see section 4.2.3).

Table 5.1 shows the laminar distribution of interneurons with each firing pattern.

Group 1 cells, which fired high frequency bursts of action potentials during epileptiform bursts, were confined to S.O. and S.P., whereas group 2 (low frequency bursts) and group 3 (single action potentials) were found in all layers.

Group 4 (stop firing during epileptiform bursts) were only seen in S.P. in this case.

	Group 1	Group 2	Group 3	Group 4
Stratum Oriens	2	2	1	0
Stratum Pyramidale	1	1	1	2
Stratum Radiatum	0	2	1	0

Table 5.1 – Laminar distribution of interneuron somata with respect to firing patterns. Firing groups are shown in Figure 4.8.

5.4 Phase relationships between interneuron firing and HFA cycles in the tetanus toxin model

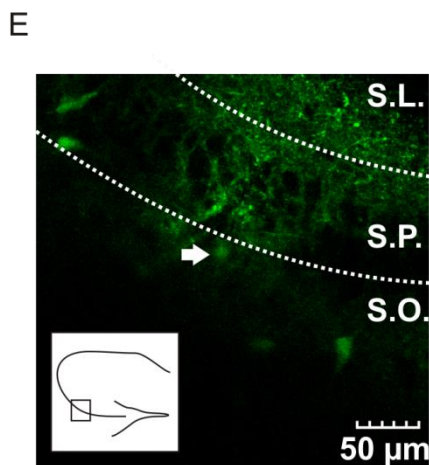
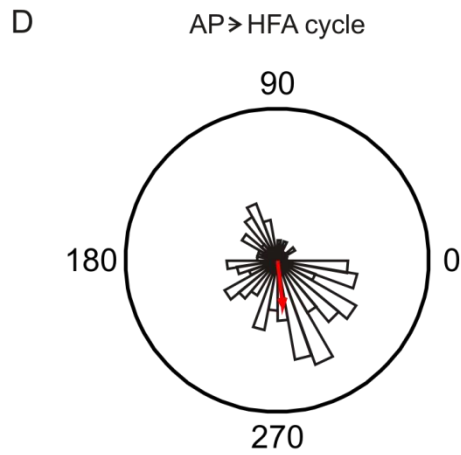
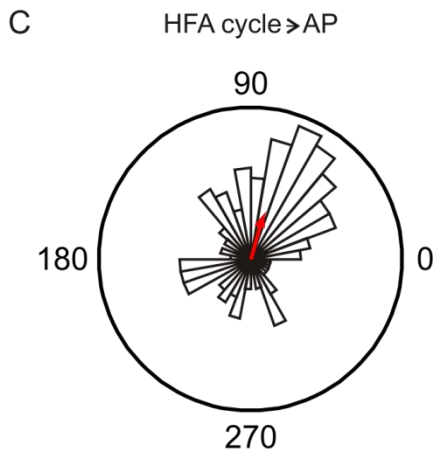
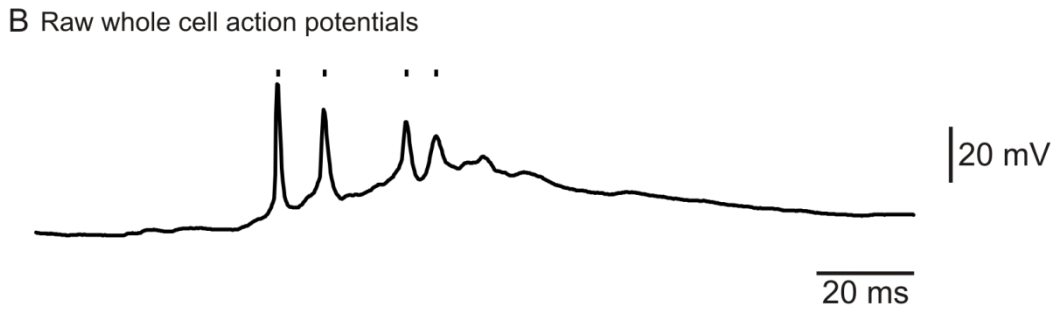
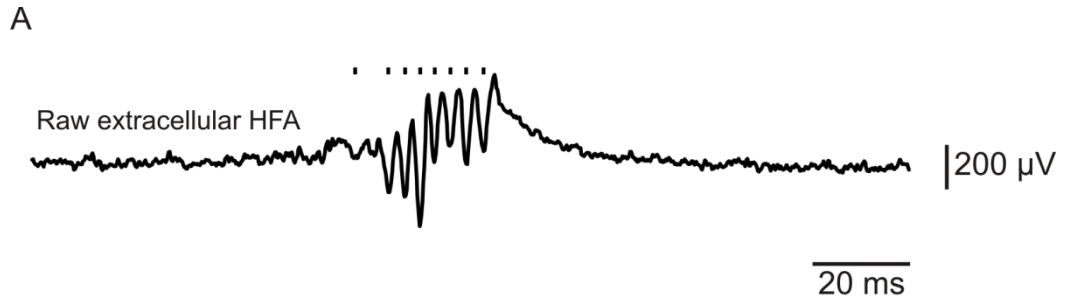
5.4.1 Phase relationships between ripple cycles and interneuron firing

5.4.1.1 HFA cycle trigger

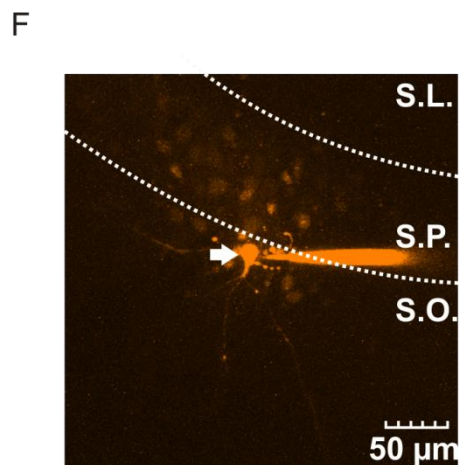
High frequency activity cycles were a significant predictor (Rayleigh statistic, $p < 0.05$) for subsequent action potentials recorded from an interneuron in 5 out of 13 recordings from TeNT treated slices. This was not significantly different from control recordings (Fisher's exact test, $p > 0.05$) where 4 out of 5 recordings showed significant correlation. Of the 5 correlated interneurons, 2 were in S.P., 2 in S.O. and 1 in S.R.. Sample correlations between ripple cycles and interneuron firing in the TeNT model are shown in Figure 5.10.

5.4.1.2 *Action potential trigger*

In this model of epilepsy, 3 of the recorded interneurons fired action potentials which were significant predictors for ripple cycles. 2 of these were found in S.O. and one in S.P.. 6 cells fired multiple action potentials during sharp waves, but were not correlated. The remaining 4 only fired one action potential during each sharp wave and so phase analysis could not be carried out in this way. In this model, there was no relationship between dominant HFA frequency and correlation to action potential firing, as was seen in the high potassium model in section 4.3.3.1.



Confocal 40x Venus
Excitation: 515 nm
Emission: 530-570 nm



Confocal 40x Alexa 647
Excitation: 635 nm
Emission: 650-750 nm

Figure 5.10 – Significant phase relationships between ripple-band HFA cycles and interneuron firing. *Ripple-band HFA (A; cycles denoted by tick marks) was compared with action potential firing in the patched interneuron (B; action potential peaks denoted by tick marks). Phase correlations using HFA cycles (C) and action potentials (D) as the causative triggers both showed a significant effect. Venus fluorescence (E-inset shows rough location of cell within the hippocampus) confirmed that the cell was an interneuron and fill with Alexa-647 (F) showed some projections.*

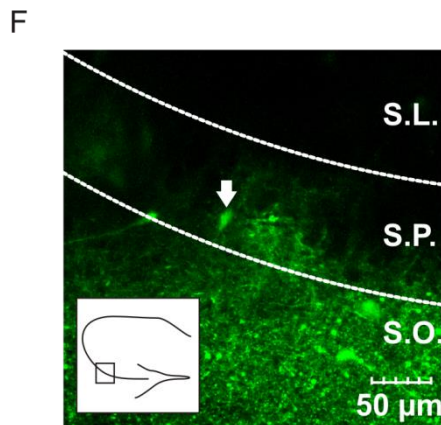
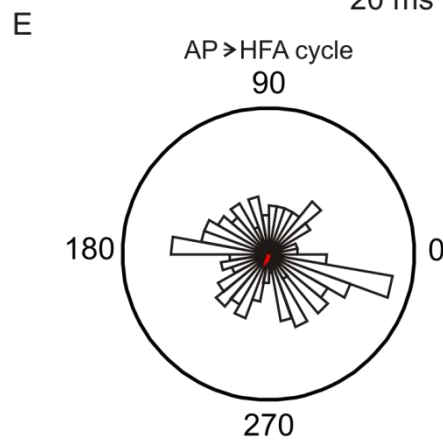
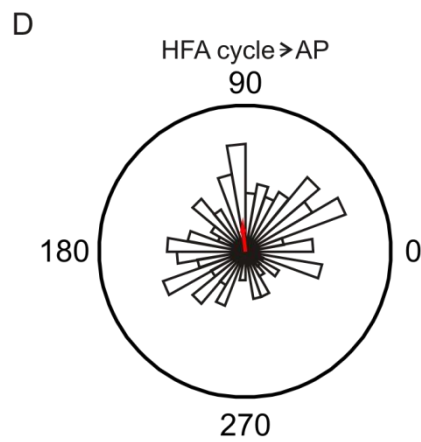
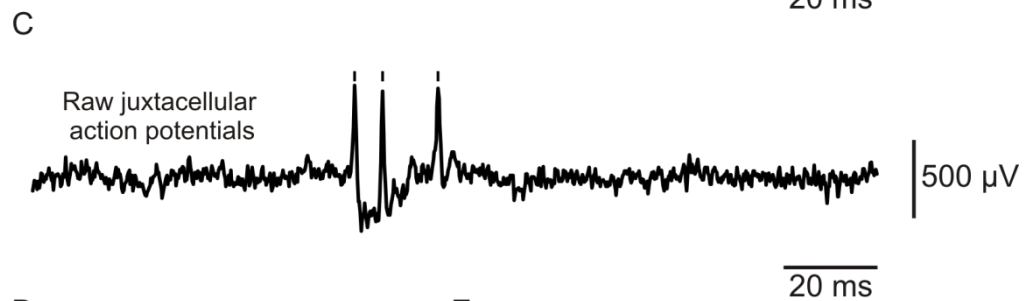
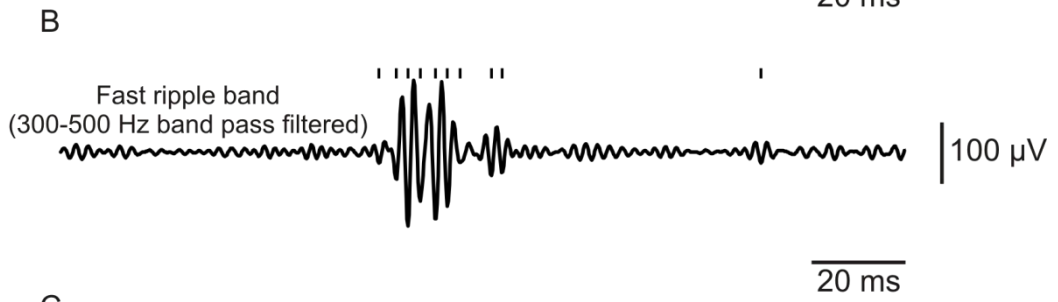
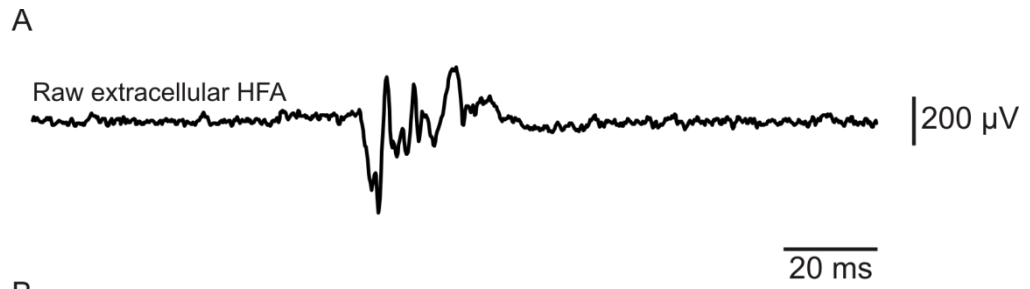
5.4.2 Phase relationships between fast ripple events and interneuron firing

5.4.2.1 HFA cycle trigger

In the 4 slices which generated fast ripple activity, these events were detected separately from ripples and then correlated with action potentials. In this case, fast ripple HFA cycles predicted interneuron firing in 2 recordings. However, these interneurons did not themselves fire at fast ripple frequency (firing at 139 and 169 Hz during epileptiform discharges). Both of these interneurons were also correlated to ripple events. One interneuron was correlated to ripple cycles, but not fast ripple cycles, and the other interneuron did not correlate with either HFA event. Sample correlations between fast ripple cycles and interneuron firing are shown in Figure 5.11.

5.4.2.2 *Action potential trigger*

Of the four cells recorded from slices which generated fast ripples, only two fired more than one action potential during each sharp wave. One cell, located in S.O., fired action potentials which were a significant predictor of fast ripple HFA cycles; the other, in S.P., did not. The correlated cell also showed a significant relationship with ripple cycles, and with both phenomena when using the HFA as a trigger.



Confocal 40x Venus
Excitation: 515 nm
Emission: 530-570 nm

Figure 5.11 – Correlations between fast ripple cycles and interneuron firing. *Raw data (A) were band-pass filtered between 300-500 Hz (B) for fast ripple cycle detection (events shown by tick marks). Action potentials fired by the interneuron (C) were detected and phase correlations using fast ripple cycles (D; significant) and action potentials (E; non-significant) were generated. Venus fluorescence (F) confirmed that the cell was an interneuron. White dotted lines on (E) indicate the rough boundaries between the layers of the hippocampus.*

6. DISCUSSION

6.1 Protocol development

6.1.1 *Slice parameters*

High frequency activity in the high potassium model was previously demonstrated in a study from this lab (Jiruska et al 10a). In this case, recordings were made from 400 μm thick brain slices, cut in the sagittal orientation. The presence of HFA in these slices made them a logical starting point for beginning a study into the mechanisms of the phenomenon. Sagittal slices only provide access to the dorsal part of the hippocampus, with the projections of the ventral portion being destroyed due to their anatomical orientation (Bragdon et al 86). However, the ventral hippocampus is more prone to epileptic-like activity (Bragdon et al 86; Gilbert et al 85; Borck and Jefferys 99) and can be accessed using slices cut in the horizontal orientation. Thus, the study began with a direct comparison between the two orientations, with the results presented in section 3.1.1. Horizontal slices were significantly more likely than sagittal slices to generate seizure-like activity. This activity was seen in both the CA1 and CA3 regions of both slices. The overall morphologies of seizure-like activity, as well as the general appearance of HFA, looked qualitatively similar in both types of slice. Indeed, there were no statistical differences in either the power or the frequency of high frequency activity generated by the two. Therefore, the only difference between the two orientations was that horizontal slices were more prone to generating seizure-like

activity, consistent with the findings of Borck and Jefferys (99). Given that, when activity was seen, both orientations generated comparable HFA, it followed that the study should progress using horizontal slices, in order to maximise the yield of experimental data and to minimise the number of animals used.

HFA is thought to be generated by local circuitry within the hippocampus, spanning around 130 microns (Jiruska et al 10a), and so a particular region of interest needed to be selected in which to investigate HFA mechanisms. The two obvious candidates for this were the CA1 and CA3 regions of the hippocampus.

Physiological HFA *in vivo* is more powerful in CA1 (Ylinen et al 95), meaning that this region could have generated more robust oscillatory activity to study.

However, pathological HFA in CA3 is strongly correlated to the occurrence of seizures (Levesque et al 11). Therefore, simultaneous recordings were made from both regions in high potassium conditions, with the results presented in section

3.1.2. The first result of note here was that some slices were capable of generating epileptic-like activity solely in CA3 and not in CA1. In contrast, no slices had activity which was limited to CA1. This suggests that CA3 could indeed be the generation site for epileptiform activity within the slice. This was further

supported by the finding that epileptiform bursts originated in CA3 and propagated to CA1 (Figure 3.2). Thus, in recordings where CA3 was not active, no activity was seen at all. This provided support for the use of the CA3 subregion in the mechanistic study. This support was consolidated by a comparison of the HFA generated in the two regions. Paired comparisons showed that CA3 exhibited significantly more powerful HFA than CA1; the frequency of the oscillations was

comparable between the two subregions. This was the key evidence in favour of the CA3 subregion because HFA, the phenomenon of interest, was so much more robust. Finally, HFA in CA3 of 300 μm thick horizontal slices was compared with that in 400 μm sections. Though 400 μm slices generated more powerful HFA (owing to a larger volume of pyramidal cells within the slice), they were considered too thick for patch clamp recording. Despite being of lower amplitude, the HFA generated in 300 μm sections was qualitatively similar to that seen in 400 μm sections, suggesting that it was the same phenomenon on a smaller scale, and that 300 μm sections still provided a valid model of HFA whilst also optimising single-cell recordings.

6.1.2 The membrane chamber

The membrane chamber (Hill and Greenfield 11) is a modified version of a conventional submerged chamber, which retains all of the desirable features of submerged designs (compatible with high magnification water immersion objectives and mechanical support for the slice), whilst also overcoming their main shortcoming – limited oxygen availability. For these reasons, it was suggested that the membrane chamber provided a novel apparatus in which simultaneous recording of epileptic fields and single cell activity was possible.

The membrane chamber had not been previously used to study epileptic-like activity. Indeed, few publications (Hill and Greenfield 13) refer to its use for other electrophysiological work. Therefore, the chamber was tested in terms of fluorescence imaging, single-cell recording and field recording before it was used

for the main groups of experiments. Figure 3.4 gives a typical example of the types of brightfield and fluorescence images that were obtained from VGAT-Venus A slices within the membrane chamber. Fluorescence imaging revealed clearly defined somata of interneurons in various layers of the hippocampus. Therefore, interneurons could be identified using VGAT-Venus A rats and the membrane chamber, permitting the study of the mechanistic role of inhibitory cells in HFA. For some interneurons, thicker projections, such as dendrites, could also be seen under Venus fluorescence imaging (Figure 3.4). However, finer projections, including axons, were difficult or impossible to visualise using the available equipment. Moreover, strong perisomatic fluorescence was seen surrounding the cell bodies of pyramidal cells in S.P., likely due to inhibitory terminals from perisomatic-targeting interneurons. This further obscured the tracking of interneuronal projections which passed through this layer. Knowledge of the targets of these projections was desirable because it can provide anatomical evidence for the specific subtypes of interneurons (Ascoli et al 08). The absence of this information from the Venus imaging necessitated the use of intracellular tracers – initially Alexa 647 and then biocytin – to enhance the imaging of all projections from recorded interneurons.

Once it was established that interneurons could be selectively targeted, trial single-cell recordings were made. For successful whole-cell patch clamp recordings to be made, slice stability is critical. This was the main shortcoming of the membrane chamber. Frequently, small mechanical disturbances whilst obtaining high resistance gigaseals, or when trying to break through into whole

cell configuration, led to recordings being lost or changing to juxtacellular configurations. Where the latter were obtained, they were continued anyway as it was considered that only the firing patterns of cells were key to this study and that they could be obtained from either juxtacellular or whole cell recordings. Though it was not investigated systematically, slice stability appeared to improve either when using slice weights made from twisted silver wire or when altering the density of the buffer material (see Figure 1.1) on the advice of the manufacturer. Despite some problems with mechanical instability, it was possible to achieve whole cell patch clamp recordings from the targeted interneurons using the membrane chamber. Once the desired configuration had been reached, the small disturbances mentioned in the previous paragraph rarely had any impact on the recording. In situations where gigaseal recordings were made, interneurons could also be filled with other fluorescent tracers, such as Alexa 647. It was hoped that axonal projections could be identified in some interneurons and putative anatomical classifications could be made. However, because many recordings were juxtacellular rather than whole-cell, not all of the interneurons were filled well or at all with Alexa 647. This eventually led to the use of biocytin, with which juxtacellular labelling is possible.

Finally, the membrane chamber was used to make field recordings from brain slices under high potassium, in order to compare the generated activity to that seen in established interface chamber models. Qualitatively, HFA seen in the membrane chamber looked comparable with that seen in the interface chamber. In each case, HFA consisted of a series of population spikes which occurred at a

frequency of between 100 and 300 Hz and were superimposed on a sharp wave discharge. This suggested that the same phenomenon was observed in both styles of recording chamber, which began to validate the use of the membrane chamber. The most notable difference when using the membrane chamber was in the overall pattern of the epileptic-like activity. In the recordings made in the interface chamber, most recordings exhibited activity which was divided into discrete seizure-like events, each separated by a relatively quiet interictal-like period. In contrast, almost all of the recordings made in the membrane chamber showed a continuous bursting profile in which each burst consisted of a pathological sharp wave with superimposed HFA and was broadly similar to the bursts seen in the clonic phase of the discrete SLE profile. This difference is likely explained by one of two causes. Potentially, despite its modified design, the membrane chamber is still not capable of supplying sufficient oxygen to support true seizure-like activity. This, however, seems unlikely because the slices do not appear to deteriorate over time (Hill and Greenfield 11), as they might if insufficient oxygen were available. Perhaps more likely is that, due to the much higher flow rate of the membrane chamber (~16 ml/min compared with ~4-6 ml/min in interface style chambers), there is a greater clearance of extracellular potassium, which results in a prolonged clonic-like brain state. Despite this gross morphological difference, there was no difference between the HFA observed in both conditions, therefore validating the use of the membrane chamber to study HFA.

6.2 HFA in the high potassium and tetanus toxin models

6.2.1 HFA in high potassium

As described in the previous section, the elicited epileptic-like activity using the high potassium model in the membrane chamber most often comprised a continuous series of epileptiform bursts. Despite the inconsistency with data from this study, and others, where high potassium elicits discrete seizure-like events, HFA was still present and was thus studied further in section 4.1.

The first result of note in this section was that cycles of high frequency activity were seen primarily superimposed on pathological sharp wave events. This is perhaps unsurprising – the sharp wave is recorded as a result of strong, synchronous dendritic excitation in a population of pyramidal cells (Ylinen et al 95). This leads to sodium ion influx in S.R., which creates an extracellular current sink. Thus, a source is created in S.P., where it can be recorded extracellularly as a large positive field potential. Therefore, most HFA events were recorded where the local cellular network was under continuous excitation, consistent with the hypothesis set out in section 1.6 that the oscillation arises from the interplay between local pyramidal cells and interneurons driven by mutual glutamatergic input.

The next stage in the investigation of this HFA was to classify it by frequency. Fast Fourier transform and average waveform analyses revealed that the HFA frequencies were normally distributed and spanned both the ripple and fast ripple

bands. At this stage, the analyses performed assumed ripples to be physiological and span 100-250 Hz (Jiruska et al 10b), with pathological fast ripples from 250-500 Hz. Boundaries from other studies extended as far as 100-300 Hz for ripples and 200-600 Hz for fast ripples (Foffani et al 07). In this case there is an overlap between the bands ranging from 200-300 Hz into which many of the data from this study fell. Further, the normal distribution implied that the HFA recorded in this study was all the same phenomenon and comparison of 'ripples' (Figure 4.3) with 'fast ripples' (Figure 4.4) showed that the two were qualitatively similar and probably the same event, with quantitatively different features. This was not compatible with the frequency bands defined previously (Jiruska et al 10a). These inconsistencies made it impossible to classify the elicited HFA based purely on frequency, a problem which has been described before (Jefferys et al 12; Karlocai et al 14). A recent study, using the high potassium model in hippocampal CA3, compared spontaneous, physiological-like 'sharp-wave ripples' with 'interictal-like events' caused by 8.5 mM K⁺ (Karlocai et al 14). This showed that physiological sharp wave ripples (not seen in the present study) and pathological epileptiform bursts occurred separately from each other, and were separated temporally by a quiet 'transitory phase'. This implied that some loss of control causes the same local circuitry to switch from a physiological to a pathological state over the quiet phase. Indeed, the physiological and pathological events were shown to have several differences. Pathological oscillations had greater amplitude, longer duration and faster underlying multi-unit activity. Therefore this study strongly suggested that HFA elicited in the high potassium model is pathological, despite

sometimes falling into the traditional ripple frequency band. Further support for the pathological nature of this HFA comes from a clinical study of outcomes following surgery to alleviate epilepsy. A positive outcome was correlated to the resection of tissue generating HFA which arose transiently from a flat, quiet baseline (Kerber et al 13). This effect was seen regardless of the frequency of the HFA, and suggested that this pattern of HFA, compared with more continuous periods of the phenomenon, was generated by the epileptic focus. HFA arising from a flat baseline was seen using the high potassium model in this study and thus, taken with the evidence from Karlocai et al, is likely to reflect a pathological situation.

All of the findings from this section suggest that HFA generated by brain slices in response to high potassium is a single pathological phenomenon, which ranges from 100-300 Hz, consistent with the boundaries set out by Foffani et al (07).

6.2.2 Dominant HFA in TeNT

Similarly, the dominant HFA in the tetanus neurotoxin model was normally distributed (though the Kolomogorov-Smirnov test used to determine this may be underpowered for the small dataset), and again ranged from 100-300 Hz. That this was a common feature between the two models perhaps suggests that this pathological 100-300 Hz activity, which rises from a flat baseline (as described by Kerber et al (13)) is more representative of epileptic HFA than are fast ripples. A direct comparison between the HFA in the high potassium model and the dominant HFA in the tetanus neurotoxin model showed that the two were very

similar in terms of appearance and that there was no difference in frequency between the two (independent samples *t*-test, $p > 0.05$).

6.2.3 Fast ripple HFA in TeNT

In 4 out of the 13 recordings made in the tetanus neurotoxin model, fast ripples were observed. The first notable point is that fast ripples were a separate phenomenon from the dominant 'ripple' oscillation. This was apparent because the two often occurred simultaneously, superimposed on pathological sharp waves (Figure 5.6), but had no temporal relationship with each other (Figure 5.7). As well as this, fast Fourier transforms of these recordings showed that the two events were entirely separated in the frequency domain, and so were not simply a continuum of the same phenomenon. This is in agreement with the findings of Bragin *et al*, who showed that ripples and fast ripples have no precise temporal relationship (Bragin *et al* 99a) in the KA model and that this produces bimodal power spectra when both are present (Bragin *et al* 04). That this has now been described in two separate chronic models of epilepsy, which use different mechanisms to induce spontaneous seizures, strongly suggests that the two are separate phenomena, rather than a continuation of the same oscillation. This observation also suggests that fast ripple generation is closely associated with the pathological circuit reorganisation that is seen in chronic models of epilepsy (see section 1.1.3).

6.3 Interneuron involvement in epileptic-like HFA

The main hypothesis for this work, set out in section 1.6, stated that each cycle of HFA would arise from the firing of a population of pyramidal cells, synchronised by the release from the inhibitory constraint of a common fast-spiking GABAergic interneuron. To test this, correlations were made between action potentials recorded from interneurons and the cycles of HFA which they were thought to underlie. Correlations were made using the phase domain, rather than the time domain, in order to normalise the sometimes variable cycle length of HFA. This then permitted the use of circular statistics in order to test the significance of correlations. The same analysis was carried out using both HFA and interneuron firing as triggers, in an effort to explore the bidirectional relationship between the two signals.

6.3.1 Interneuron participation in pathological 100-300 Hz HFA

In the high potassium model, when using HFA cycles as the trigger for the phase correlations, 14 out of 37 (38%) interneurons were significantly correlated to the dominant pathological ripple oscillation. The same percentage of interneurons was entrained by the pathological ripples in the tetanus neurotoxin model (5 out of 13 cells, 38%). This finding alone was important because it was the first demonstration, to the author's knowledge, that interneuron firing and pathological HFA are related on a millisecond timescale. Mechanistically, this implied that the population of pyramidal cells, whose firing underlies the HFA, caused feedforward excitation of the correlated interneurons. This would require

an excitatory input from the pyramidal population into the correlated cells. This lends some weight to the hypothesis that HFA arises from recurrent interplay between pyramidal cells and interneurons, by suggesting that the pyramidal cells are capable of providing the requisite feedback to the interneuron. However, to fully support the hypothesis, interneurons must not only be caused to fire by the pyramidal cells, but they must also entrain the pyramidal cells to fire synchronously. This was tested by reversing the putative causative trigger in the analysis, so that high frequency cycles were detected with reference to the firing of the interneuron. In this case, 11 out of the 37 interneurons (30%) in the high potassium model showed a significant correlation. Therefore the firing of these 11 interneurons served to predict pathological ripple cycles, suggesting that they imposed synchronous IPSPs on their target pyramidal cells and entrained them to fire together and form one HFA event. In the TeNT model, a lower percentage of interneurons were predictors of pathological ripples (3 out of 13, 23%), perhaps due to the diminished inhibitory transmission which is a feature of this model. However, this effect was not statistically significant (Fisher's exact test, $p > 0.05$). It would be desirable to have gained a larger dataset for the TeNT model, in order to use the more powerful Chi-Square test to examine this difference. It should also be noted that VAMP, and so inhibitory transmission, could have started to recover at this point (Ferecsko et al 14).

In order to be compatible with the hypothesis set out in this study, correlations between the two signals were required in both directions. Significant correlations using action potentials as a trigger lent weight to the idea that inhibitory signalling

could entrain the oscillation, whilst those using HFA as a trigger suggested that the pyramidal cells provided feedback to the interneuron. This was the case for 8 interneurons in the high potassium model and 3 interneurons in the TeNT model. For the 8 correlated interneurons in the high potassium model, the mean phase lags for the two triggers added to almost exactly 360° (Table 4.2), implying a cyclical relationship between the two signals. However, significant correlations were, in some cases, slightly misleading. A significant correlation simply meant that action potentials and HFA were correlated when both were happening. This meant that some interneurons could fire only once or twice during a pathological ripple (see groups 2 and 3 in Figure 4.8) but, because this limited number of action potentials were correlated with the HFA, the Rayleigh statistic was positive. Clearly, an interneuron which fired only one action potential during a sharp-wave ripple complex did not pace the entire oscillation as hypothesised, because it only provided one IPSP to any target. Thus, to truly be a candidate for pacing pathological ripples, interneurons had to fire a high frequency burst of action potentials (group 1 in Figure 4.8) which was correlated using both HFA cycles and cellular firing as triggers. Further, the duration of the action potential burst had to be at least as long as the field burst to support the notion that each action potential triggered each cycle³. In the high potassium model, 4 interneurons met all of these criteria – 3 from stratum oriens and 1 from stratum pyramidale. In the tetanus neurotoxin model, only one cell, located in stratum oriens, did so.

³ As a caveat here, it is possible that interneurons could form a network, possibly linked by gap junctions, whereby each individual interneuron need not fire on every cycle of HFA, as long as one interneuron within the network did so. It would require multiple simultaneous patch clamp recordings from interneurons, during epileptiform bursts, to test this hypothesis.

When taken together, the results from the two models showed that interneurons located in stratum oriens were the most likely candidates to support the hypothesised mechanism. However, this conclusion was not satisfactory because multiple subtypes of interneurons have cell bodies in S.O., including O-LM cells and trilaminar cells (Freund and Buzsaki 96). Immunohistochemistry and anatomical reconstruction of the cells discussed so far were unsuccessful for reasons suggested in section 6.4.1. Thus a small further study, using the high potassium model and focussing on interneurons in S.O., was carried out. An anatomical reconstruction was possible for one cell, summarised in Figure 6.1. This interneuron markedly reduced its firing during sharp wave events, compatible with one of the functional sub-divisions of O-LM cells shown by Spampanato and Mody. This was likely due to GABAergic feedback via interneuron-interneuron interactions, though depolarisation block may play a role. However, prior to ceasing firing, the cell did fire some action potentials and these showed significant correlations with field HFA cycles. Perhaps, therefore, some interneurons are capable of playing a role in HFA, but those which enter are prevented from firing throughout have a limited role. It is important to note that this is only one cell and that anatomically similar interneurons have been shown to have a functional diversity during HFA (Spampanato and Mody 07).

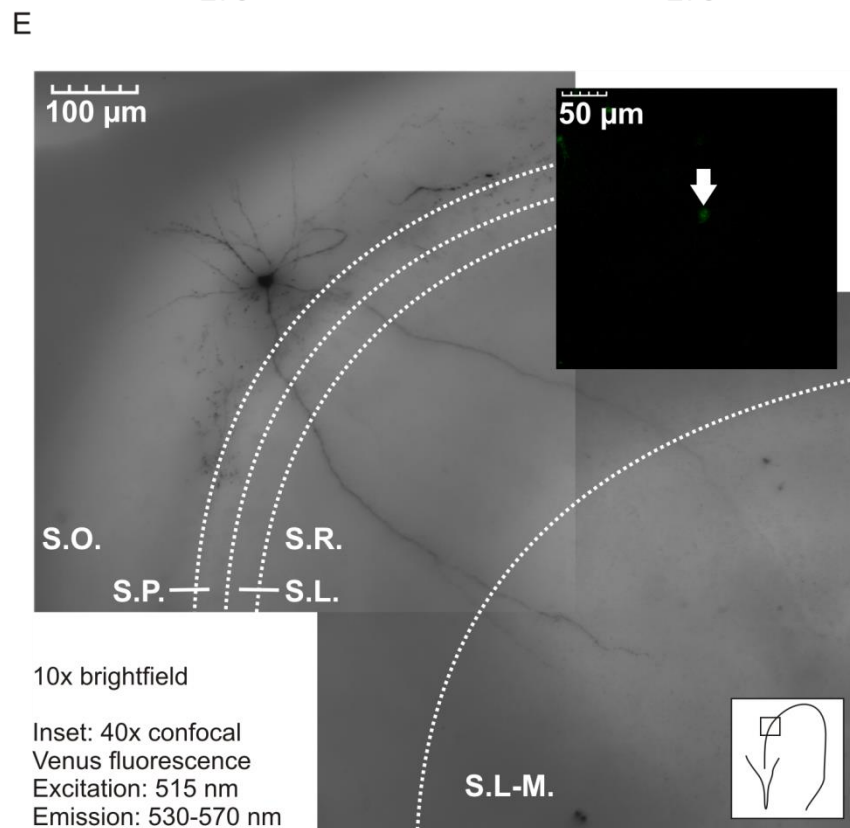
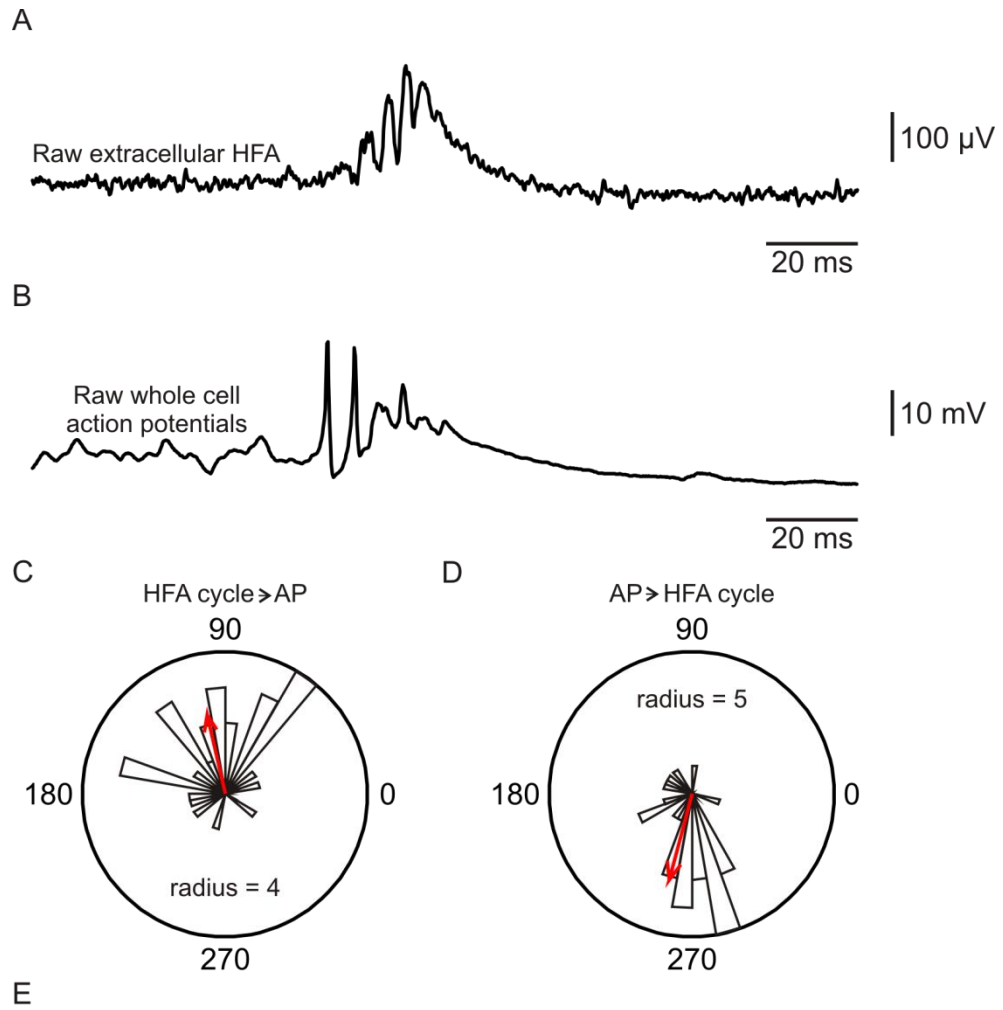


Figure 6.1 – Phase relationships in a visualised CA3 interneuron. *Raw field data (A) and action potentials recorded in whole cell configuration (B) were correlated with each other. Phase correlations using HFA (C) and action potentials (D) as the causative triggers were both significant (Rayleigh statistic, $p < 0.001$). Partial visualisation (E) and Venus fluorescence (E - inset) confirmed that the cell was an interneuron. White dotted lines indicate rough boundaries between the layers of the hippocampus.*

Two other studies into the role of interneurons in HFA, which are comparable with this work, have been published (Karlocai et al 14; Spampanato and Mody 07). This work differs from the former because it examined the precise relationships between the interneurons' firing and HFA and it differs from the latter because it looked at all interneuron sub-types, rather than just one. However, comparisons between the three studies can be beneficial in determining the role of interneurons in HFA.

Using the acute *in vitro* low magnesium model of epilepsy, Spampanato and Mody showed that approximately half of O-LM cells, identified by transgenic fluorescent labelling, in CA3 fired in response to the convulsant perfusate (this is in contrast with the results here from the high potassium model, in which all recorded interneurons fired in some way). Further, amongst those that did fire, there was still a functional diversity within anatomically similar O-LM cells, with some firing high frequency bursts comparable to those in group 1 (Figure 4.8) and some not

firing at all, as in group 4, perhaps due to depolarisation block. Crucially, in those O-LM cells which did fire high frequency bursts throughout HFA, Spampanato and Mody showed that their firing had no relationship with the phase of the field oscillation. Whilst not definitive, this suggests that the correlated interneurons from this study may not have been O-LM cells. Further, that some interneurons are candidates to pace HFA is a novel finding, not seen before in similar studies.

The study by Karlocai et al (14) may shed further light on to the identity of the correlated interneurons. In this work, Karlocai et al recorded the activity of CA3 neurons during spontaneous sharp wave ripples, and compared this behaviour to that during epileptic-like bursts elicited by high potassium. They did not, however, compare the firing of each population of cells with the field oscillation and so their classifications of interneurons, based upon firing patterns in high K^+ , could help to identify the candidate cells for pacing HFA, as identified earlier in this section.

Parvalbumin expressing basket cells were shown to be particularly vulnerable to suppressed firing during epileptic-like field bursts and so were seen to stop firing as HFA cycles began. This effectively rules them out as candidates for pacing HFA. Further, using recordings from pyramidal cells under high K^+ , they showed that IPSCs from basket cells and axo-axonic cells were greatly reduced during field bursts. However, the inhibitory activity of CCK-expressing basket cells remained intact.

Combining the evidence of the present study with that of Spampanato and Mody and Karlocai et al, it appears that CCK-expressing basket cells are a good candidate

for pacing HFA. Firstly, the current work showed that correlated interneurons were limited to those with somata in S.P. and, mainly, in S.O.. This ruled out all of those interneurons with cells bodies in S.R.. Secondly, the work of Spampanato and Mody suggests that O-LM cells, whilst being capable of high frequency bursting during HFA, do not correlate with the field oscillation. Finally, PV-positive basket cells and axo-axonic cells were ruled out by Karlocai et al, who showed that the former are vulnerable to suppressed firing, and thus an absence of firing, during epileptic bursts, and that both of these interneuron subtypes exhibit diminished inhibitory abilities during HFA.

Thus, to summarise, the novel finding of this work was that some interneurons, located in S.O. or S.P., are compatible with the hypothesis of pacing HFA through recurrent high frequency IPSPs. This is the first demonstration that interneuron firing can be correlated with pathological HFA. Anatomical identification of the particular types of interneuron involved was not possible because visualisation with biocytin did not work, but comparison with similar studies suggests that the candidate interneurons may be CCK-expressing basket cells.

6.3.2 Interneurons as a rate-limiting step in pathological 100-300 Hz HFA

The results presented in section 6.3.1 showed that interneurons, which could be CCK-expressing basket cells, are compatible with the hypothesis that they pace HFA via recurrent inhibition. However, in light of other work, this hypothesis may be unrealistic. First of all, both the bicuculline (see appendix) and low calcium (Jiruska et al 10a; Jefferys and Haas 82) acute models of epilepsy produce HFA. In

the former, GABAergic transmission is blocked and in the latter, all synaptic transmission is abolished. That HFA is still present in the absence of synaptic transmission strongly implies that this type of cellular communication is not necessary for the generation of HFA and provides robust evidence against the hypotheses of pacing by interneurons (section 1.2.4.1) and synaptic pyramidal cell coupling (section 1.2.4.2). Nevertheless, this work demonstrated some interneuronal involvement with HFA, though it is unclear what this may be. The finding that oscillations in which interneurons serve as reliable predictors are generally slower (section 4.3.3.1) may provide clarification. Perhaps it is the case that, where interneurons are sufficiently interconnected, they can participate in all (firing pattern group 1) or part (firing pattern group 2) of an oscillation, providing a rate-limiting step and thus slowing the overall frequency. This work thus speculates that epileptiform HFA is generated by another, non-synaptic mechanism, but interneurons do indeed play a role in the modulation of the oscillation. As inhibitory transmission is diminished in chronic epilepsy, interneurons could lose their influence over local circuits. This would result in hyperexcitable networks of pyramidal cells which could be coupled to directly neighbouring cells via gap junctions, giving rise to fast ripple oscillations. This hypothesis is summarised in Figure 6.2.

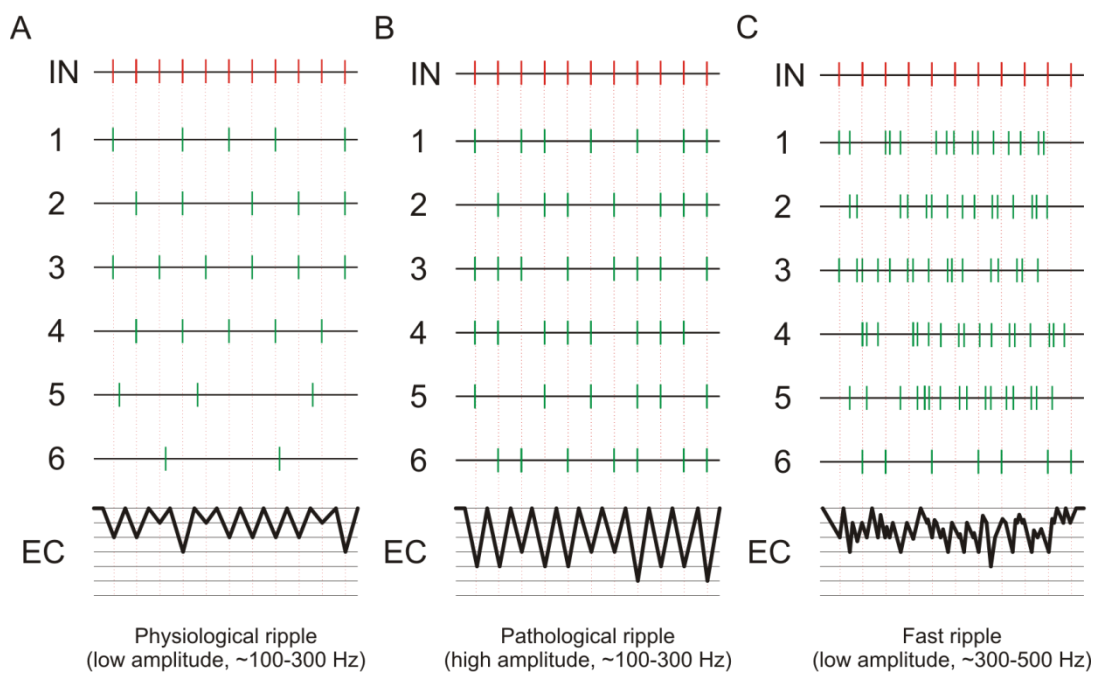
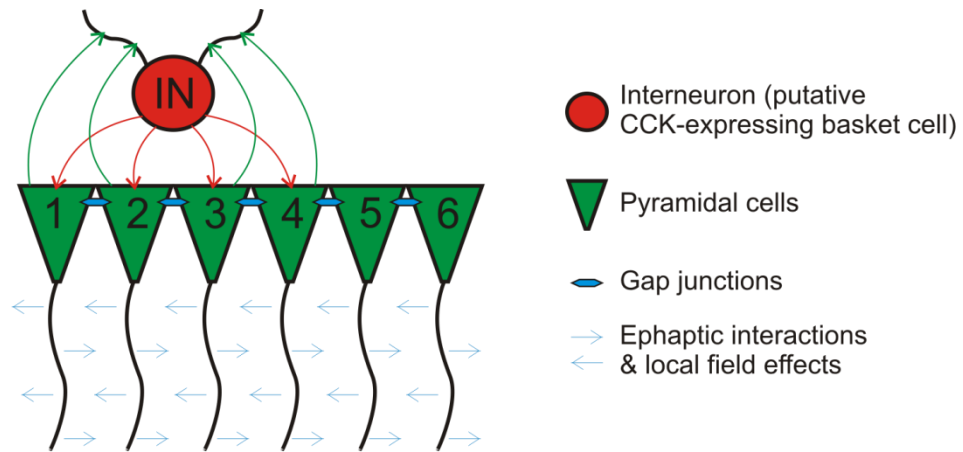


Figure 6.2 - Hypothesised mechanisms for the transition from physiological to pathological HFA. The upper panel shows the hypothesised local circuitry for the generation of HFA. The population of pyramidal cells (green cells, 1-6) output onto a local interneuron (IN) which provides recurrent feedback. In physiological conditions (A), the firing of connected pyramidal cells (1-4) is strongly entrained by the firing of IN (Ylinen et al 95). Each pyramidal cell (1-4) only participates in every second or third HFA cycle, giving rise to a low amplitude ripple band oscillation,

whose maximum frequency is determined by the firing rate of the interneuron. As excitation is increased (B, as in acutely and chronically epileptic tissue), pyramidal cells 1-4 are still entrained by the interneuron, but their enhanced excitability means that they begin to participate in more HFA cycles. Other pyramidal cells, which are not part of the physiological network (cells 5 and 6) also become loosely entrained by other mechanisms such as gap junctional coupling and field interactions, as these effects are more likely to synchronise slightly depolarised neurons (Draguhn et al 98). Therefore a greater number of pyramidal cells participate in each cycle. This gives rise to a larger amplitude oscillation, but the frequency is still dictated by IN. This is hypothesised to be the case for those interneurons shown in figures 4.9 and described in section 4.3.3.1, where phase locking to interneuron firing was associated with slower oscillations. In chronically epileptic tissue (C), the interneuron firing no longer controls the oscillation. This could be due to suppressed interneuron firing (Karlocai et al 14). In this case, other synchronizing mechanisms such as direct coupling between neighbouring pyramidal cells via gap junctions could be important. This would result in small aggregates of highly excitable pyramidal cells. Due to the extremely local nature of this synchronising mechanism, each aggregate would not phase lock to others, giving rise to the low amplitude, high frequency fast ripple oscillation. IN may still be able to have a weak influence on the oscillation if its firing and GABAergic signaling are not entirely impaired. This is thought to be the case in figure 5.11. Thus, the transition from physiological HFA to pathological-like ripples (as seen acutely) and finally fast ripples (unique to chronically epileptic tissue) is thought to

be caused by the gradual decline in the ability of IN to influence to firing of the pyramidal cells.

6.4 Further experimental work

Several limitations mean that it is impossible to definitively state if HFA arises from the inhibitory constraints of a sub-type of interneuron.

6.4.1 Anatomical identification of interneuron subtypes

Firstly, as was attempted for this study, recorded interneurons need to be anatomically reconstructed in order to define the activity of each sub-type during epileptic-like bursts. This required the visualisation of axonal projections from each interneuron (Karlocai et al 14). Identification of these projections was impossible using the VGAT-Venus transgene, due to background fluorescence and overlapping with axons from other interneurons, and so other methods were tried. For this work, recorded cells were filled initially with Alexa 647 in an effort to identify them. This proved problematic for several reasons. Firstly, those recordings made in juxtacellular configuration – which provided acceptable electrophysiological records of firing patterns – did not fill the targeted interneuron with fluorescent dye. In these cases, attempts were made to ‘break through’ the cell membrane following juxtacellular recording in order to fill the interneurons but this did not work – at best the somata would fill and the required projections still could not be seen. As discussed in section 6.1.2, the

membrane chamber did not always supply the mechanical stability required for whole cell recordings and as a result many recordings were made in juxtacellular configuration and thus did not fill with dye. For the TeNT treated slices and the later subset of high K^+ treated slices, the targeted interneurons were filled with biocytin for subsequent processing using DAB staining. For the high K^+ slices, the only successfully filled and stained cell (see Figure 6.1) was recorded in whole cell configuration; juxtacellular labelling was attempted but did not work in the other four. In the TeNT treated slices, even those interneurons which were successfully recorded in whole cell configuration did not show any staining. The reason for this remains unclear – the slices were processed in exactly the same way and with the same reagents at the same time as the successful high K^+ cell. It is possible that interneurons were damaged when removing the patch pipette, causing them to rupture and biocytin to leak out and wash away.

To improve on this, future work must be more discerning in the quality of recordings obtained. It was assumed here that juxtacellular recording was adequate to answer the question set out, because the firing pattern could still be seen. However, whole cell recordings are necessary for sufficient filling and so in future every effort must be made to obtain them. Where juxtacellular recordings are obtained due to failures in obtaining gigaseal recordings caused by mechanical instability, a new electrode must be placed following the juxtacellular recording and a whole cell recording must be obtained with this second electrode in order to gain sufficient filling for DAB staining, as in Karlocai et al (14). The electrophysiology alone is not enough to define specific subtypes of interneuron.

At least with this study the candidate cells were narrowed down to primarily S.O. and occasionally S.P., and so these regions could be targeted by future work.

Efforts were made to speculate as to the identity of the correlated cells using data from similar studies (section 6.3.1), and logical elimination of other cells suggested that CCK expressing basket cells could be involved, because correlated interneurons do exist but many other common sub-types appear to have been ruled out. However, this cannot be stated with any confidence until electrophysiological recordings obtained from anatomically identified CCK positive basket cells are made and fulfil the criteria for pacing HFA.

6.4.2 Establishing causality

One of the major difficulties in interpreting the circular data from this study was that of causality. A correlation between the two signals merely provided evidence of some relationship between the two and gave no indication as to which signal led the other. However, because the hypothesis stated that there was a circular interaction between the pyramidal cell population and a fast-spiking interneuron, it is not necessarily crucial to know which fires first, provided that there is evidence that the firing of one triggers the firing of the other, as is shown by phase correlations using both directions of phase relationship. To be rigorous, it must also be considered that a third event (perhaps the excitatory sharp wave) could cause both the interneuron and pyramidal cells to fire in bursts. It is feasible that the firing of the two populations could not be at all directly related and that they simply fire at similar frequencies in response to the same sharp wave, thus

showing significant correlation and suggesting spurious relationships between the two. This seems unlikely, because it is known that pyramidal cells and perisomatic-targeting interneurons are closely interconnected, as is seen in physiological ripples (Ylinen et al 95). Thus, it is known that the requisite circuitry for interplay between the two is in place and very unlikely that the firing of one population would not affect the other in some way. As a final note, there is some evidence of a collapse in inhibitory transmission in models of epilepsy (Ferecsko et al 14; Karlocai et al 14) and so it could be feasible that the two populations are not capable of interacting in these conditions, despite the circuitry being present.

Clearly, further experiments are required to fully establish causality, and they must be designed carefully. Several attempts were made during this study to ascertain causality, though each suffered its own pitfalls. In the first instance, interneurons held in whole cell current clamp configuration were hyperpolarised using negative holding currents, in order to modulate their firing. If the interneuron were integral to the field HFA, it would follow that the oscillation should change. This was not seen, but it was noted that the hyperpolarisation of one interneuron may not be sufficient to disrupt HFA, as pyramidal cells receive input from multiple interneurons (Traub et al 99) and so another could effectively take over from the hyperpolarised interneuron. Subsequently, experiments using bicuculline to modulate GABAergic inhibition throughout all interneurons were used (see appendix). However, this proved unreliable because bath application of drugs affects the entire slice, rather than just the local circuitry which is hypothesised to generate HFA. It is most desirable to be able to control a specific

population of cells with both temporal and spatial selectivity. This was achieved to an extent by focally applying bicuculline to different layers of CA3 using a picospritzer. Early results hinted that HFA was modulated only when applying the drug to S.O. (A Powell, unpublished observations). This is compatible with the present study, in which interneurons involved with HFA were mainly located in S.O.. This could be explored further by using optogenetic technology (Wykes et al 12), which provides precise temporal and spatial control over a genetically targeted group of cells.

6.4.3 Use of a different chronic model

Whilst the similarities between HFA seen in the two models were fairly convincing, it must also be noted that to induce HFA in the TeNT model, subtle increases in extracellular potassium, usually to 6 mM, were still necessary. Thus it could be argued that, while TeNT treatment had rendered the slices hyperexcitable, the actual epileptic-like response and HFA were induced by an increase in K^+ and so it is unsurprising that the two are so similar. To counter this, it would perhaps have been desirable to prepare *ex vivo* brain slices from chronically epileptic rats at an earlier point in the time course of seizures. Slices were prepared at around 3 weeks post-injection, because VAMP cleavage (Ferecsko et al 14), and so inhibitory transmission, would be recovered by this time point. However, examination of Figure 5.1 shows that animals had typically gained or were nearing remission from spontaneous seizures here and so perhaps this explains why no spontaneous activity was seen in *ex vivo* conditions. To

address concerns about limited inhibitory transmission at this stage during the TeNT model, an alternative model, such as the kainic acid model which is based upon enhanced excitation rather than limited inhibition, could have been used. In this case it could be assumed that inhibitory synapses were intact throughout epileptogenesis and so perhaps would be more appropriate in the investigation of this study's main hypothesis, which relied upon GABAergic inhibition to pace HFA.

6.4.4 *Studying non-synaptic mechanisms*

As suggested in section 6.3.2, it could be that HFA is generated by a non-synaptic mechanism, with interneurons having a modulatory role in the oscillation.

Therefore, whilst the experiments described in sections 6.4.1 and 6.4.2 would serve to discover the role that interneurons play in the phenomenon,

investigations into the outright mechanism of HFA should focus on the non-synaptic hypotheses of synchronisation via gap junctions (section 1.2.4.3) or field effects (section 1.2.4.4). Specific modulation of gap junctions is difficult, due to off-target effects of most pharmacological agents which affect their function.

Perhaps the use of a cre-lox genetic system (Ventura et al 04), to knock out genes encoding gap junctions in specific cells within the hippocampus, could be a method to selectively target gap junctions in just the region of interest. This could be carried out either *in vivo* or *ex vivo*. Gap junctions between interneurons throughout the hippocampus contain connexin 36 (Allen et al 11). The same protein is expressed in CA3 pyramidal cells (Condorelli et al 00) and so it could be a potential target for knock-out. Several studies described in the introduction

have used field effects to modulate cellular excitability *in vitro* in hippocampal slices, though none has ever analysed the effects of applied electrical fields on HFA. Fields could be applied locally to the region of interest using a monopolar stimulating electrode and any number of stimulation parameters. Thus, this would provide spatial and temporal control over the applied fields and provide a method to study their effect on HFA.

6.5 Concluding remarks

This study set out to investigate whether HFA arises as a result of recurrent inhibition from perisomatic-targeting interneurons, and to do this it was also necessary to establish the use of the membrane chamber.

The first novel finding of the study was that the membrane chamber facilitated simultaneous extracellular and intracellular recordings, as well as high magnification imaging, whilst retaining robust slice physiology. It therefore provides a valuable new tool for *in vitro* electrophysiology.

The second novel finding was the presence of a pathological ripple oscillation common to both models of epilepsy. Conventionally, oscillations from 100-200/250 Hz have been considered physiological, though more recently doubt has been correctly cast over the use of frequency alone as a classifier. A pathological ripple oscillation, between 100-300 Hz, was different from both spontaneous

physiological sharp wave ripples observed by others (Karlocai et al 14) and epileptic-like fast ripples seen in this study in the TeNT model.

Finally, this work showed for the first time that interneurons, located mainly in S.O. and possibly CCK-expressing basket cells, can correlate with pathological HFA. Previous work has shown that firing of interneurons correlate with physiological HFA (Ylinen et al 95) but, where correlations have been made between certain interneurons and pathological oscillations, no relationship was found (Spampanato and Mody 07). However, it is probably spurious to state that interneurons provide the outright mechanism for HFA because the phenomenon can occur in absence of inhibitory synaptic transmission. Therefore, this study suggests that the role of interneurons in pathological HFA is modulatory and serves to slow down existing oscillations, which arise from non-synaptic mechanisms.

REFERENCE LIST

Alberts,B., Johnson,A., Lewis,J., Raff,M., Roberts,K. & Walter,P. (2008) *Molecular Biology of the Cell* Garland Science.

Allen,K., Fuchs,E.C., Jaschonek,H., Bannerman,D.M. & Monyer,H. (2011) Gap junctions between interneurons are required for normal spatial coding in the hippocampus and short-term spatial memory. *J.Neurosci.*, **31**, 6542-6552.

Allen,P.J., Fish,D.R. & Smith,S.J. (1992) Very high-frequency rhythmic activity during SEEG suppression in frontal lobe epilepsy. *Electroencephalogr.Clin.Neurophysiol.*, **82**, 155-159.

Amaral,D.G. (1993) Emerging principles of intrinsic hippocampal organization. *Curr.Opin.Neurobiol.*, **3**, 225-229.

Arvanitaki,A. (1942) Effects Evoked in an Axon by the Activity of a Contiguous One. *J.Neurophysiol.*, **5**, 89-108.

Ascoli,G.A., Alonso-Nanclares,L., Anderson,S.A., Barrionuevo,G., Benavides-Piccione,R., Burkhalter,A., Buzsaki,G., Cauli,B., Defelipe,J., Fairen,A., Feldmeyer,D., Fishell,G., Fregnac,Y., Freund,T.F., Gardner,D., Gardner,E.P., Goldberg,J.H., Helmstaedter,M., Hestrin,S., Karube,F., Kisvarday,Z.F., Lambolez,B., Lewis,D.A., Marin,O., Markram,H., Munoz,A., Packer,A., Petersen,C.C., Rockland,K.S., Rossier,J., Rudy,B., Somogyi,P., Staiger,J.F., Tamas,G., Thomson,A.M., Toledo-Rodriguez,M., Wang,Y., West,D.C. & Yuste,R. (2008) Petilla terminology: nomenclature of features of GABAergic interneurons of the cerebral cortex. *Nat.Rev.Neurosci.*, **9**, 557-568.

Axmacher,N., Mormann,F., Fernandez,G., Elger,C.E. & Fell,J. (2006) Memory formation by neuronal synchronization. *Brain Res.Rev.*, **52**, 170-182.

Babiloni C, Babiloni F, Carducci F, Cincotti F, Rosciarelli F, Arendt-Nielsen L, Chen AC, Rossini PM (2002) Human brain oscillatory activity phase-locked to painful electrical stimulations: a multi-channel EEG study. *Hum Brain Mapp* 15:112-123.

Banerjee,P.N., Filippi,D. & Allen,H.W. (2009) The descriptive epidemiology of epilepsy-a review. *Epilepsy Res.*, **85**, 31-45.

Bikson,M., Fox,J.E. & Jefferys,J.G. (2003) Neuronal aggregate formation underlies spatiotemporal dynamics of nonsynaptic seizure initiation. *J.Neurophysiol.*, **89**, 2330-2333.

Bikson,M., Inoue,M., Akiyama,H., Deans,J.K., Fox,J.E., Miyakawa,H. & Jefferys,J.G. (2004) Effects of uniform extracellular DC electric fields on excitability in rat hippocampal slices in vitro. *J.Physiol*, **557**, 175-190.

Bliss,T.V. & Lomo,T. (1973) Long-lasting potentiation of synaptic transmission in the dentate area of the anaesthetized rabbit following stimulation of the perforant path. *J.Physiol*, **232**, 331-356.

Borck,C. & Jefferys,J.G. (1999) Seizure-like events in disinhibited ventral slices of adult rat hippocampus. *J.Neurophysiol.*, **82**, 2130-2142.

Bragdon,A.C., Taylor,D.M. & Wilson,W.A. (1986) Potassium-induced epileptiform activity in area CA3 varies markedly along the septotemporal axis of the rat hippocampus. *Brain Res.*, **378**, 169-173.

Bragin,A., Azizyan,A., Almajano,J., Wilson,C.L. & Engel,J., Jr. (2005) Analysis of chronic seizure onsets after intrahippocampal kainic acid injection in freely moving rats. *Epilepsia*, **46**, 1592-1598.

Bragin,A., Engel,J., Jr., Wilson,C.L., Fried,I. & Buzsaki,G. (1999a) High-frequency oscillations in human brain. *Hippocampus*, **9**, 137-142.

Bragin,A., Engel,J., Jr., Wilson,C.L., Fried,I. & Mathern,G.W. (1999b) Hippocampal and entorhinal cortex high-frequency oscillations (100--500 Hz) in human epileptic brain and in kainic acid--treated rats with chronic seizures. *Epilepsia*, **40**, 127-137.

Bragin,A., Engel,J., Jr., Wilson,C.L., Vizentin,E. & Mathern,G.W. (1999c) Electrophysiologic analysis of a chronic seizure model after unilateral hippocampal KA injection. *Epilepsia*, **40**, 1210-1221.

Bragin,A., Wilson,C.L., Almajano,J., Mody,I. & Engel,J., Jr. (2004) High-frequency oscillations after status epilepticus: epileptogenesis and seizure genesis. *Epilepsia*, **45**, 1017-1023.

Bragin,A., Wilson,C.L. & Engel,J. (2003) Spatial stability over time of brain areas generating fast ripples in the epileptic rat. *Epilepsia*, **44**, 1233-1237.

Buckmaster,P.S. & Lew,F.H. (2011) Rapamycin suppresses mossy fiber sprouting but not seizure frequency in a mouse model of temporal lobe epilepsy. *J.Neurosci.*, **31**, 2337-2347.

Buzsaki,G. (1986) Hippocampal sharp waves: their origin and significance. *Brain Res.*, **398**, 242-252.

Buzsaki,G., Horvath,Z., Urioste,R., Hetke,J. & Wise,K. (1992) High-frequency network oscillation in the hippocampus. *Science*, **256**, 1025-1027.

Cavazos,J.E., Jones,S.M. & Cross,D.J. (2004) Sprouting and synaptic reorganization in the subiculum and CA1 region of the hippocampus in acute and chronic models of partial-onset epilepsy. *Neuroscience*, **126**, 677-688.

Cavazos,J.E. & Sutula,T.P. (1990) Progressive neuronal loss induced by kindling: a possible mechanism for mossy fiber synaptic reorganization and hippocampal sclerosis. *Brain Res.*, **527**, 1-6.

Cohen,I. & Miles,R. (2000) Contributions of intrinsic and synaptic activities to the generation of neuronal discharges in in vitro hippocampus. *J.Physiol*, **524 Pt 2**, 485-502.

Condorelli,D.F., Belluardo,N., Trovato-Salinaro,A. & Mudo,G. (2000) Expression of Cx36 in mammalian neurons. *Brain Res.Brain Res.Rev.*, **32**, 72-85.

Coulter,D.A., Yue,C., Ang,C.W., Weissinger,F., Goldberg,E., Hsu,F.C., Carlson,G.C. & Takano,H. (2011) Hippocampal microcircuit dynamics probed using optical imaging approaches. *J.Physiol*, **589**, 1893-1903.

Csicsvari,J., Hirase,H., Czurko,A., Mamiya,A. & Buzsaki,G. (1999) Oscillatory coupling of hippocampal pyramidal cells and interneurons in the behaving Rat. *J.Neurosci.*, **19**, 274-287.

Deans,J.K., Powell,A.D. & Jefferys,J.G. (2007) Sensitivity of coherent oscillations in rat hippocampus to AC electric fields. *J.Physiol*, **583**, 555-565.

Deuchars J, Thomson AM (1996) CA1 pyramid-pyramid connections in rat hippocampus in vitro: dual intracellular recordings with biocytin filling. *Neuroscience* 74:1009-1018.

Draguhn,A., Traub,R.D., Schmitz,D. & Jefferys,J.G. (1998) Electrical coupling underlies high-frequency oscillations in the hippocampus in vitro. *Nature*, **394**, 189-192.

Dudek,F.E., Yasumura,T. & Rash,J.E. (1998) 'Non-synaptic' mechanisms in seizures and epileptogenesis. *Cell Biol.Int.*, **22**, 793-805.

Dzhala,V.I. & Staley,K.J. (2004) Mechanisms of fast ripples in the hippocampus. *J.Neurosci.*, **24**, 8896-8906.

Engel,J., Jr. (2001) A proposed diagnostic scheme for people with epileptic seizures and with epilepsy: report of the ILAE Task Force on Classification and Terminology. *Epilepsia*, **42**, 796-803.

Ferecsko,A.S., Jiruska,P., Foss,L., Powell,A.D., Chang,W.C., Sik,A. & Jefferys,J.G. (2014) Structural and functional substrates of tetanus toxin in an animal model of temporal lobe epilepsy. *Brain Struct.Funct.*.

Fisher,N.I. (1995) *Statistical Analysis of Circular Data* Cambridge University Press.

- Fisher,R.S., Webber,W.R., Lesser,R.P., Arroyo,S. & Uematsu,S. (1992) High-frequency EEG activity at the start of seizures. *J.Clin.Neurophysiol.*, **9**, 441-448.
- Foffani,G., Uzcategui,Y.G., Gal,B. & Menendez,d.I.P. (2007) Reduced spike-timing reliability correlates with the emergence of fast ripples in the rat epileptic hippocampus. *Neuron*, **55**, 930-941.
- Francis,J.T., Gluckman,B.J. & Schiff,S.J. (2003) Sensitivity of neurons to weak electric fields. *J.Neurosci.*, **23**, 7255-7261.
- Freund,T.F. & Buzsaki,G. (1996) Interneurons of the hippocampus. *Hippocampus*, **6**, 347-470.
- Fukuda,T. & Kosaka,T. (2000) Gap junctions linking the dendritic network of GABAergic interneurons in the hippocampus. *J.Neurosci.*, **20**, 1519-1528.
- Gilbert,M., Racine,R.J. & Smith,G.K. (1985) Epileptiform burst responses in ventral vs dorsal hippocampal slices. *Brain Res.*, **361**, 389-391.
- Girardeau,G., Benchenane,K., Wiener,S.I., Buzsaki,G. & Zugaro,M.B. (2009) Selective suppression of hippocampal ripples impairs spatial memory. *Nat.Neurosci.*, **12**, 1222-1223.

Goldensohn,E.S. & Purpura,D.P. (1963) Intracellular potentials of cortical neurons during focal epileptogenic discharges. *Science*, **139**, 840-842.

Grenier,F., Timofeev,I., Crochet,S. & Steriade,M. (2003) Spontaneous field potentials influence the activity of neocortical neurons during paroxysmal activities in vivo. *Neuroscience*, **119**, 277-291.

Haas,K.F. & Macdonald,R.L. (1999) GABAA receptor subunit gamma2 and delta subtypes confer unique kinetic properties on recombinant GABAA receptor currents in mouse fibroblasts. *J.Physiol*, **514 (Pt 1)**, 27-45.

Hajos,N., Ellender,T.J., Zemanekovics,R., Mann,E.O., Exley,R., Cragg,S.J., Freund,T.F. & Paulsen,O. (2009) Maintaining network activity in submerged hippocampal slices: importance of oxygen supply. *Eur.J.Neurosci.*, **29**, 319-327.

Hajos,N. & Mody,I. (2009) Establishing a physiological environment for visualized in vitro brain slice recordings by increasing oxygen supply and modifying aCSF content. *J.Neurosci.Methods*, **183**, 107-113.

Hamzei-Sichani,F., Davidson,K.G., Yasumura,T., Janssen,W.G., Wearne,S.L., Hof,P.R., Traub,R.D., Gutierrez,R., Ottersen,O.P. & Rash,J.E. (2012) Mixed Electrical-Chemical Synapses in Adult Rat Hippocampus are Primarily Glutamatergic and Coupled by Connexin-36. *Front Neuroanat.*, **6**, 13.

Hill,M.R. & Greenfield,S.A. (2011) The membrane chamber: a new type of in vitro recording chamber. *J.Neurosci.Methods*, **195**, 15-23.

Hill,M.R. & Greenfield,S.A. (2013) Characterization of early cortical population response to thalamocortical input in vitro. *Front Neurosci.*, **7**, 273.

Jefferys,J.G. (1981) Influence of electric fields on the excitability of granule cells in guinea-pig hippocampal slices. *J.Physiol*, **319**, 143-152.

Jefferys,J.G. (1989) Chronic epileptic foci in vitro in hippocampal slices from rats with the tetanus toxin epileptic syndrome. *J.Neurophysiol.*, **62**, 458-468.

Jefferys,J.G. (1995) Nonsynaptic modulation of neuronal activity in the brain: electric currents and extracellular ions. *Physiol Rev.*, **75**, 689-723.

Jefferys,J.G. & Haas,H.L. (1982) Synchronized bursting of CA1 hippocampal pyramidal cells in the absence of synaptic transmission. *Nature*, **300**, 448-450.

Jefferys,J.G., Menendez,d.I.P., Wendling,F., Bragin,A., Avoli,M., Timofeev,I. & Lopes da Silva,F.H. (2012) Mechanisms of physiological and epileptic HFO generation. *Prog.Neurobiol.*, **98**, 250-264.

Jiruska,P., Csicsvari,J., Powell,A.D., Fox,J.E., Chang,W.C., Vreugdenhil,M., Li,X., Palus,M., Bujan,A.F., Dearden,R.W. & Jefferys,J.G. (2010a) High-frequency

network activity, global increase in neuronal activity, and synchrony expansion precede epileptic seizures in vitro. *J.Neurosci.*, **30**, 5690-5701.

Jiruska,P., Finnerty,G.T., Powell,A.D., Lofti,N., Cmejla,R. & Jefferys,J.G. (2010b) Epileptic high-frequency network activity in a model of non-lesional temporal lobe epilepsy. *Brain*, **133**, 1380-1390.

Jiruska,P., Powell,A.D., Chang,W.C. & Jefferys,J.G. (2010c) Electrographic high-frequency activity and epilepsy. *Epilepsy Res.*, **89**, 60-65.

Karlocai,M.R., Kohus,Z., Kali,S., Ulbert,I., Szabo,G., Mate,Z., Freund,T.F. & Gulyas,A.I. (2014) Physiological sharp wave-ripples and interictal events in vitro: what's the difference? *Brain*, **137**, 463-485.

Kerber,K., Dumpelmann,M., Schelter,B., Le,V.P., Korinthenberg,R., Schulze-Bonhage,A. & Jacobs,J. (2013) Differentiation of specific ripple patterns helps to identify epileptogenic areas for surgical procedures. *Clin.Neurophysiol.*

Khazipov,R., Congar,P. & Ben-Ari,Y. (1995) Hippocampal CA1 lacunosum-moleculare interneurons: modulation of monosynaptic GABAergic IPSCs by presynaptic GABAB receptors. *J.Neurophysiol.*, **74**, 2126-2137.

Klausberger,T. & Somogyi,P. (2008) Neuronal diversity and temporal dynamics: the unity of hippocampal circuit operations. *Science*, **321**, 53-57.

Kohrman,M.H. (2007) What is epilepsy? Clinical perspectives in the diagnosis and treatment. *J.Clin.Neurophysiol.*, **24**, 87-95.

Levesque,M., Bortel,A., Gotman,J. & Avoli,M. (2011) High-frequency (80-500 Hz) oscillations and epileptogenesis in temporal lobe epilepsy. *Neurobiol.Dis.*, **42**, 231-241.

Li,X.G., Somogyi,P., Tepper,J.M. & Buzsaki,G. (1992) Axonal and dendritic arborization of an intracellularly labeled chandelier cell in the CA1 region of rat hippocampus. *Exp.Brain Res.*, **90**, 519-525.

Lian,J., Bikson,M., Sciortino,C., Stacey,W.C. & Durand,D.M. (2003) Local suppression of epileptiform activity by electrical stimulation in rat hippocampus in vitro. *J.Physiol*, **547**, 427-434.

MacVicar,B.A. & Dudek,F.E. (1981) Electrotonic coupling between pyramidal cells: a direct demonstration in rat hippocampal slices. *Science*, **213**, 782-785.

Maris,E., van,V.M. & Kahana,M. (2011) Spatially distributed patterns of oscillatory coupling between high-frequency amplitudes and low-frequency phases in human iEEG. *Neuroimage.*, **54**, 836-850.

McBain,C.J., Traynelis,S.F. & Dingledine,R. (1990) Regional variation of extracellular space in the hippocampus. *Science*, **249**, 674-677.

Mellanby,J., George,G., Robinson,A. & Thompson,P. (1977) Epileptiform syndrome in rats produced by injecting tetanus toxin into the hippocampus.

J.Neurol.Neurosurg.Psychiatry, **40**, 404-414.

Nagai,T., Ibata,K., Park,E.S., Kubota,M., Mikoshiba,K. & Miyawaki,A. (2002) A variant of yellow fluorescent protein with fast and efficient maturation for cell-biological applications. *Nat.Biotechnol.*, **20**, 87-90.

Oliva,A.A., Jr., Jiang,M., Lam,T., Smith,K.L. & Swann,J.W. (2000) Novel hippocampal interneuronal subtypes identified using transgenic mice that express green fluorescent protein in GABAergic interneurons. *J.Neurosci.*, **20**, 3354-3368.

Peinado,A., Yuste,R. & Katz,L.C. (1993) Extensive dye coupling between rat neocortical neurons during the period of circuit formation. *Neuron*, **10**, 103-114.

Pellizzari,R., Rossetto,O., Schiavo,G. & Montecucco,C. (1999) Tetanus and botulinum neurotoxins: mechanism of action and therapeutic uses.

Philos.Trans.R.Soc.Lond B Biol.Sci., **354**, 259-268.

Perez-Velazquez,J.L., Valiante,T.A. & Carlen,P.L. (1994) Modulation of gap junctional mechanisms during calcium-free induced field burst activity: a possible role for electrotonic coupling in epileptogenesis. *J.Neurosci.*, **14**, 4308-4317.

Racine,R.J. (1972) Modification of seizure activity by electrical stimulation. II.

Motor seizure. *Electroencephalogr.Clin.Neurophysiol.*, **32**, 281-294.

Rudy,B. & McBain,C.J. (2001) Kv3 channels: voltage-gated K⁺ channels designed for high-frequency repetitive firing. *Trends Neurosci.*, **24**, 517-526.

Schiavo,G., Matteoli,M. & Montecucco,C. (2000) Neurotoxins affecting neuroexocytosis. *Physiol Rev.*, **80**, 717-766.

Schmitz,D., Schuchmann,S., Fisahn,A., Draguhn,A., Buhl,E.H., Petrasch-Parwez,E., Dermietzel,R., Heinemann,U. & Traub,R.D. (2001) Axo-axonal coupling. a novel mechanism for ultrafast neuronal communication. *Neuron*, **31**, 831-840.

Shin,M.C., Nonaka,K., Wakita,M., Yamaga,T., Torii,Y., Harakawa,T., Ginnaga,A., Ito,Y. & Akaike,N. (2012) Effects of tetanus toxin on spontaneous and evoked transmitter release at inhibitory and excitatory synapses in the rat SDCN neurons. *Toxicon*, **59**, 385-392.

Siddiqui,A.H. & Joseph,S.A. (2005) CA3 axonal sprouting in kainate-induced chronic epilepsy. *Brain Res.*, **1066**, 129-146.

Spampanato,J. & Mody,I. (2007) Spike timing of lacunosom-moleculare targeting interneurons and CA3 pyramidal cells during high-frequency network oscillations in vitro. *J.Neurophysiol.*, **98**, 96-104.

Standen,N.B. (1994) *Microelectrode Techniques: The Plymouth Workshop Handbook* Company of Biologists.

Tamamaki,N., Yanagawa,Y., Tomioka,R., Miyazaki,J., Obata,K. & Kaneko,T. (2003) Green fluorescent protein expression and colocalization with calretinin, parvalbumin, and somatostatin in the GAD67-GFP knock-in mouse. *J.Comp Neurol.*, **467**, 60-79.

Tellez-Zenteno,J.F. & Hernandez-Ronquillo,L. (2012) A review of the epidemiology of temporal lobe epilepsy. *Epilepsy Res.Treat.*, **2012**, 630853.

Tovar,K.R., Maher,B.J. & Westbrook,G.L. (2009) Direct actions of carbenoxolone on synaptic transmission and neuronal membrane properties. *J.Neurophysiol.*, **102**, 974-978.

Traub,R., Jefferys,J.G. & Whittington,M.A. (1999) *Fast Oscillations in Cortical Circuits* MIT Press.

Traub,R.D., Dudek,F.E., Snow,R.W. & Knowles,W.D. (1985) Computer simulations indicate that electrical field effects contribute to the shape of the epileptiform field potential. *Neuroscience*, **15**, 947-958.

Traynelis,S.F. & Dingledine,R. (1988) Potassium-induced spontaneous electrographic seizures in the rat hippocampal slice. *J.Neurophysiol.*, **59**, 259-276.

Uematsu,M., Hirai,Y., Karube,F., Ebihara,S., Kato,M., Abe,K., Obata,K., Yoshida,S., Hirabayashi,M., Yanagawa,Y. & Kawaguchi,Y. (2008) Quantitative chemical composition of cortical GABAergic neurons revealed in transgenic venus-expressing rats. *Cereb.Cortex*, **18**, 315-330.

van Drongelen,W. (2010) *Signal Processing for Neuroscientists, A Companion Volume: Advanced Topics, Nonlinear Techniques and Multi-Channel Analysis* Elsevier Insights.

Ventura,A., Meissner,A., Dillon,C.P., McManus,M., Sharp,P.A., Van,P.L., Jaenisch,R. & Jacks,T. (2004) Cre-lox-regulated conditional RNA interference from transgenes. *Proc.Natl.Acad.Sci.U.S.A*, **101**, 10380-10385.

Vivar,C., Traub,R.D. & Gutierrez,R. (2012) Mixed electrical-chemical transmission between hippocampal mossy fibers and pyramidal cells. *Eur.J.Neurosci.*, **35**, 76-82.

Vreugdenhil,M., Hack,S.P., Draguhn,A. & Jefferys,J.G. (2002) Tetanus toxin induces long-term changes in excitation and inhibition in the rat hippocampal CA1 area. *Neuroscience*, **114**, 983-994.

Weiss,S.A., McKhann,G., Jr., Goodman,R., Emerson,R.G., Trevelyan,A., Bikson,M. & Schevon,C.A. (2013) Field effects and ictal synchronization: insights from in homine observations. *Front Hum.Neurosci.*, **7**, 828.

White,W.F., Nadler,J.V. & Cotman,C.W. (1978) A perfusion chamber for the study of CNS physiology and pharmacology in vitro. *Brain Res.*, **152**, 591-596.

Whittington,M.A., Traub,R.D. & Jefferys,J.G. (1995) Synchronized oscillations in interneuron networks driven by metabotropic glutamate receptor activation. *Nature*, **373**, 612-615.

Wiebe,S., Blume,W.T., Girvin,J.P. & Eliasziw,M. (2001) A randomized, controlled trial of surgery for temporal-lobe epilepsy. *N.Engl.J.Med.*, **345**, 311-318.

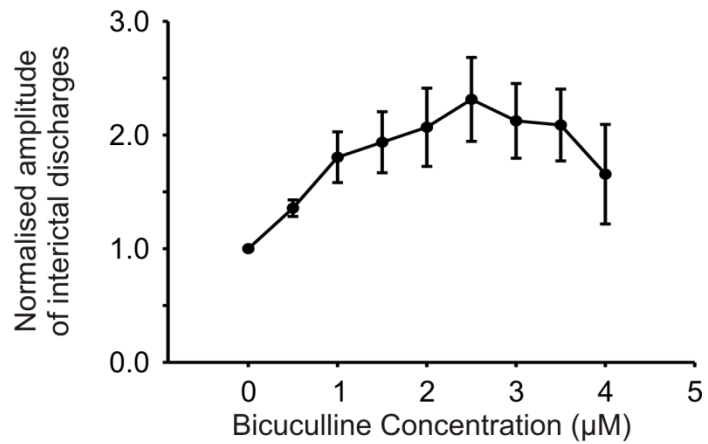
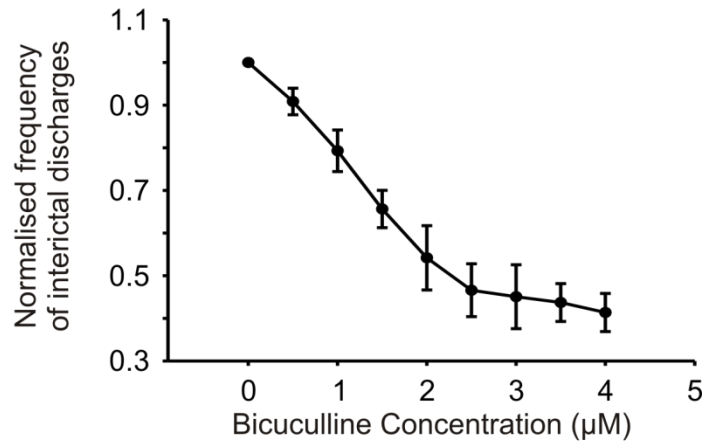
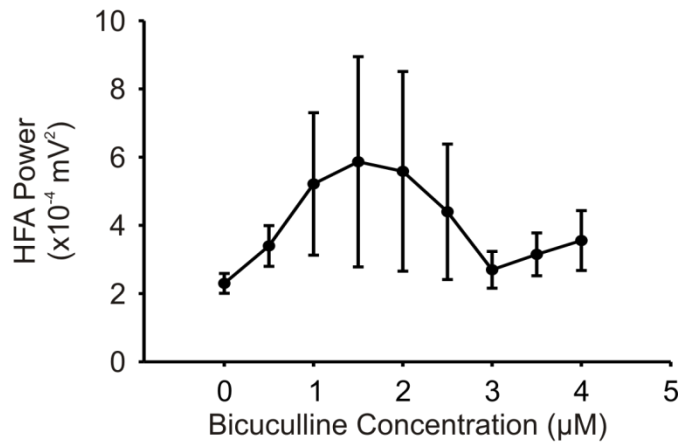
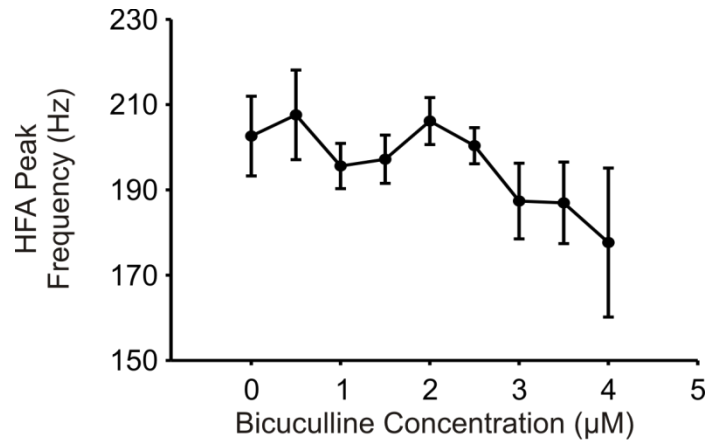
Wykes,R.C., Heeroma,J.H., Mantoan,L., Zheng,K., MacDonald,D.C., Deisseroth,K., Hashemi,K.S., Walker,M.C., Schorge,S. & Kullmann,D.M. (2012) Optogenetic and potassium channel gene therapy in a rodent model of focal neocortical epilepsy. *Sci.Transl.Med.*, **4**, 161ra152.

Ylinen,A., Bragin,A., Nadasdy,Z., Jando,G., Szabo,I., Sik,A. & Buzsaki,G. (1995) Sharp wave-associated high-frequency oscillation (200 Hz) in the intact hippocampus: network and intracellular mechanisms. *J.Neurosci.*, **15**, 30-46.

APPENDIX – PHARMACOLOGICAL MANIPULATION OF

HFA

The following page contains graphs which display the changes in various parameters of epileptiform bursts and HFA in response to slowly increasing concentrations of bicuculline methiodide. These data do not provide a reliable indicator of the effect of local interneuron circuits on HFA, because the drug was bath applied and so modulated GABAergic inhibition throughout the slice and lacked the spatial stability that is required for the probing of local circuitry (see section 6.4.2). Nevertheless, the observation that HFA was still present when GABAergic inhibition was blocked showed that the generation of HFA did not rely on interneuronal signalling of any kind.



APPENDIX – PUBLISHED ABSTRACTS

International Union of Physiological Sciences – Poster presentation, Birmingham, July 2013

Morris, G, Jiruska, P, Chang, W, Powell, AD, Jefferys, JGR

Investigating the role of interneurons in epileptic high frequency activity

Temporal Lobe Epilepsy is the most common form of epilepsy - a neurological disorder characterised by abnormal excitation and synchronisation of neuronal networks. High frequency activity (HFA) is defined as network activity with frequency of over 100 Hz and is a biomarker for the epileptic hippocampus. The underlying mechanism is unknown, but it is hypothesised that interneurons, which are capable of firing action potentials (APs) at frequencies in the HFA range, could synchronise local pyramidal cell activity. High frequency interneuronal firing imposes synchronous IPSPs upon on a population of pyramidal cells, creating temporal windows in which they can fire. This could lead to synchronised high frequency population events. Using the VGAT-Venus A strain of rats that selectively express the fluorescent Venus protein in interneurons, we have examined the role of hippocampal interneurons in the genesis of HFA. Adult VGAT-Venus A rats were anaesthetised with 0.24mg/kg medetomidine and 58.2mg/kg ketamine via I.P. injection before transcardial perfusion with sucrose

aCSF, and 300 μm horizontal brain slice preparation. Extracellular recordings were made from stratum pyramidale (SP) in hippocampal region CA3b. Interictal-like discharges (ILDs) were induced by superfusion of the slices with high potassium (9mM). Following induction of ILDs, whole-cell patch clamp recordings were made from interneurons, irrespective of location, which were identified using fluorescence microscopy. Data is given as the mean \pm SEM. Superfusion of high potassium generated ILDs (frequency = $0.72 \pm 0.04 \text{ Hz}$; $n=11$), on which HFA ($190.6 \pm 9.8 \text{ Hz}$; $n=10$) was superimposed. Interneurons were divided into four categories, as defined by their firing pattern. Group 1 neurons fired throughout ILDs and correlated with HFA (mean max. firing frequency = 207.5 ; $n=2$), whilst group 2 neurons fired throughout ILDs but were not correlated with HFA ($182.50 \pm 20.4 \text{ Hz}$; $n=4$). Group 3 neurons fired a single AP on each ILD ($n=2$) whereas group 4 neurons fired randomly except for 2-3 APs at the onset of each ILD ($120 \pm 31.8 \text{ Hz}$; $n=3$). Those neurons whose activity correlated with HFA were found in SP and stratum oriens and those which fire single APs were found in SP and stratum radiatum. Interneurons which are capable of maintaining HFA frequency firing, but do not correlate with HFA, were found throughout the layers of the hippocampus. These results show that a sub-population of interneurons correlate with HFA and are candidates for pacing this activity. Pharmacological or electrophysiological manipulation of candidate cells has the potential to affect epileptic field activity by reducing the pathological synchronisation of pyramidal cell activity.

Where applicable, experiments conform with Society ethical requirements.

American Epilepsy Society – Poster presentation,

Washington, D.C., December 2013

Morris, G., Powell, A.D., Jiruska, P., Jefferys, J.G.R.

Interneuron firing patterns during High Frequency Activity

Rationale

High frequency activity (HFA) is defined as brain activity faster than 100Hz. It can be subdivided into ripples (100-~200Hz), which occur during normal function, and fast ripples (~200-500Hz), which are associated with epileptic tissue. HFA requires the synchronisation of pyramidal cells on a millisecond timescale and the mechanism for this is unclear. One hypothesis is that fast-spiking interneurons create this synchronisation by imposing short temporal windows on their many target pyramidal cells, causing them to fire in synchrony at high frequency.

Methods

300µm horizontal brain slices were prepared from VGAT-Venus A rats, which selectively express a fluorescent protein in interneurons that enables visually targeted recordings. Extracellular fields in hippocampal CA3b stratum pyramidale were recorded simultaneously with single cell interneuron activity under 9mM potassium. Event correlation, on a 10 ms timescale, between HFA troughs and action potential peaks determined the temporal relationship of each interneuron with the oscillation. Event correlations were tested for statistical significance using

a Kolmogorov-Smirnov test against a uniform distribution ($\alpha=0.05$). Results are presented as mean \pm SEM.

Results

HFA (frequency $212\pm 9\text{Hz}$; power $820\pm 150\mu\text{V}^2$; $n=18$ slices), which was superimposed on interictal-like discharges (frequency = $0.8\pm 0.04\text{Hz}$), was induced in elevated potassium. 14 out of 19 recorded cells increased firing frequency by $463\pm 87\%$ during interictal discharges and the remaining 5 fired exclusively during interictal discharges. In all cells, action potential amplitude decreased during interictal discharges to an average of $47\pm 6\%$. 7 out of 19 cells showed significant correlation, of which 6 were located in stratum oriens and 1 in stratum pyramidale. The 12 uncorrelated cells were found in all layers of the hippocampus.

Conclusions

A subset of interneurons is involved in HFA and is located in stratum oriens and stratum pyramidale. Targeted manipulation of these interneurons has the potential to modulate HFA and epileptic pathophysiology.

Physiology 2014 - Oral Presentation

London, June 2014

Examining the role of interneurons in high frequency activity

in vitro

High frequency activity (HFA) is a phenomenon where neuronal networks oscillate at frequencies faster than 100 Hz. Physiological HFA ('ripple band') is implicated in learning and memory and has a frequency of around 100-200 Hz. Network ripples in the hippocampus *in vivo* are tightly phase-locked to the firing of certain interneurons, implying a causative relationship and a pacemaker role for the interneuron within the oscillation (Csicsvari et al 99; Ylinen et al 95). HFA that is faster than 200 Hz ('fast ripple band') is unique to the epileptic brain (Bragin et al 99). The mechanism underlying fast ripples is unknown and could give an insight into the pathophysiology of epilepsy, with the potential to identify new therapeutic targets. This work examined the relationship between interneuron firing and HFA in the acute high potassium model of epilepsy *in vitro*.

300 μ m horizontal brain slices were prepared from adult VGAT-Venus A rats (Uematsu et al 08), following cardiac perfusion with sucrose aCSF. Rats were anaesthetised with 0.24mg/kg medetomidine and 58.2mg/kg ketamine via i.p. injection. Epileptic-like activity, including HFA, was induced by bath perfusion of 9mM potassium. Field activity was recorded from stratum pyramidale in hippocampal CA3b and simultaneous single-cell recordings were made from

interneurons, as identified by the fluorescent Venus transgene. The phase relationship between HFA cycles and interneuronal action potentials was determined using a custom made MatLab script; the significance of these relationships was determined using Rayleigh statistics ($\alpha=0.05$). Averages are presented as mean \pm SEM.

Perfusion of 9mM potassium caused epileptic-like discharges, including HFA, in 83 out of 131 slices. Traces where HFA was acquired simultaneously with successful single-cell recordings were analysed further (n=36). Peak HFA frequency was normally distributed (Kolmogorov-Smirnov test, $p>0.05$), with a mean of 216 ± 5 Hz, and spanned both the ripple (n = 8) and fast ripple (n=28) bands. Using interneuronal action potentials as a reference, 11 cells showed significant phase correlation with HFA cycles. Despite the unimodal distribution of HFA frequencies, ripples were significantly more likely than fast ripples to be correlated with interneuronal activity (Fisher's exact test, $p<0.001$).

This suggests a fundamental mechanistic difference between ripple and fast ripple band activity, which hints at a failure of interneurons to modulate high frequency activity in the epileptic brain.

APPENDIX – MATLAB SCRIPTS

In several instances, data analysis was carried out using custom-made scripts in MatLab. This allowed analysis to be automated to an extent, providing advantages in both speed and the removal of bias and error. Full readouts of the scripts described in the methods section are included here. Text following ‘%’ symbols is not read by MatLab during data processing and is included here only as a guide to the logical flow of the scripts.

Phase analysis between HFA and action potential events

The following script required an input of HFA cycles, action potentials and sharp wave events, which were detected manually and represented as discrete points in time. The output contained histograms and rose plots representing correlations in the phase domain, as well as the p value of the Rayleigh test, the mean vector angle, mean vector length and circular standard deviation of the phase data.

```
%Phase Analysis with no event detection

clear all
close all

AP = input('Enter action potentials: ')
HFA = input('Enter HFA: ')
SPW = input('Enter sharp waves: ')
AP=AP';
HFA=HFA';
SPW=SPW';

%HFA trigger
%Calculate phase differences in positive direction
i=1;%index for HFA
i2=1;%index for AP
i3=1;%index for phase differences
i4=1;%index for sharp waves
phasediffs=[];
```

```

for i4=1:length(SPW)%for each SPW
for i=1:(length(HFA)-1)%for each HFA cycle
    totalcycle=HFA(1,i+1)-HFA(1,i);
    if all([totalcycle<=0.01 , HFA(1,i)>=(SPW(1,i4)-0.05) ,
HFA(1,i)<=(SPW(1,i4)+0.05)])==1 %if the cycle is greater than 100
Hz and occurs within 50 ms of a sharp wave
        for i2=1:length(AP)
            if all([(AP(1,i2)-HFA(1,i))<totalcycle, (AP(1,i2)-
HFA(1,i))>=0])==1
                timeintocycle=AP(1,i2)-HFA(1,i);
                fractionintocycle=timeintocycle/totalcycle;
                radians=fractionintocycle*2*pi;
                phasediffs(1,i3)=radians;
                i3=i3+1;
            end
            i2=i2+1;
        end
    end
    i=i+1;
end
i=1;
i2=1;
i4=i4+1
end
%Rayleigh Statistics
C=sum(cos(phasediffs));
S=sum(sin(phasediffs));
Rsq=((C^2) + (S^2));
R=sqrt(Rsq);
if all([S>0, C>0])==1;
    posmeanangle=atan(S/C);
elseif all([S<0, C>0]);
    posmeanangle=atan(S/C)+(2*pi);
elseif C<0;
    posmeanangle=atan(S/C)+pi;
end
posmeanvectorangle=360*(posmeanangle/(2*pi));
posmeanvectorlength=R/length(phasediffs);
Z=(length(phasediffs))*(posmeanvectorlength^2);
HFATriggerP=exp(-Z);
HFATriggerCircVar=1-posmeanvectorlength;
HFATriggerCircSD=((-2*log(1-HFATriggerCircVar))^0.5)*(180/pi);

```

```

%Using AP trigger:

```

```

%Calculate phase differences in positive direction
iI=1;%index for AP
i2I=1;%index for HFA
i3I=1;%index for phase differences
i4I=1;%index for SPWs
phasediffsI=[];
for i4I=1:length(SPW)
for iI=1:(length(AP)-1)
    totalcycleI=AP(1,iI+1)-AP(1,iI);
    if all([totalcycleI<=0.01 , AP(1,iI)>=(SPW(1,i4I)-0.05) ,
AP(1,iI)<=(SPW(1,i4I)+0.05)])==1

```

```

    for i2I=1:length(HFA)
        if all([(HFA(1,i2I)-AP(1,iI))<totalcycleI, (HFA(1,i2I)-
AP(1,iI))>=0])==1
            timeintocycleI=HFA(1,i2I)-AP(1,iI);
            fractionintocycleI=timeintocycleI/totalcycleI;
            radiansI=fractionintocycleI*2*pi;
            phasediffsI(1,i3I)=radiansI;
            i3I=i3I+1;
        end
        i2I=i2I+1;
    end
    end
    iI=iI+1;
end
iI=1;
i2I=1;
i4I=i4I+1
end
%Rayleigh Statistics
%Positive
CI=sum(cos(phasediffsI));
SI=sum(sin(phasediffsI));
RsqrI=((CI^2) + (SI^2));
RI=sqrt(RsqrI);
if all([SI>0, CI>0])==1;
    posmeanangleI=atan(SI/CI);
elseif all([SI<0, CI>0]);
    posmeanangleI=atan(SI/CI)+(2*pi);
elseif CI<0;
    posmeanangleI=atan(SI/CI)+pi;
end
posmeanvectorangleI=360*(posmeanangleI/(2*pi));
posmeanvectorlengthI=RI/length(phasediffsI);
ZI=(length(phasediffsI))* (posmeanvectorlengthI^2);
APTriggerP=exp(-ZI);
APTriggerCircVar=1-posmeanvectorlengthI;
APTriggerCircSD=((-2*log(1-APTriggerCircVar))^0.5)*(180/pi);

%plot histogram and rose plots for HFA trigger
figure;
hist((phasediffs),36);title('Phase differences 0 - 360 degrees -
HFA trigger')
xlim([min(phasediffs) max(phasediffs)])

figure;
posrose=subplot(1,1,1);
posroseplot=rose(phasediffs,36); title('Positive phase differences
0-360 degrees - HFA trigger')
hold on
backtoradians=posmeanvectorangle*pi/180;
xlim=get(posrose,'XLim');
sigh=max(xlimit)*posmeanvectorlength;
[poscart1,poscart2]=pol2cart(backtoradians ,sigh);
meanplot=compass(poscart1,poscart2);
set(meanplot,'LineWidth',1,'color','r');

```

```

%plot histogram and rose plots for AP trigger
figure;
hist((phasediffsI),36);title('Phase differences 0 - 360 degrees -
AP trigger')
xlim([min(phasediffsI) max(phasediffsI)])

figure;
posroseI=subplot(1,1,1);
posroseplotI=rose(phasediffsI,36); title('Positive phase
differences 0-360 degrees - AP trigger')
hold on
backtoradiansI=posmeanvectorangleI*pi/180;
xlimI=get(posroseI,'XLim');
sighI=max(xlimI)*posmeanvectorlengthI;
[poscart1I,poscart2I]=pol2cart(backtoradiansI ,sighI);
meanplotI=compass(poscart1I,poscart2I);
set(meanplotI,'LineWidth',1,'color','r');

HFATriggerP
HFATriggerCircVar
HFATriggerCircSD
posmeanvectorangle
APTriggerP
APTriggerCircVar
APTriggerCircSD
posmeanvectorangleI

```

Comparing interneuron firing frequencies during and separate from sharp wave events

The following script was used to analyse the differences in interneuron firing frequency between action potentials that occurred during sharp wave excitation and those which did not. The script required an input of manually detected sharp waves and action potentials, represented as discrete time points. The use of this script permitted the analysis of many sharp wave events, in order to calculate an average value for this effect.

```

%Measuring firing frequency in and out of SPWs

%input event times
clear all
AP=input('Paste action potentials times')
SPW=input('Paste SPW times')
AP=AP';
SPW=SPW';

%median max freq during SPW
iSPW=1;
iAP=1;
itemp=1;
ifreq=1;
duringfreqs=[];
for iSPW=1:length(SPW)
    for iAP=1:length(AP)
        if all([AP(1,iAP)>=(SPW(1,iSPW)-0.05) ,
AP(1,iAP)<=(SPW(1,iSPW)+0.05)])==1 %if an action potential is
within 50 ms of a sharp wave
            temp(1,itemp)=AP(1,iAP); %then it is stored in a
temporary matrix
                itemp=itemp+1; %and the script moves on to the next
entry in that matrix
                    end
                end
            if length(temp)>1
                timediffs=diff(temp);%calculate the time differences between
the temporarily stored action potentials
                duringfreqs(1,ifreq)=1/(min(timediffs)); %stores the maximum
temp value into a different matrix
                ifreq=ifreq+1; %moves onto next permanent storage value
            end
            iSPW=iSPW+1; %moves onto next sharp wave
            iAP=1; %resets action potential index
            itemp=1; %resets temporary storage index
            temp=[]; %clears temporary storage
        end
    end
    medianduringfreq=median(duringfreqs)

%median max freq outside SPWs
iSPW=1;
iAP=1;
itemp=1;
ifreq=1;
notduringfreqs=[];
for iSPW=1:length(SPW)-1
    for iAP=1:length(AP)
        if all([AP(1,iAP)>=(SPW(1,iSPW)+0.05) ,
AP(1,iAP)<=(SPW(1,iSPW+1)-0.05)])==1
            temp(1,itemp)=AP(1,iAP); %then it is stored in a
temporary matrix
                itemp=itemp+1; %and the script moves on to the next
entry in that matrix
                    end
                end
            if length(temp)>1

```

```

    timediffs=diff(temp);%calculate the time differences between
the temporarily stored action potentials
    notduringfreqs(1,ifreq)=1/(min(timediffs)); %stores the maximum
temp value into a different matrix
    ifreq=ifreq+1; %moves onto next permanent storage value
end
    iSPW=iSPW+1; %moves onto next sharp wave
    iAP=1; %resets action potential index
    itemp=1; %resets temporary storage index
    temp=[]; %clears temporary storage
end
mediannotduringfreq=median(notduringfreqs)

```